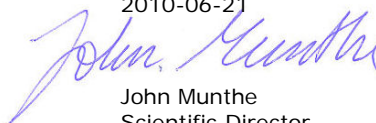


# On the increasing levels of NO<sub>2</sub> in some cities

The role of primary emissions  
and shipping

Marie Haeger-Eugensson, Jana Moldanova, Martin Ferm,  
Martin Jerksjö and Erik Fridell  
Juni 2010  
B1886

This report approved  
2010-06-21



John Munthe  
Scientific Director



<p><b>Organization</b> IVL Swedish Environmental Research Institute Ltd.</p>	<p><b>Report Summary</b></p>
<p><b>Address</b> P.O. Box 5302 SE-400 14 Gothenburg</p>	<p><b>Project title</b></p>
<p><b>Telephone</b> +46 (0)31-725 62 00</p>	<p><b>Project sponsors</b> The Swedish Environmental Protection Agency, Sveriges Ingenjörers Miljöfond, The Foundation for the Swedish Environmental Research Institute (SIVL).</p>
<p><b>Authors</b> Marie Haeger-Eugensson, Jana Moldanova, Martin Ferm, Martin Jerksjö and Erik Fridell.</p>	
<p><b>Title and subtitle of the report</b> On the increasing levels of NO<sub>2</sub> in some cities. The role of primary emissions and shipping.</p>	
<p><b>Summary</b> See below</p>	
<p><b>Keyword</b> nitrogen dioxide, emissions, dispersion modelling</p>	
<p><b>Bibliographic data</b> IVL Report B1886</p>	
<p><b>The report can be ordered via</b> Homepage: <a href="http://www.ivl.se">www.ivl.se</a>, e-mail: <a href="mailto:publicationservice@ivl.se">publicationservice@ivl.se</a>, fax+46 (0)8-598 563 90, or via IVL, P.O. Box 21060, SE-100 31 Stockholm Sweden</p>	



## **Foreword**

Financial support from Sveriges Ingenjörer, The Swedish Environmental Protection Agency and The Foundation for the Swedish Environmental Research Institute (SIVL) is gratefully acknowledged. We thank Maria Holmes at the Environmental Agency in Gothenburg for providing emission data and results from their dispersion modelling. Thanks to Åke Sjödin, IVL for providing FEAT data.



## Summary

This report is an attempt to investigate the background to the high NO<sub>2</sub> levels in Gothenburg and the reason for the slowing decrease in NO<sub>2</sub> observed during the last years. Two possible reasons for these observations are investigated: contribution from shipping to NO<sub>2</sub> emissions, and increased fraction of NO<sub>2</sub> in the NO<sub>x</sub> emissions from modern diesel engines. The issue was studied through emission measurement, passive sampling, dispersion modelling and atmospheric chemistry studies

Two possible reasons for the high NO<sub>2</sub> levels in Gothenburg were investigated: 1) increased fraction of NO<sub>2</sub> in the NO<sub>x</sub> emissions from modern diesel engines, and 2) increasing total emission of NO<sub>x</sub> due to increasing contribution from shipping. The results also showed that local mixing conditions greatly influenced the dispersion of especially local and ground-based emissions. This was mainly due to their main location within the Göta älv valleys where the dispersion becomes particularly poor during high pressure conditions. The effect of ship emissions in the Gothenburg area was very dominant along the harbour. At distances of about 1-2 km from the harbour area the ship contribution was still more than 30 % of the total NO<sub>x</sub> concentration level.

The modelled concentration data was compared to measurement results from passive sampling performed mainly along the river but also with the continuous monitoring at the Femman site. In general, the NO<sub>2</sub> concentrations were underestimated, the SO<sub>2</sub> mainly coincided well and the O<sub>3</sub> concentrations were somewhat overestimated in the calculations with the TAPM model. Variation in concentrations due to varying weather conditions were reproduced well but the modelled peaks are sometimes lower than the monitored concentration peaks.

There are several explanations for the increased proportions of NO<sub>2</sub> in the primary emissions of NO<sub>x</sub>. First the increase in the fraction of diesel vehicles by ca. 15% (as vehicle-km) during the last decade. Diesel vehicles generally have a higher fraction of NO<sub>2</sub> in their NO<sub>x</sub> emissions than gasoline cars. On top of this, the large increase of diesel vehicles over the last decade was accompanied by a simultaneous increase of the NO<sub>2</sub> fraction in NO<sub>x</sub> emissions from diesel trucks with Euro3 and Euro4 standards which became compulsory in 2000 and 2005, respectively. Measurements of NO<sub>2</sub> and NO<sub>x</sub> concentrations in tunnels, and at sites largely dominated by primary emissions, indicated an increase in the NO<sub>2</sub>/NO<sub>x</sub> partitioning from 4-6% in the 1980s, and at the beginning of the 1990s, to today's 13%. The tunnel-model study indicated that the actual NO<sub>2</sub>/NO<sub>x</sub> fraction could be even larger if effects of the NO<sub>2</sub> sinks in the tunnel are taken into account.

The modelling results show that the increase in the NO<sub>2</sub> share of the NO<sub>2</sub> concentrations was greatest close to the sources since the NO in the primary emission reacted with ambient ozone forming NO<sub>2</sub> on a time-scale of minutes and the NO<sub>2</sub>/NO<sub>x</sub> ratio quickly increased, approaching a photo-stationary state between NO, NO<sub>2</sub> and ozone. The simultaneous measurements of NO<sub>2</sub>, NO (or NO<sub>x</sub>) and ozone indicated that the fraction of primary and secondary NO<sub>2</sub> in the city varied largely depending on mixing and photochemical conditions.

A sensitivity study with the city scale dispersion model was performed by raising the NO<sub>2</sub>/NO<sub>x</sub> emission ratio from 5 to 20%. The change in NO<sub>2</sub> concentrations showed that the effect of the higher share of NO<sub>2</sub> within the NO<sub>x</sub> emissions can affect the NO<sub>2</sub> concentration level close to the source up to a distance of about 500-700m.

The chemical development in ship plumes was studied with a detailed photochemical plume model to ensure that the simple chemistry treatment of the TAPM model accurately described the processes affecting the NO/NO<sub>2</sub> distribution and NO<sub>x</sub> oxidation. Comparison of the detailed chemistry with the simplified version showed a significant similarity during day hours when chemistry is, to a large extent, driven by NO<sub>2</sub> photolysis. The night-time chemistry of NO<sub>x</sub>, driven by nitrate radical and oxidation of N<sub>2</sub>O<sub>5</sub> is not included in the TAPM chemical scheme which may lead to an underestimation of NO<sub>x</sub> oxidation during dark hours.

## Contents

Summary .....	3
1 Introduction .....	5
1.1 NO <sub>2</sub> in Gothenburg .....	5
1.2 Photochemistry in urban air .....	11
1.3 Outline.....	12
2 FEAT measurements .....	13
2.1 Instrumentation and procedure .....	13
2.2 Results .....	14
3 Trends in vehicle fleet composition.....	16
4 Estimation of primary emitted NO <sub>2</sub> concentration in ambient air.....	18
5 Passive sampling of ambient air in Gothenburg .....	19
5.1 Principle of diffusive sampling .....	19
5.2 Results .....	19
6 Emissions.....	22
6.1 Emission data for Gothenburg .....	22
6.2 Emission trends .....	26
7 Tunnel study .....	27
7.1 Measurements .....	28
7.1.1 Early measurements .....	28
7.1.2 Measurements in a long road tunnel .....	29
7.2 Modelling .....	30
7.2.1 Model description.....	31
7.2.2 Modelling results.....	32
8 Ship plume chemistry.....	36
8.1 Plume-model description .....	36
8.2 Results .....	37
9 Dispersion modelling.....	40
9.1 The TAPM dispersion model.....	40
9.2 The modelling .....	40
9.3 Results .....	41
9.3.1 Meteorological simulation with TAPM.....	41
9.3.2 Dispersion calculations.....	44
9.3.2.1 Calculations with TAPM .....	44
9.3.2.2 Calculations with Enviman .....	46
9.3.3 Evaluation of air pollution calculations.....	48
9.3.4 Sensitivity study of the NO <sub>2</sub> /NO <sub>x</sub> emission ratio .....	54
9.4 Separate calculations for different emission sources .....	56
10 Discussion.....	59
11 References.....	61
Appendix 1. Description of the TAPM model .....	65



# 1 Introduction

The ambient air concentration of NO<sub>2</sub> at urban background stations in Sweden (4 – 8 m above street level in the city centre) has decreased since catalytic converters were introduced from car model year 1989 and the NO<sub>x</sub> emission per vehicle and kilometre became lower. In small and medium sized towns, the NO<sub>2</sub> concentration has decreased by about 35 % since the mid 1980s (Persson et al., 2007). During the last few years this trend has changed in some towns, in which the decrease in NO<sub>2</sub> concentration appears to have halted.

There are not many long-term series of NO<sub>2</sub> and NO<sub>x</sub> measurements at street level, but the trend is that the NO<sub>2</sub> concentration does not decrease as fast as expected or does not decrease at all. This study looks at possible reasons for this trend.

## 1.1 NO<sub>2</sub> in Gothenburg

Air pollution measurements have been performed in the centre of Gothenburg at roof level (25 m above the ground) since 1975. According to the result presented in Figure 1 the NO<sub>x</sub> and NO<sub>2</sub> concentrations decreased significantly in Gothenburg from 1975 to 1983. After 1985, the concentrations have continued to decrease but not to the same degree. However, the NO<sub>x</sub> concentration decreases faster than the NO<sub>2</sub> concentration, implying that the NO<sub>2</sub> fraction (NO<sub>2</sub>/NO<sub>x</sub> ratio) increases with time from about 45 % in 1975 to 60 % in 2008. Measurements in regional background at Rörvik, outside Gothenburg, started in 1982. The concentration of NO<sub>x</sub> at this, and similar sites, consists mainly of NO<sub>2</sub>. The annual average between 1982 and 2005 decreases almost continuously from about 9 to about 4.5 µg m<sup>-3</sup>. The O<sub>3</sub> concentration, on the other hand, decreased between 1975 and 1990 and then started to increase.

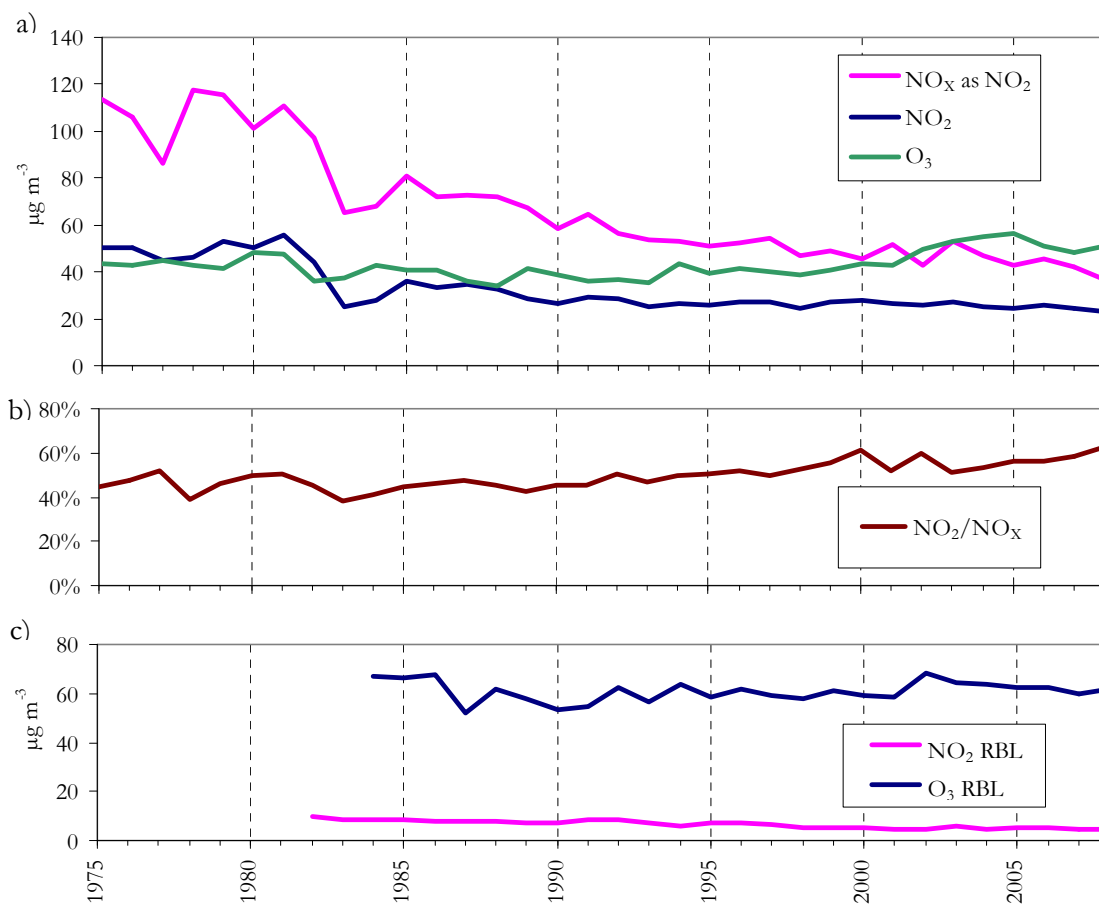


Figure 1. a) -  $\text{NO}_x$ ,  $\text{NO}_2$  and  $\text{O}_3$  concentrations measured under period 1975 – 2008 on a roof-level at station 'Femman' in Gothenburg, Figure 1. b) - The  $\text{NO}_2/\text{NO}_x$  ratio of the concentrations measured at Femman, and Figure 1. c) –  $\text{NO}_2$  and  $\text{O}_3$  concentration measured at background station c.a. 40 km south of Gothenburg at the coast (Rörvik/Råö) (all yearly averages, RBL means regional background level).

The  $\text{NO}_2$  concentration in urban background (UB) in Gothenburg is known to be rather high compared to other towns. In Figure 2, the mean UB concentrations for about four winter half-years are shown for about 40 towns. A large part of the  $\text{NO}_2$  concentration originates from the same sources as the locally developed  $\text{PM}_{10}$ ; and the ratio of the two parameters is similar in urban areas of southern Sweden (Sjöberg et al. 2008).

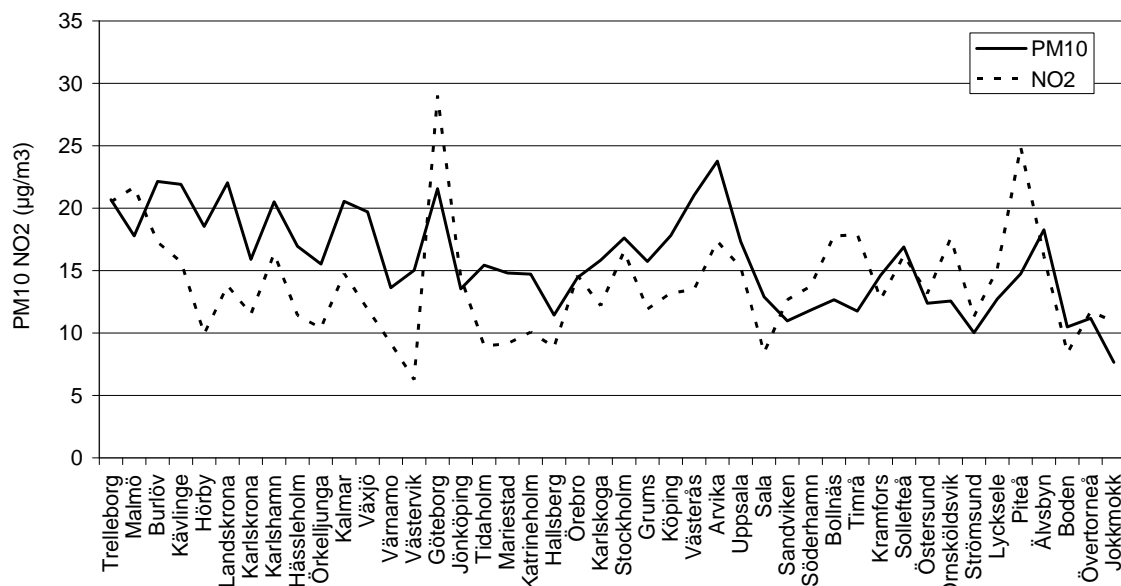


Figure 2. Monitored winter half-year means (for about 4 years, 2002 - 2006) of NO<sub>2</sub> and PM<sub>10</sub> of varying sizes of towns plotted from south to north (urban background).

According to the result presented in Figure 2, the ratio of the NO<sub>2</sub> concentration to the PM<sub>10</sub> concentration is high in Gothenburg compared to the majority of the other towns in southern Sweden. It also becomes clear that in southern Sweden, up to the latitude of about Uppsala/Sala, the PM<sub>10</sub> concentration in urban background is higher than the NO<sub>2</sub> concentration. North of Sala, the relationship between the two parameters changes to higher or similar NO<sub>2</sub> concentrations; this is perhaps partly due to meteorological factors resulting in decreased local dispersion, leading to high concentrations of locally developed pollutants, such as NO<sub>2</sub>. This, therefore, suggests that local factors to a large extent influence the total NO<sub>2</sub> urban background concentration in this part of the country. To the contrary, for PM<sub>10</sub>, large-scale processes govern the total concentration level, specifically the influence from long-distance transportation which is a considerable part of the PM<sub>10</sub> concentration in urban background air in southern Sweden. The observed trend may also to some extent be influenced by an increasing fraction of studded tyres from south to north. Thus, when plotting the PM<sub>10</sub> to NO<sub>2</sub> ratio calculated from the data in Figure 2, it becomes clear that the ratio differs substantially for Gothenburg compared to most of the other towns in southern Sweden (Figure 3). Due to the above-mentioned processes, the PM<sub>10</sub> to NO<sub>2</sub> ratio thus depends on the latitude, since the relationship between the locally-developed and the long-distance transported part of the urban background concentrations varies differently for NO<sub>2</sub> and PM<sub>10</sub> (Haeger-Eugensson et al. 2002, Sjöberg et al. 2008). Thus, one can conclude that the observed levels of NO<sub>2</sub> in Gothenburg stick out as high which may be due to unusual local topography or metrology or to that the emission situation in Gothenburg is different from other cities.

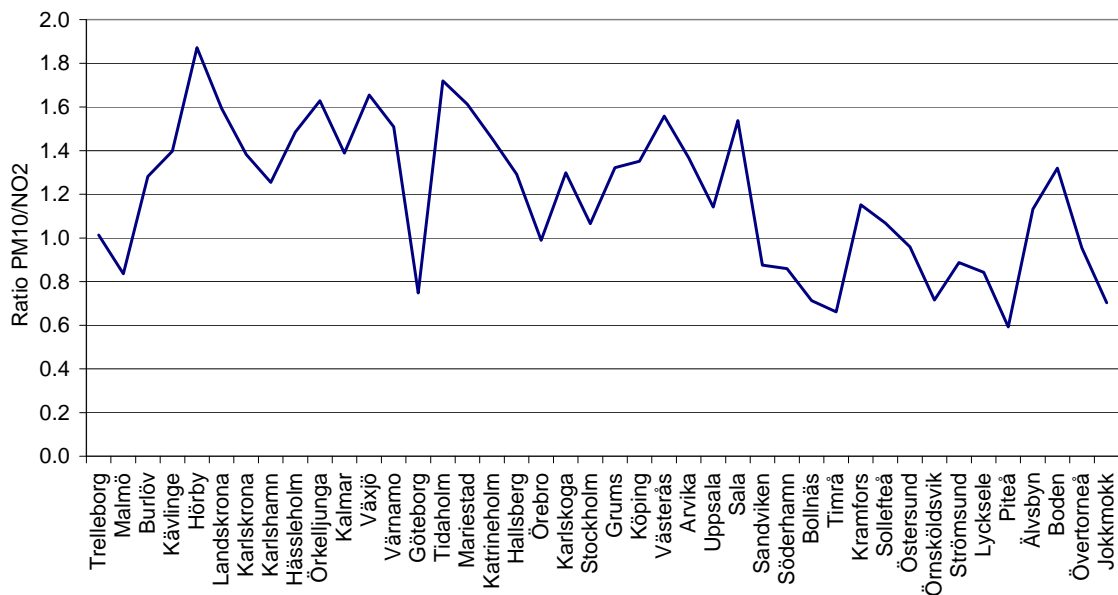


Figure 3. Ratio calculations of monitored winter half-year mean averages of NO<sub>2</sub> and PM<sub>10</sub> (for about 4 years) for a number of cities (from southern to northern Sweden).

In order to show the latitudinal change, the ratios above (Figure 3) have also been plotted towards the southerly-northerly coordinate (x and y coordinates RT90). It is clear that the ratio decreases towards the north but with some exceptions, namely Trelleborg, Malmö and Gothenburg. Of these three towns, it is Gothenburg that stands out the most, compared to the mean value representative for the respective latitude.

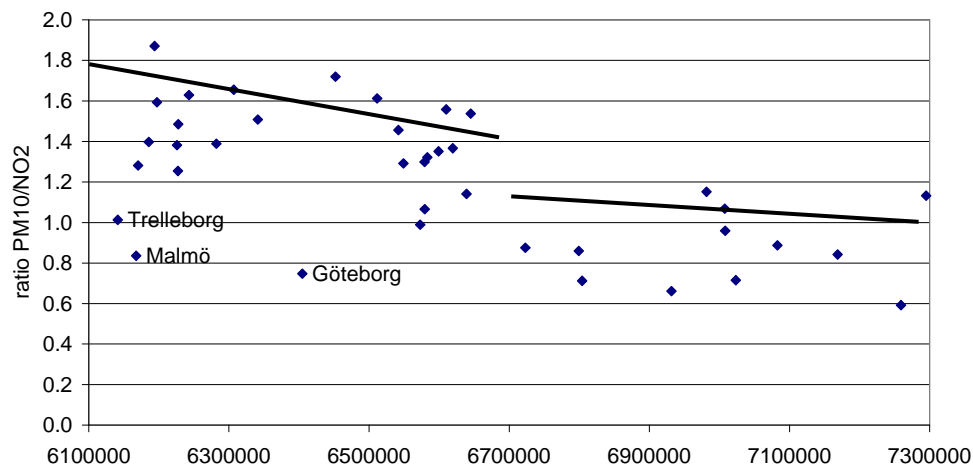


Figure 4. Mean ratios of PM<sub>10</sub>/NO<sub>2</sub> based on monitoring data. The X-axis shows the local coordinates (RT90) from the south to the north of Sweden.

The Gothenburg area is known to have relatively limited dispersion, mainly due to complex terrain and its closeness to the sea (see Figure 5). The complexity of the terrain consists of valleys carved down (from 50-200 m) into the rather flat surrounding plateau (see Figure 6). This morphology causes rapid development of stable air and inversions within the valleys. The vertical temperature structure gives rise to developments of both local and mesoscale modifications of the wind systems in the area (Haeger-Eugensson, 1999). The dispersion conditions are therefore rather complex in

both winter and summer. The air quality, especially for locally developed air pollutants, is thus worse than what would have been expected for a typical Scandinavian town of this size.

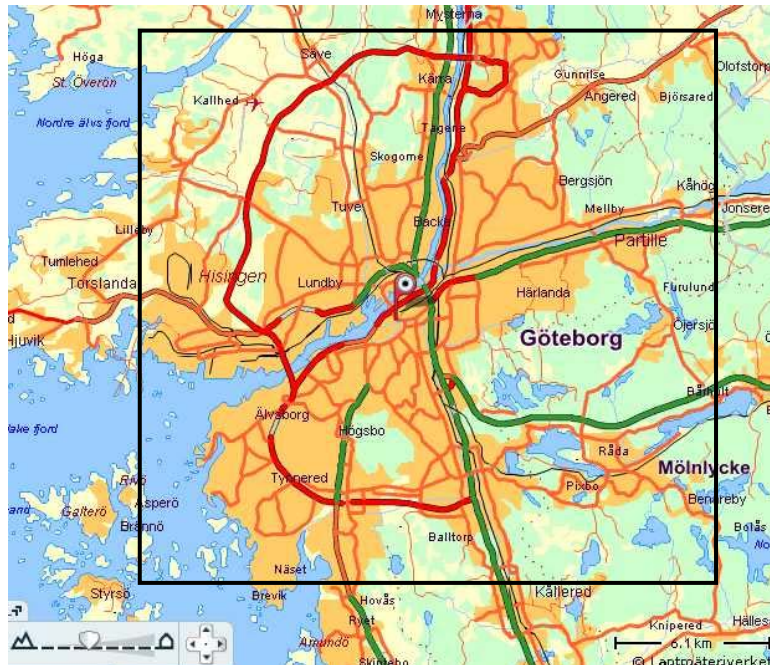


Figure 5. Map of Gothenburg. Yellow areas show urban areas, red and green lines show major roads. The frame indicates the calculation area. The monitoring point Femman is marked.

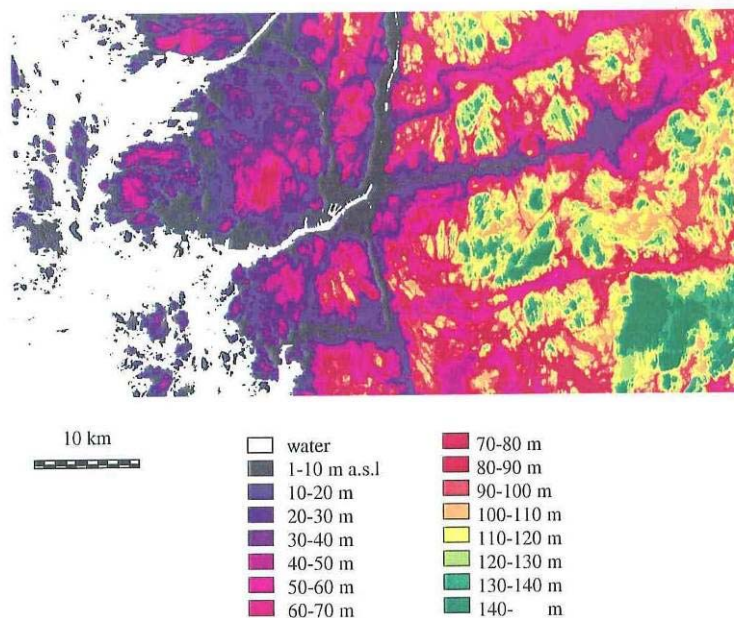


Figure 6. Topographical map of the Gothenburg area (from Haeger-Eugensson 1999).

In Figure 7, historical measurement data are presented for two urban background sites: the Femman site (in the city centre and close to the harbour), and the Kungsportsplatsen site (also in the city centre but farther away from the harbour). According to this data, the measured concentrations at the two sites agreed well initially but drifted apart from about 1998/1999.

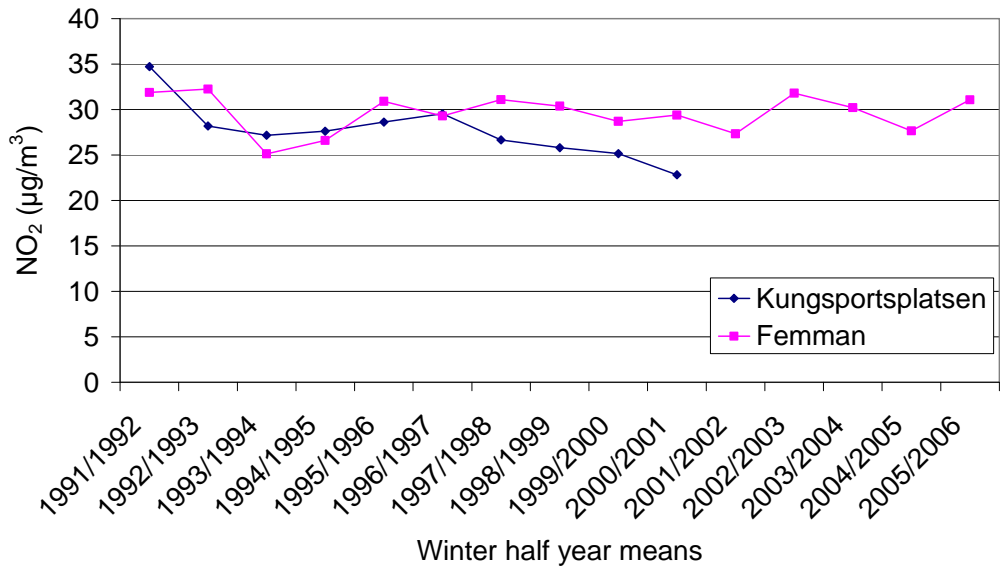


Figure 7. Historical monitoring data at two sites in Gothenburg (see also map in Figure 46).

When plotting the mean SO<sub>2</sub> and NO<sub>2</sub> concentrations against the different wind directions a very different pattern occurs for the different parameters (Figure 8).

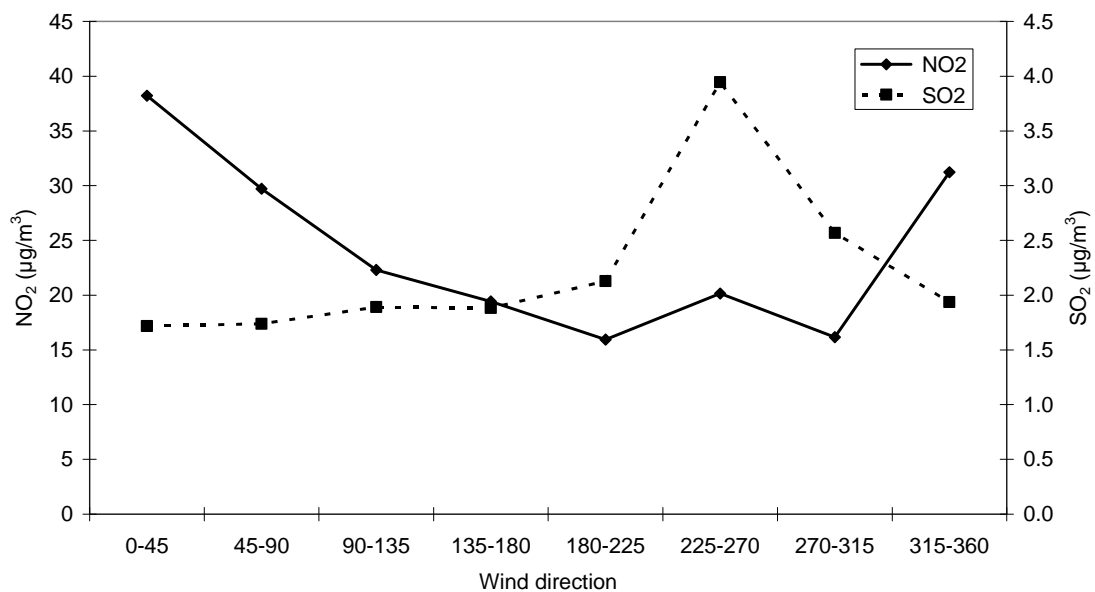


Figure 8. Measured hourly mean NO<sub>2</sub> and SO<sub>2</sub> concentration data for each wind direction class (each 45 deg) for one year at the Femman station.

The highest NO<sub>2</sub> concentrations occur when the wind direction is from the north-west (315-360), the north-east (0-45), and east (45-90). For SO<sub>2</sub>, the highest concentrations arise when the wind direction is from the south-west (225-270); this is the direction of the river, while the northerly to easterly directions are from heavy traffic areas. In Figure 9 the pattern of O<sub>3</sub> shows the opposite pattern to NO; the reason for this is possibly that most of the O<sub>3</sub> is consumed during the chemical reaction where NO is oxidised to NO<sub>2</sub> (see next chapter).

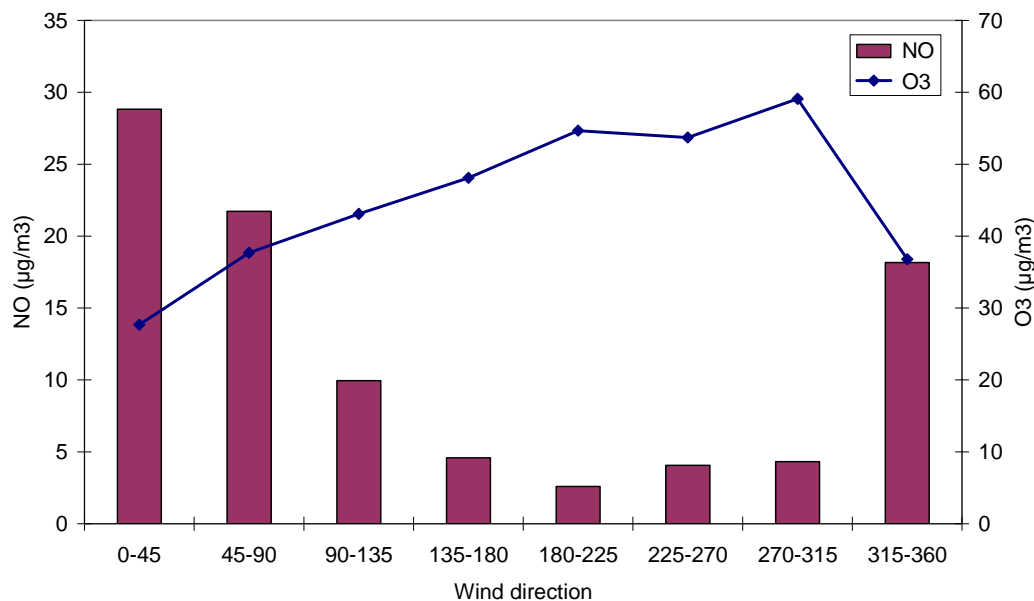


Figure 9. Yearly mean NO and O<sub>3</sub> concentration data (based on hourly mean-values) for each of the wind direction classes (each 45 deg) at the Femman station.

## 1.2 Photochemistry in urban air

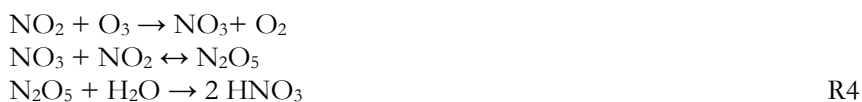
The NO<sub>x</sub> emissions from combustion engines contain to the larger part NO with a smaller part of NO<sub>2</sub>. NO will, at a high rate, react with ozone present in the background air in the following reaction:



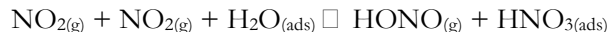
This reaction increases the NO<sub>2</sub>/NO ratio in the air compared to the fresh exhaust. In the daytime NO<sub>2</sub> reacts to form NO in a photolytic reaction and the NO<sub>2</sub>/NO ratio in the air is mainly decided through equilibration between R1 and this photolytic reaction:



NO can also be oxidized by hydro-peroxy (HO<sub>2</sub>) and organic-peroxy (RO<sub>2</sub>) radicals which increase the NO<sub>2</sub>/NO ratio and at the same time increase the ozone concentration (**Error! Reference source not found.**). The main NO<sub>2</sub> sinks are the gas-phase oxidation of NO<sub>2</sub> to HNO<sub>3</sub> by the OH radical during the daytime (R3) and oxidation through nitrate radical and the dinitrogen pentoxide formation at night-time (R4):



Further, NO<sub>2</sub> adsorbed on a wet surface can recombine giving nitrous acid, HONO and HNO<sub>3</sub>:



R5

Where (g) is gas-phase and (ads) are species adsorbed on a surface. NO<sub>2</sub> is also subjected to dry deposition. Figure 10 shows the main processes affecting the NO<sub>x</sub> and ozone concentrations in urban air.

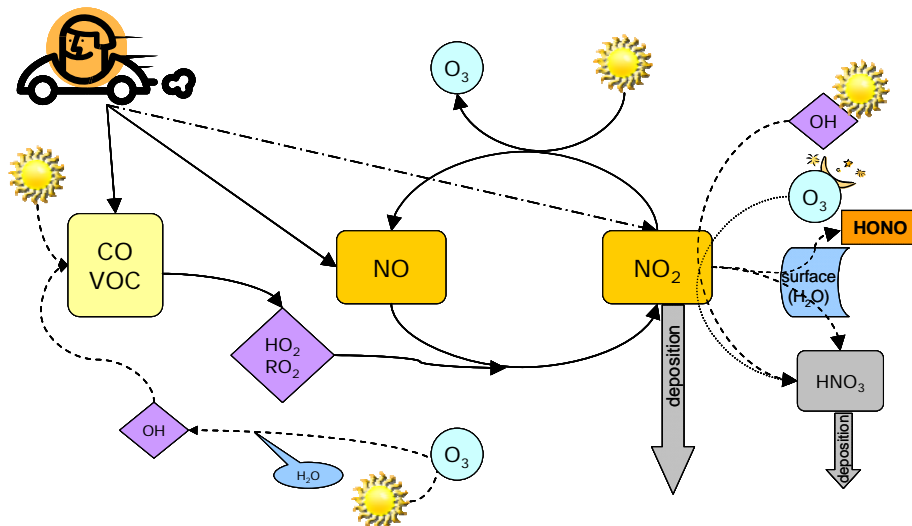


Figure 10. Scheme of NO<sub>x</sub> conversion and removal processes.

### 1.3 Outline

This report is an attempt to investigate the background to the high NO<sub>2</sub> levels in Gothenburg and the reason for the slowing decrease in NO<sub>2</sub> observed during the last years. Two possible reasons for these observations are investigated: contribution from shipping to NO<sub>2</sub> emissions, and increased fraction of NO<sub>2</sub> in the NO<sub>x</sub> emissions from modern diesel engines. In order to investigate, a number of studies have been undertaken as described in the preceding chapters. In order to study the influence of changes in the ratio of NO<sub>2</sub> to NO in the exhaust, the NO<sub>2</sub> emissions were measured for vehicles in real traffic situations. In Chapter 2, results of these measurements of primary emissions are briefly reported. Further, passive samplers were used in order to study the decrease in NO<sub>2</sub> concentration (and SO<sub>2</sub>) as the distance from pollution sources increase. The data from these samplers are also used to validate the dispersion modelling. Chapter 5 contains the results from the passive sampling of NO<sub>2</sub>, O<sub>3</sub> and SO<sub>2</sub> in Gothenburg. In order to investigate the NO<sub>2</sub> levels with dispersion modelling, a database with emissions is required. In Chapter 6, the emissions data for Gothenburg is described and in Chapter 7 modelling and measurements of NO<sub>2</sub>, NO and O<sub>3</sub> levels in a tunnel are reported. The latter study was undertaken in order to verify the NO chemistry that takes place in the vicinity of traffic locations. In order to model the contribution to NO<sub>2</sub> levels of ship emissions it is essential to have a correct description of the chemical reactions taking place in the exhaust plume. Chapter 8 describes the plume model used to study the evolution of NO<sub>2</sub> in a ship plume. Chapter 9 describes the dispersion modelling for Gothenburg using TAPM and Enviman with the emissions data described in Chapter 6. The dispersion modelling is also evaluated towards the passive sampling results in Chapter 5. Discussion follows in chapter 10.



## 2 FEAT measurements

Two measurement campaigns were carried out in the Gothenburg area in order to investigate the primary emissions of NO and NO<sub>2</sub> from different vehicles (one within this project). In both cases the measurements were done with the Fuel Efficiency Automobile Test (FEAT) technique. The FEAT system at IVL can only measure NO and not NO<sub>2</sub>. Therefore the system was complemented for these studies. In the first study, a system was constructed together with Chalmers University in the framework of a master's thesis. The FEAT system at IVL was then complemented with another light source and a spectrometer, thus allowing for detection of NO<sub>2</sub>. This system was tested in a number of field studies to obtain the emissions of NO and NO<sub>2</sub> in real traffic situations. In the second system, a new version of the FEAT equipment was rented. This system allowed for simultaneous measurements of NO and NO<sub>2</sub> and was used in measurements for a few months. The data about the vehicles were obtained by noting the licence numbers and obtaining information from the Swedish vehicle registry. The methods and results from these campaigns are described by Thomar (2008) and Sjödin et al. (2009) and are only briefly reported here.

### 2.1 Instrumentation and procedure

The measurements were carried out with the FEAT technique where light absorption is used to measure the concentration of a number of exhaust components in relation to CO<sub>2</sub>. The instruments generated and monitored a co-linear beam of IR- and UV-light emitted and reflected approximately 30 centimetres above a single lane road. When a car passed, the absorption in the exhaust plume at some specific wavelengths was measured. Because the path length within the plume was not known, Lambert Beer's Law did not give the absolute concentration of pollutants in the exhaust plume. However the concentrations of CO, HC and NO relative to the CO<sub>2</sub> concentration could be determined. These quotas were then recalculated and the instrument provided emissions data as volume% (or ppm by volume) in the undiluted exhaust.

For the measurements in the first campaign, NO<sub>2</sub> was measured using the Differentiated Optical Absorption Spectroscopy (DOAS) technique. This was done with a separate set-up but the probe volume was the same as for the other exhaust components (Thomar, 2008).

The measurements in the second campaign were carried out using the most recent remote sensing (FEAT) technology developed by the University of Denver, which is capable of measuring individual vehicle raw exhaust concentrations of NO<sub>2</sub>, NH<sub>3</sub> and SO<sub>2</sub>, in addition to the "traditional" remote sensing parameters CO<sub>2</sub>, CO, HC and NO (Burgard, 2006). The remote sensing instrument provided also speed and acceleration measurements of individual light-duty vehicles. The measurements followed the normal procedures for remote sensing operation with regard to instrument calibration, vehicle license plate recognition etc., that have been described in detail in earlier work (Ekström, 2004), with the only difference being that now also NO<sub>2</sub>, NH<sub>3</sub> and SO<sub>2</sub> were included in the measurements.

Four different sites were included in the measurements, all of which exhibited a weak to moderate inclination:

- Site 1: A sharply curved city freeway interchange ramp with a speed limit of 30 km/h.
- Site 2: A slightly curved city freeway off-ramp with a speed limit of 70 km/h.
- Site 3: A straight single-lane city freeway with a speed limit of 70 km/h.
- Site 4: A single-lane access road in the city for buses only.

By default, the remote sensor provides emission data as volume-% in the undiluted (raw) exhaust. However, from the definition of the remote sensing measurement principle, the volume-% emissions may also be converted to corresponding fuel-specific emissions, expressed as grams of pollutant emitted per litre or kg of fuel burnt. In this study the conversion of the remote sensing emission data in volume-% to g/kg fuel burnt was done in accordance with the formulas and methods as described in detail in Ekström (2004). Cold-start enrichment operation was considered negligible for all sites, thus it was assumed that the remote sensing data represent hot emissions only.

## 2.2 Results

In this report only a selection of the results is presented. Figure 11 shows the emissions of NO and NO<sub>2</sub> for cars with different Euro classes, broken down into petrol or diesel engine categories. For petrol cars the NO<sub>x</sub> emissions decrease with newer Euro class and the NO<sub>2</sub> fraction is very low. For diesel cars the NO<sub>x</sub> emissions also decrease but here the NO<sub>2</sub> fraction is significant and increasing with newer cars.

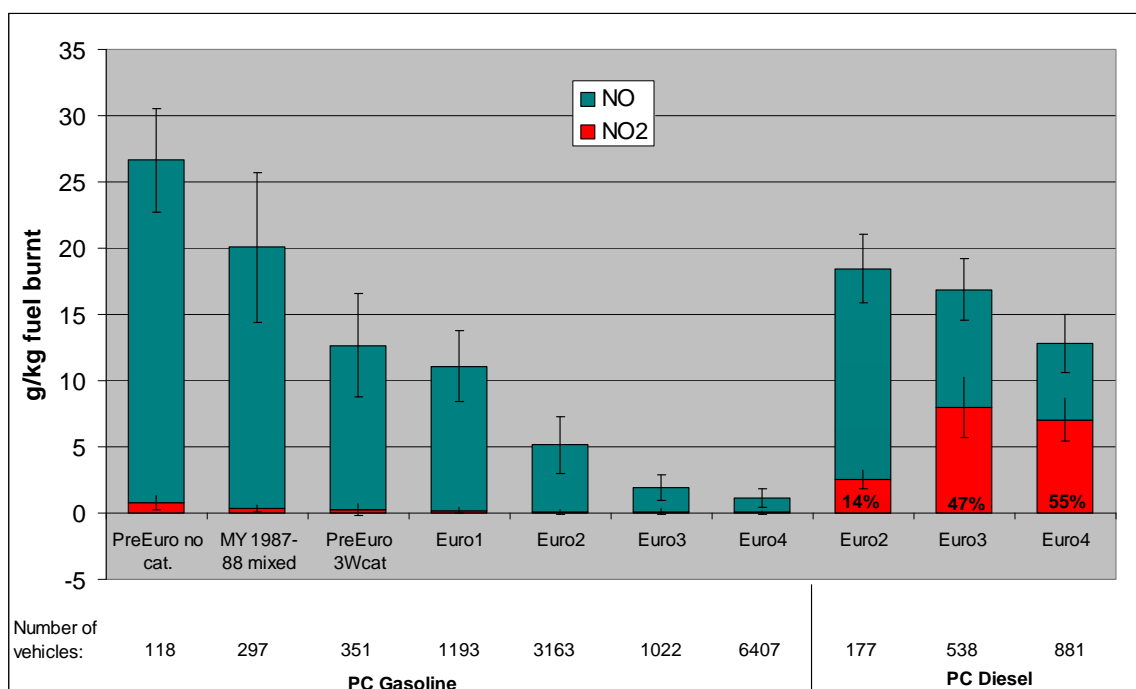


Figure 11. Average NO and NO<sub>2</sub> emissions in g/kg fuel per Euro class for gasoline (petrol) and diesel passenger cars according to the remote sensing measurements. From Sjödin et al. (2009).

Figure 12 shows the emissions of NO and NO<sub>2</sub> for heavy-duty buses with different Euro classes and abatement technologies. The dataset comprises total measurements of more than 500 buses. For Euro 2 and Euro 3 there was a mix of conventional buses, with CPF- and CPF plus EGR-equipped buses. From Figure 12, a general downward trend in NO<sub>x</sub> emissions with increasing Euro class can be observed for conventional buses, resulting in approximately a 30% reduction in NO<sub>x</sub> emissions from Euro 2 to Euro 5. The lowest NO<sub>x</sub> emissions were observed for CNG-buses, which were just slightly lower than Euro 5. NO<sub>2</sub>/NO<sub>x</sub>-fractions were generally high (25-50%), except for CNG-buses (6%). There was no clear trend in the NO<sub>2</sub>/NO<sub>x</sub>-fraction for the diesel-fuelled buses, however Euro 3 CPF- and EGR-equipped buses showed the highest fraction (52%), as well as the highest NO<sub>x</sub> emission.

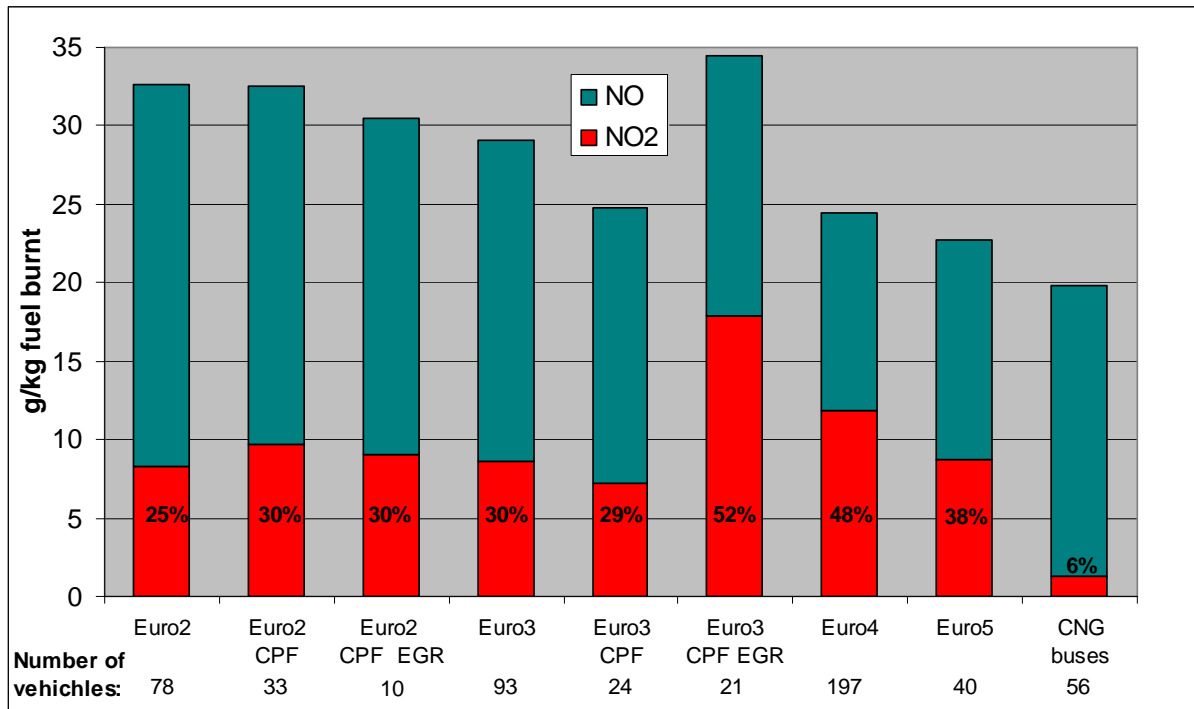


Figure 12. Average NO and NO<sub>2</sub> emissions in g/kg fuel per Euro class for heavy-duty buses according to the remote sensing measurements. Data from sites 1-4 combined. From Sjödin et al. (2009).

There is thus support from this data that newer diesel cars have a higher fraction of NO<sub>2</sub> in the NO<sub>x</sub> emissions than older ones. However, at the same time the NO<sub>x</sub> emissions are decreasing, as expected, with newer models.

### 3 Trends in vehicle fleet composition

In order to understand the different primary NO<sub>2</sub> fractions in NO<sub>x</sub> emissions, differences in the vehicle fleet were studied for different years. Data for the share of traffic activity of diesel vehicles in Sweden 1980 - 2008 compared to total traffic activity were taken from the ARTEMIS Road Model (<http://www.trl.co.uk/artemis/index.htm>). The ARTEMIS model version that was used, comprises Swedish statistical data from 1980 until 2008. Between 1994 and 2008 the fraction of vehicle-kilometres using diesel increased by a factor of 2.5, see Figure 13. Annual averages are plotted in Figure 14. The lowest recorded number of diesel vehicle-kilometres is reported for 1993.

This increase in the fraction of diesel cars, together with the observed increase in the NO<sub>2</sub> to NO fraction in the exhaust reported in Chapter 2, may lead to an increased NO<sub>2</sub> to NO ratio in the emission from road traffic with time. Since the NO<sub>2</sub> emissions from petrol cars are very low, the NO<sub>2</sub> emissions from road traffic can be approximated to follow the use of diesel vehicles. From the increase in the latter (Fig. 13) and the fraction of NO<sub>2</sub> (Figs 11, 12) one can expect that the NO<sub>2</sub> emissions from traffic is doubled between 1994 and 2008. If the NO<sub>2</sub> emission is a limiting factor for the measured NO<sub>2</sub> levels, this could be a reason to the observed high levels.

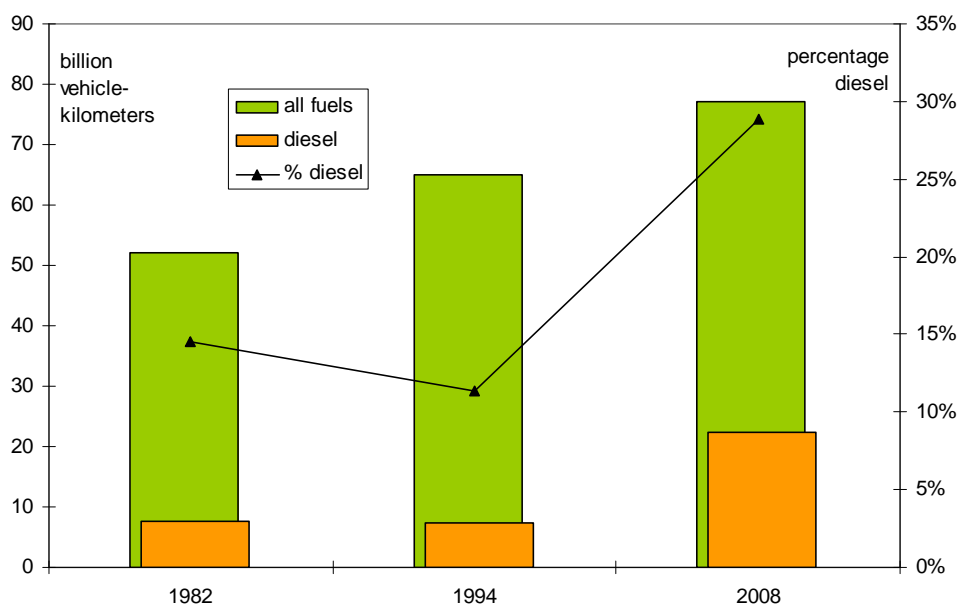


Figure 13. Billions (10<sup>9</sup>) of vehicle-kilometres from all fuels (including diesel) and the separate diesel fraction for three sample years.

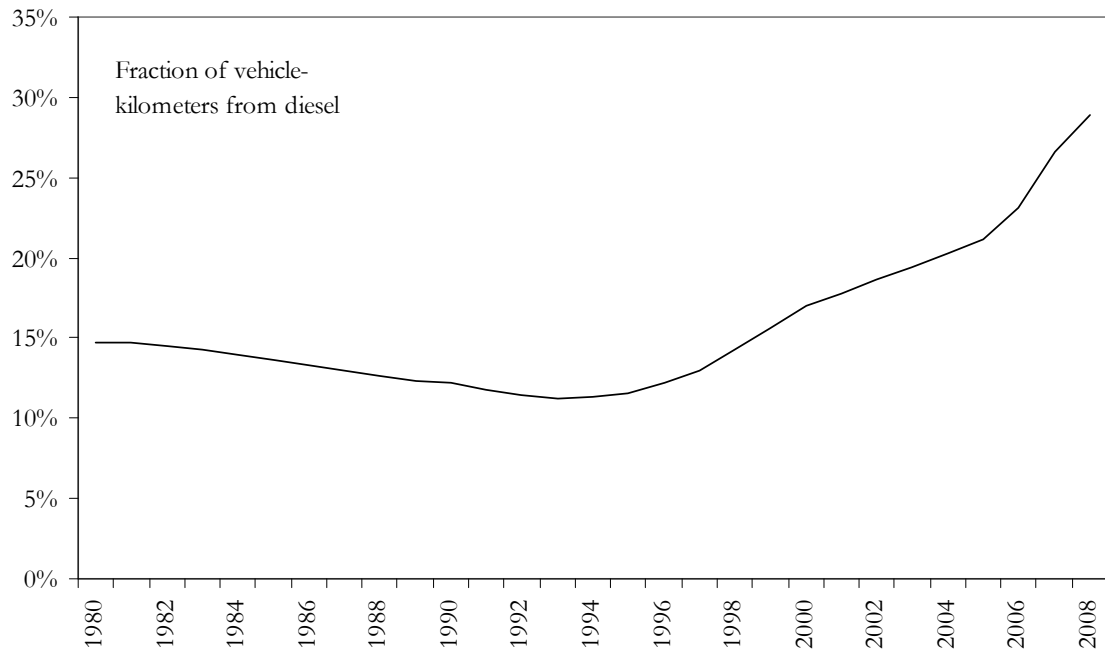


Figure 14. Annual fraction of vehicle-kilometres from diesel fuel from 1980 to 2008 in Sweden.

## 4 Estimation of primary emitted NO<sub>2</sub> concentration in ambient air

The ozone loss at a polluted site at street level compared to an urban background reference site is mainly caused by the reaction with nitric oxide (NO). This ozone loss should therefore reflect the secondary-formed NO<sub>2</sub>. Ozone is monitored at many sites in Sweden, but normally not at street level in cities. Data are available only from two street-level sites: Dalaplan in Malmö and Gårda in Gothenburg.

By analysing the decrease in ozone concentration at street level in relation to urban background, the formation of secondary NO<sub>2</sub>, from the reaction between NO and O<sub>3</sub>, can be obtained. In Figure 15, the measured NO<sub>2</sub> concentration difference ( $\Delta$  NO<sub>2</sub>) at Dalaplan is plotted as a function of the NO<sub>2</sub> concentration calculated as the sum of the primary emitted fraction ( $\Delta$ NO<sub>x</sub> • 0.13, see section 7.1) and the secondary-formed fraction ( $-\Delta$ O<sub>3</sub> • 46/48).  $\Delta$  means the concentration difference between street level and a reference measurement representing urban background air. The roof of the town hall was used as reference to the street-level station at Dalaplan in Malmö. The factor 46/48 is used to convert one mole of ozone to one mole of nitrogen dioxide. As can be seen from Figure 15, the calculated NO<sub>2</sub> concentrations are higher than those measured. A possible explanation could be that ozone is consumed by other reactions than NO oxidation.

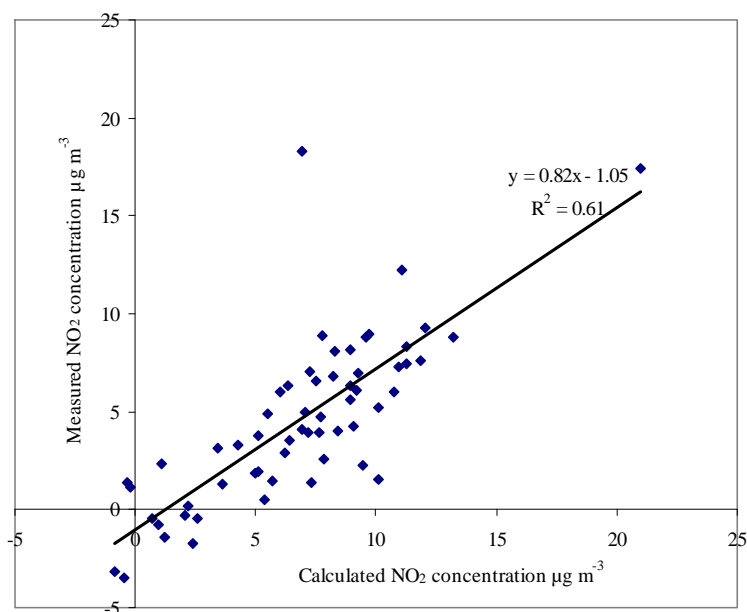


Figure 15. Measured change in NO<sub>2</sub> concentration relative urban background vs. the NO<sub>2</sub> concentration calculated from primary and secondary NO<sub>2</sub> at Dalaplan in Malmö. January – February 2007.

## 5 Passive sampling of ambient air in Gothenburg

### 5.1 Principle of diffusive sampling

Diffusive sampling is a passive sampling technique for air quality measurements in which no pump is needed for collecting the air; this offers many advantages when selecting sampling points. The samplers are small, lightweight (ca 2 g), silent, and do not need mains power. The samplers can therefore be placed almost anywhere. The costs are low, thus making it feasible to use a large number of sampling points simultaneously. Diffusive samplers are frequently used for model validations. The sampling principle is based on molecular diffusion (Ferm 2001). An impregnated filter that quantitatively sorbs the gas in question is placed in one end of a tube. The other end of the tube is protected by a membrane that prevents wind-induced turbulent diffusion inside the tube, but allows gas molecules to permeate through it at a high flux. After a short while (a matter of seconds), there is a concentration gradient of the targeted gas inside the tube. The flux (sampling rate) is directly proportional to this gradient. Since the concentration of the gas is zero at the sorbent, the gradient is determined by the ambient air gas concentration. After analysis, the average concentration during the exposure time is calculated using Fick's first law of diffusion.

Two different samplers for measuring concentrations of NO<sub>2</sub> and SO<sub>2</sub> have been developed at IVL (Ferm and Rodhe 1997, Ferm and Svanberg 1998). Another sampler has been developed for the measurement of ozone (Ferm 2001, Sjöberg *et al.*, 2001).

### 5.2 Results

The first experiment was carried out in 2007. A park (Slottsskogen) was used as a reference point. Average concentrations of NO<sub>2</sub>, NO and O<sub>3</sub> were determined at ground level (3 m) using this technique. The results are shown in Table 1.

Table 1. Average measured concentrations of NO<sub>2</sub>, NO and O<sub>3</sub> between 2007-11-26 and 2007-11-30 in µg m<sup>-3</sup> at STP (20 °C, 1013 mbar).

Place	NO <sub>2</sub>	NO	O <sub>3</sub>
<b>Urban Background</b>			
Slottsskogen No 2	20.3	7.4	32.0
Slottsskogen No 1	19.8	6.9	28.8
<b>Street level</b>			
Sprängkullsgatan nr 1 (tree)	39.0	25.6	26.5
Femman	34.5	36.5	26.3
Nya Allén	35.0	22.8	24.2
Sprängkullsgatan No 3	29.9	12.0	23.9
Sprängkullsgatan No 2	35.3	29.6	23.9
Nils Ericsson nr 1	52.5	62.3	23.8
Järntorget	44.5	50.3	22.4
Järntorget	42.8	52.9	22.3
Järntorget	43.8	49.5	22.1
Hjalmar Brantingsplatsen No 2	45.5	60.4	21.9
Järntorget	44.2	45.2	21.5
Nils Ericsson nr 2	67.6	92.5	21.1
Nils Ericsson nr 3	69.1	104.8	20.6
Hjalmar Brantingsplatsen No 1	57.6	68.9	19.5

A plot of the measured NO<sub>2</sub> concentration as a function of the sum of the primary fraction and the secondary-formed fraction (as discussed in Chapter 4) of the data in Table 1 is shown in Figure 16. Here the correlation coefficient is better than in Malmö, but the calculated concentrations are lower than those measured.

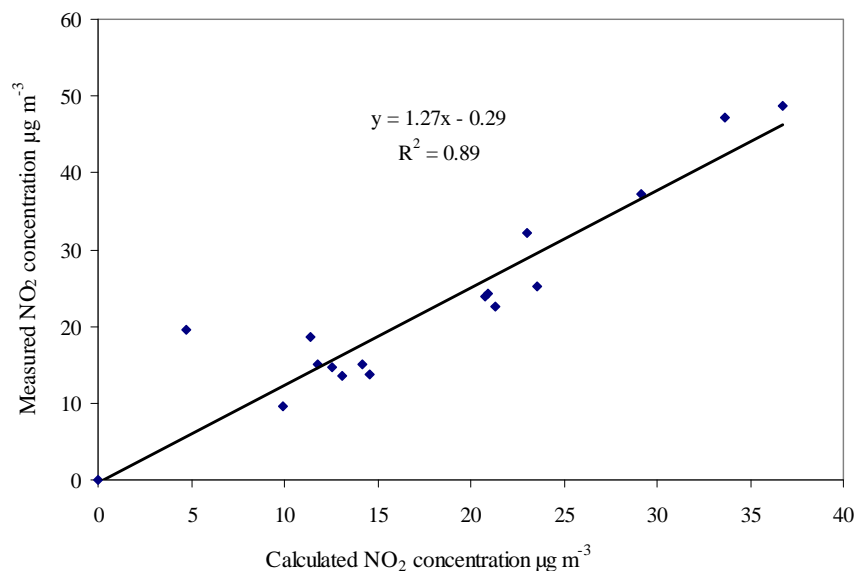


Figure 16. Measured NO<sub>2</sub> concentration as a function of the calculated NO<sub>2</sub> concentration obtained from both the primary-emitted and secondary-formed fractions. Measurements of NO, NO<sub>2</sub> and O<sub>3</sub> were carried out in Gothenburg during 4 days in November 2007 using diffusive samplers.

The measurements were repeated in 2008, without NO measurements, but with SO<sub>2</sub> measurements to gauge the influence of shipping. The sites are shown on a map in Figure 46. Unfortunately several diffusive samplers were lost in this campaign, among them the earlier used reference point for the calculations (Slottsskogen). Results from 2008 are shown in Table 2. The results from Arendal were used as a reference point in this campaign.

The secondary-formed NO<sub>2</sub> ( $-\Delta\text{O}_3 \cdot 46/48$ ) was on average 74 % of the average NO<sub>2</sub> concentration. Two sites had to be removed from this calculation, since the secondary-formed fraction exceeded 100 %. In the 2007 experiments the secondary-formed NO<sub>2</sub>, calculated in the same way constituted only 19 % of the average NO<sub>2</sub> concentration. This may be because the ozone concentrations were much higher in the 2008 campaign than in the 2007 campaign and the NO<sub>2</sub> concentrations much lower.

Table 2. Average measured concentrations between 2008-10-01 and 2008-10-22 in µg m<sup>-3</sup> at STP (20°C, 1013 mbar).

Place	NO <sub>2</sub>	SO <sub>2</sub>	O <sub>3</sub>
Arendal	9.8	25.0	57.5
Länsmansgården	9.0	1.8	53.7
Möndals centrum	12.4	0.6	43.4
Kielterminalen	16.9	3.2	43.4
Järntorget	23.9	3.4	42.9
Suckarnas kaj	21.1	1.7	41.7
Amerikaskjulet	22.9	3.5	40.8
Joten (Söderleden)	10.8	0.7	*
Masthuggskyrkan	12.3	2.9	*

\*sampler lost



We have so far not succeeded in balancing the calculated NO<sub>2</sub> concentration from the estimated concentration of primary-emitted NO<sub>2</sub> (0.14 NO<sub>x</sub> concentration) and the secondary-formed NO<sub>2</sub> ( $-\Delta O_3 \cdot 46/48$ ) with the measured concentration. In Malmö, the calculated NO<sub>2</sub> concentration was overestimated and in Gothenburg it was underestimated. More experimental work is clearly needed. The diffusive NO sampler might need to be improved and better criteria for choosing the reference point (for measuring the urban background of ozone at street level) have to be found.

## 6 Emissions

### 6.1 Emission data for Gothenburg

In this project, two dispersion models were used to calculate the concentrations of air pollutants in the Gothenburg area, TAPM and Enviman (see chapter 7). The emission database used for the modelling was originally developed by the Environmental Agency in Gothenburg and built within the Enviman modelling system. The TAPM database is based on the original database, but some modifications have been done.

Both emission databases are for 2005 and include emissions from traffic, industry, heating, road machinery and ships. For the modelling simulations, point and line sources are handled the common way for advanced dispersion models. In the TAPM database, a typical Swedish monthly and daily time variation, recommended for urban areas, has been applied to the traffic emissions. The emissions from ships are characterized as line sources, with a general 24-hour variation all through the year. The point sources have a typical monthly variation.

In Figure 17 some examples from the Enviman database, the traffic and ship emissions, are shown. Here the main roads are clearly visible together with ship emissions in the harbour.

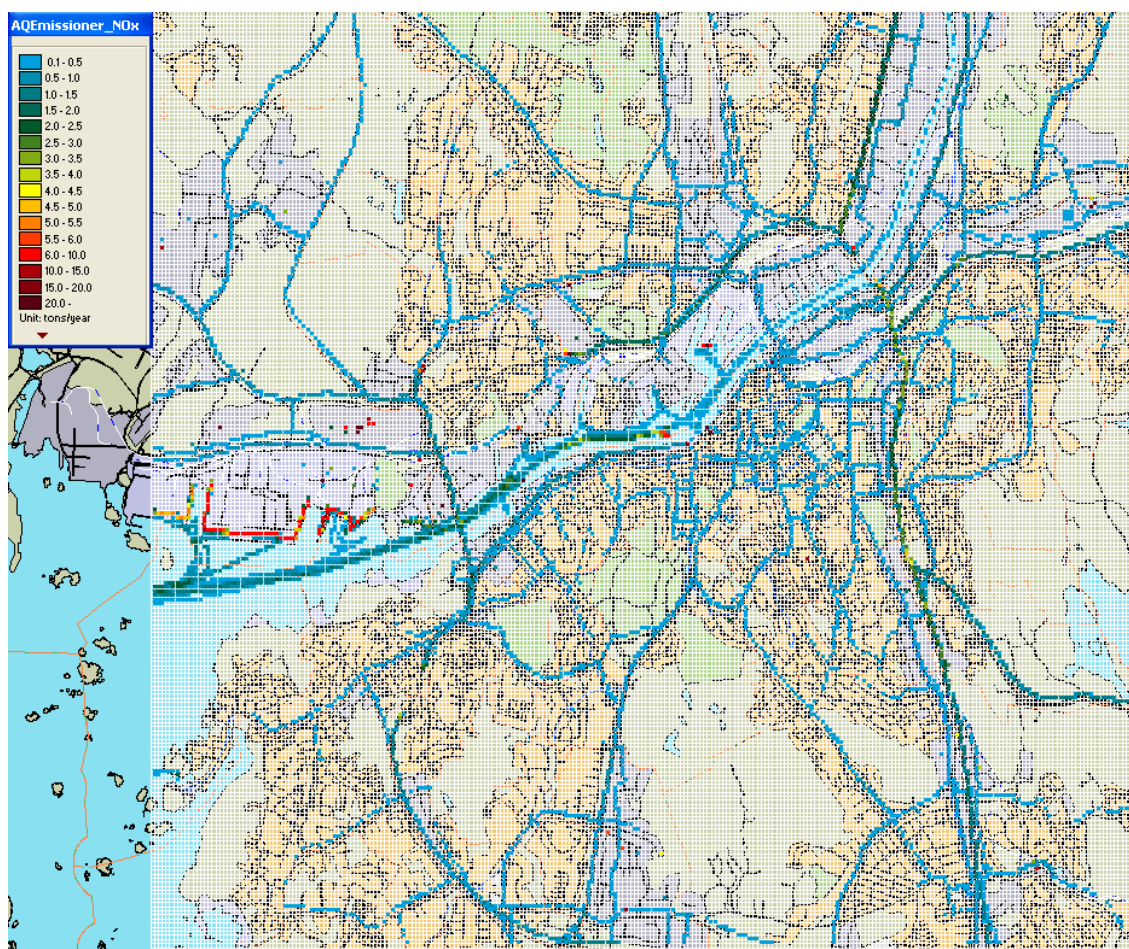


Figure 17. NO<sub>x</sub> emission data for traffic used in the Enviman modelling.

For the TAPM database some simplifications have been made compared to the original database, i.e. vehicle emissions were recategorised from line to area sources. The total  $\text{NO}_x$ ,  $\text{PM}_{10}$  and  $\text{SO}_2$  emissions distributed over the area, are shown in Figures 18 - 20. In these maps the emissions are presented in a 500 m x 500 m grid resolution, while the grid resolution in the calculations is 100 m x m 100 for vehicle emissions, 500 m x 500 m for area emissions and ship emissions are described as line sources and point sources including the common parameters connected to this emission type. Figure 18 shows the total  $\text{NO}_x$  emissions, Figure 19 the  $\text{PM}_{10}$  emissions, and Figure 20 the  $\text{SO}_2$  emissions from all sources. After the simplifications, the road pattern shown in Figure 17 is still visible, even though it has become less distinct.

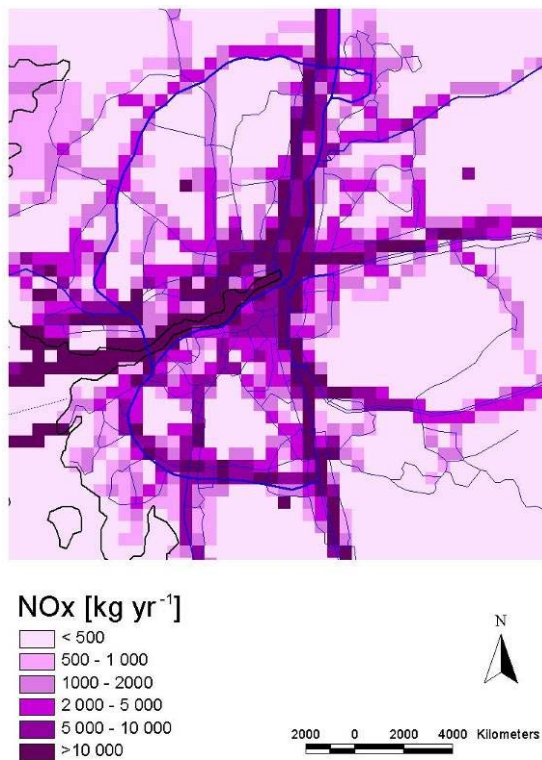


Figure 18. Total  $\text{NO}_x$  emissions (2005) for the calculation area. The blue lines indicate the main roads.

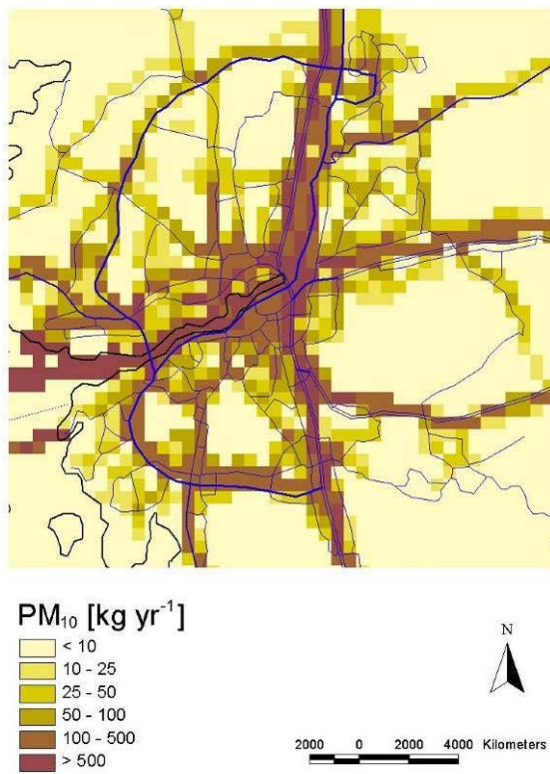


Figure 19. PM<sub>10</sub> emissions (2005) for the calculation area. The blue lines indicate the main roads.

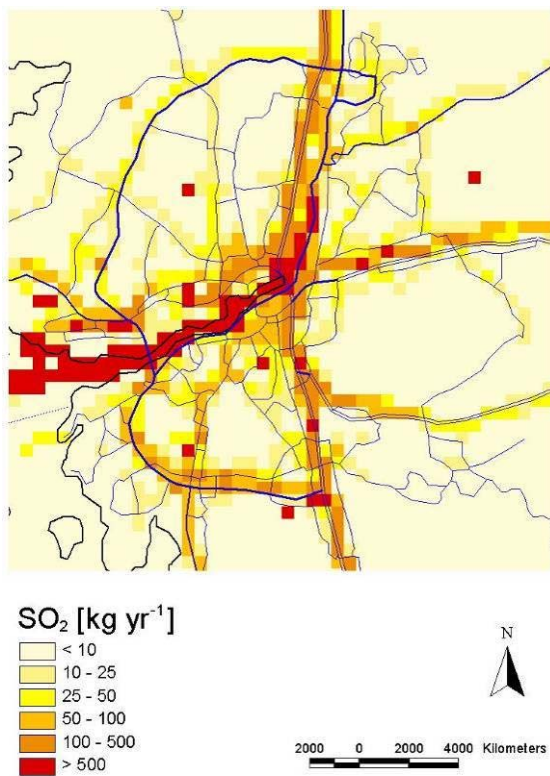


Figure 20. SO<sub>2</sub> emissions (2005) for the calculation area. The blue lines indicate the main roads.

The pattern of total NO<sub>x</sub> and PM<sub>10</sub> distribution is rather similar, while the highest levels for SO<sub>2</sub> are more localized to the river and at some places showing point source locations. The total emissions from all sources and parameters used in the TAPM modelling are shown in Figure 21. The percentage contribution between the different sources is shown in Figure 22. According to that result the major part of the PM<sub>10</sub> emissions are emitted from roads and from ships. The area distribution of PM<sub>10</sub> is thus along major roads and from ships both located in, and passing, the harbour. The NO<sub>x</sub> emissions come from both ships and road traffic as well as from point/area sources, while most of the SO<sub>2</sub> comes from ships but also a minor part from point sources.

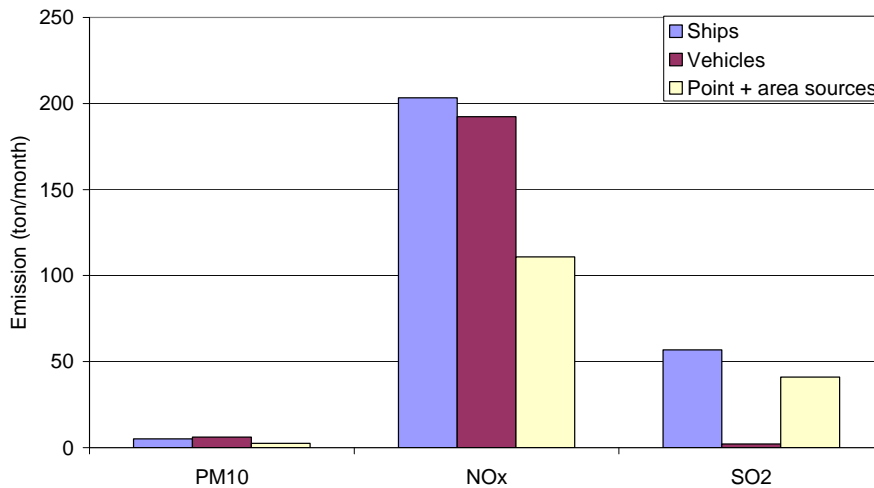


Figure 21. Emissions from the parameters PM<sub>10</sub>, NO<sub>x</sub> and SO<sub>2</sub> used in the TAPM modelling.

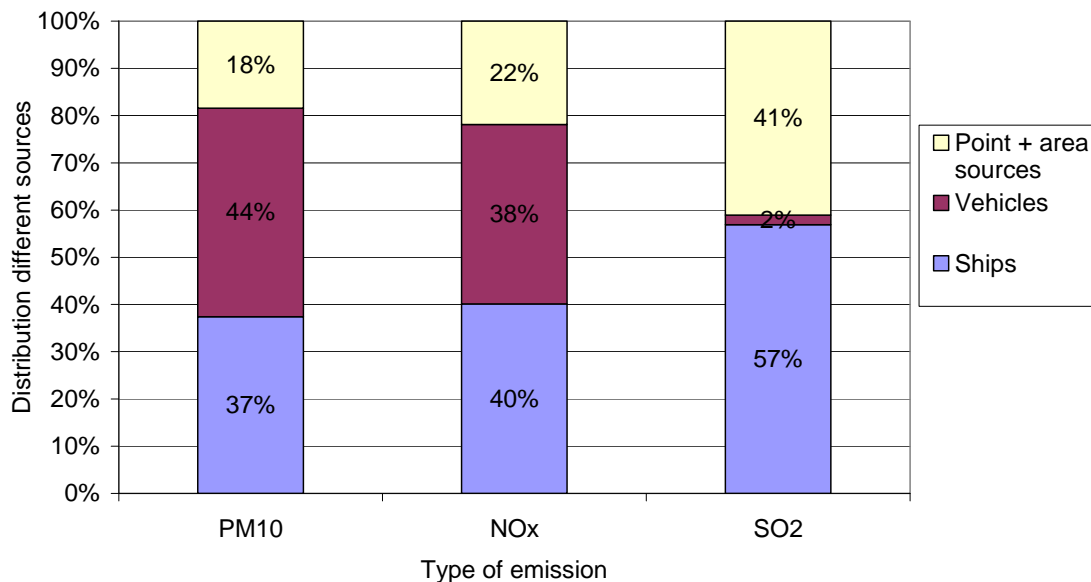


Figure 22. Percentage distribution of emissions from the different sources.

In Figure 23 a comparison has been done between the NO<sub>x</sub> emissions used in the two different models and for each source type. The total emissions used in the TAPM model are a bit lower than that used for the modelling in Enviman even if the emissions from ships are somewhat higher.

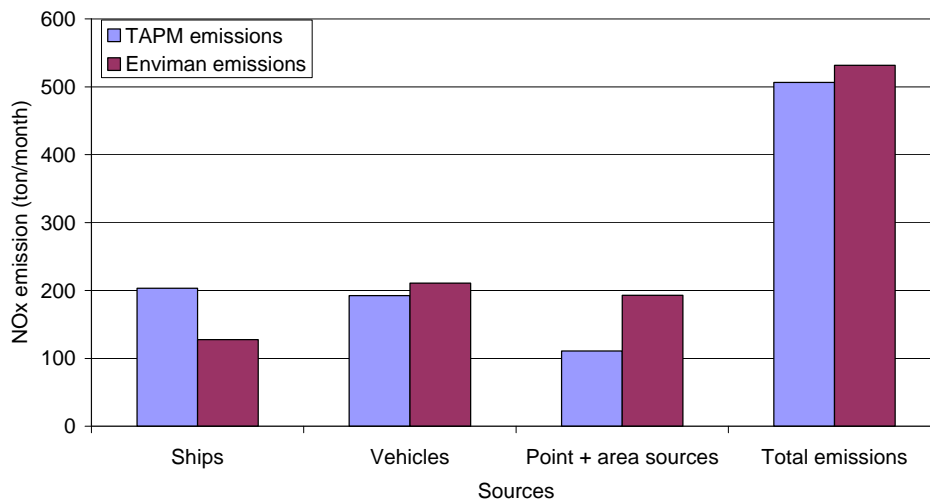


Figure 23. Comparison between the NO<sub>x</sub> emissions used for the TAPM and the Enviman modelling respectively.

## 6.2 Emission trends

The emission trends for the Gothenburg region for vehicles and ships are presented in Figure 24. According to the figure, the road traffic emissions have slowly decreased from 1998 to 2007. However, while the ship emissions were lower in 2004 they had increased again by 2007.

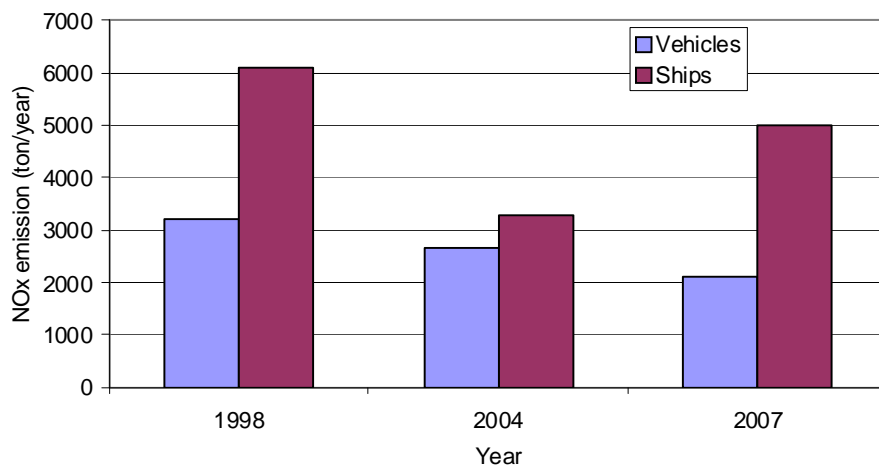


Figure 24. Emission trends for NO<sub>x</sub> in Gothenburg (from Environmental agency of Gothenburg).

## 7 Tunnel study

Measurements of air pollutants in road tunnels are often used to derive emission factors for aggregated car fleets. According to the mass-conservation law, the difference between concentration of a species in tunnel inflow and outflow air  $\Delta c_i$  (in g/m<sup>3</sup>) multiplied by ventilation flow (also air change rate) of the tunnel  $ACR$  (m<sup>3</sup>/s) is equal to the mass of the species emitted in the tunnel  $m_i$  (g) ( $m_i = \Delta c_i \times ACR$ ). When dividing this mass by length of the tunnel  $L$  (km) and the traffic flow  $f_i$  (vehicles/s) an emission factor  $Ef$  per vehicle-meter (g/vkm) ( $Ef = m_i \times L \times f_i$ ) is obtained. By further analysis of correlation of the concentration data with composition, speed and fluency of the traffic flow, one can obtain more specific emission factors such as those for mean passenger and heavy-duty vehicles (Sjödín et al. 2000, Rodler et al., 2005). This approach assumes that the species is not deposited or transformed by chemical processes on the timescale of air exchange in tunnel through ventilation.

The tunnel measurements also give information about distribution of oxides of nitrogen within the emitted NO<sub>x</sub> total. However, this partition can not be assumed as constant and it is also necessary to take into account chemical processes taking place in the air package during its passage through the tunnel. The car NO<sub>x</sub> emissions consist to the larger part of NO and to a smaller part of NO<sub>2</sub>. Part of the emitted NO will in a fast-rate react with ozone infiltrating into the tunnel (R1, see Chapter 1) and this reaction increases the NO<sub>2</sub>/NO<sub>x</sub> ratio. Considering only reaction R1, the NO<sub>2</sub> concentration originating from primary emission from the vehicles in the tunnel can be calculated accordingly:

$$[\text{NO}_2]_{\text{primary}} = [\text{NO}_2]_{\text{tunnel}} - [\text{NO}_2]_{\text{entering}} \quad \text{R6}$$

$$[\text{NO}_2]_{\text{entering}} = [\text{NO}_2]_{\text{background}} + [\text{O}_3]_{\text{background}} \quad \text{R7}$$

The primary emitted NO can be calculated from:

$$[\text{NO}]_{\text{primary}} = [\text{NO}]_{\text{tunnel}} - [\text{NO}]_{\text{entering}} + [\text{NO}]_{\text{oxidized}} \quad \text{R8}$$

$$[\text{NO}]_{\text{oxidized}} = [\text{O}_3]_{\text{background}} \quad \text{R9}$$

The slope of a plot NO<sub>2</sub> (primary) against NO (primary) gives the partition NO/NO<sub>2</sub> in the primary emission.

However, other processes such as gas-phase and surface chemical reactions and dry deposition can affect the NO<sub>2</sub>/NO<sub>x</sub> ratios under conditions of tunnel measurements (compare with Figure 10). In the lack of sunlight, the processes decreasing the NO<sub>2</sub>/NO<sub>x</sub> ratios are those that are also main NO<sub>x</sub> sinks: NO<sub>2</sub> dry deposition, the gas-phase oxidation of NO<sub>2</sub> by the OH radical (R4) and the heterogeneous HONO formation (R5). HONO affects our understanding of NO<sub>2</sub>/NO<sub>x</sub> distribution also indirectly; when using the chemiluminescence technique, HONO is measured as NO<sub>2</sub>. Mixing ratios of HONO measured in tunnels were as high as 10 – 50 ppb (this study, Kurtenbach et al., 2001) and hence understanding of the role of HONO in emissions and conversion of oxides of nitrogen is important and needs to be improved.

## 7.1 Measurements

### 7.1.1 Early measurements

In order to investigate historical development of the NO<sub>2</sub>/NO<sub>x</sub> partition in car exhaust gas one can look at earlier studies that included roadside and tunnel measurements. Figure 25 and Figure 26 show plots of NO<sub>2</sub> against NO<sub>x</sub> measured in 1982 at a roadside under low mixing conditions. Since there are no ozone measurements for this period, the slope of the regression lines will represent the primary-emitted NO<sub>2</sub> fraction instead of the  $[\text{NO}_2]_{\text{primary}}$  to  $[\text{NO}_x]_{\text{primary}}$ . This slope is an upper limit of the partitioning of the primary NO<sub>x</sub> emissions from equations R6 – R9. Considering the high level of NO<sub>x</sub> concentrations in the plots, and the fact that the measurements were performed in December when photochemical activity is very low, the effect of ozone titration of the primary emissions is probably unimportant. The slopes of the plots indicate NO<sub>2</sub>/NO<sub>x</sub> partitioning of 4 - 6 %.

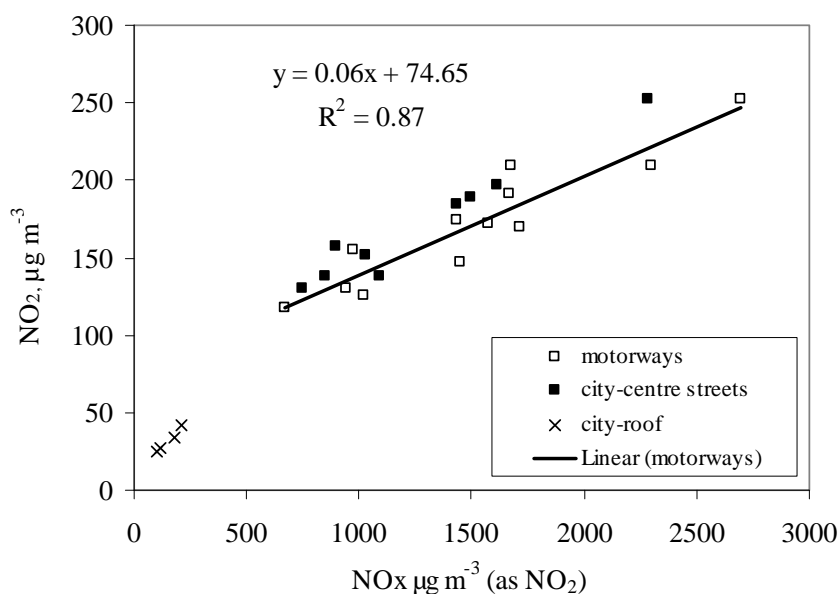


Figure 25. Measurements along roads before a temperature inversion 1982-12-03.



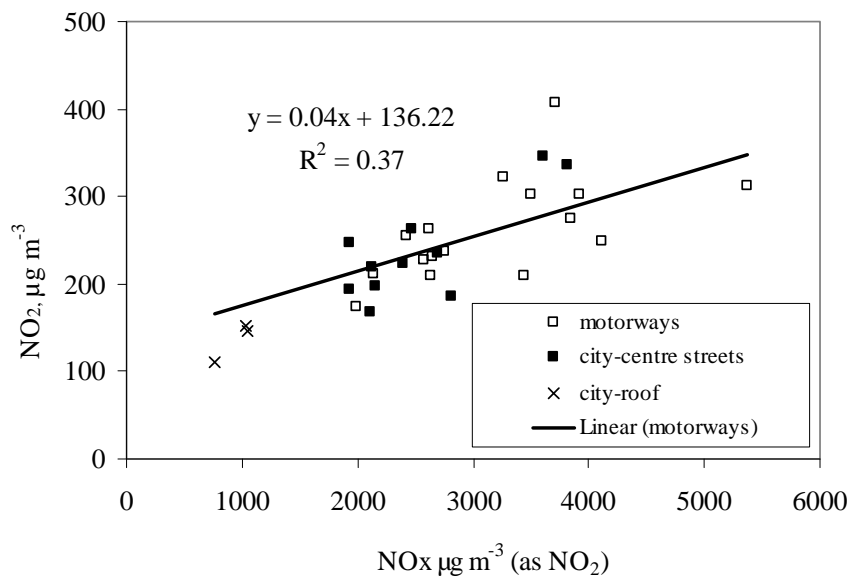


Figure 26. Measurements along roads during a temperature inversion 1982-12-13.

From the results of roadside measurements of exhaust-gas composition of individual vehicles performed in 1994, Sjödin et al. (1998) concluded that the NO<sub>2</sub>/NO<sub>x</sub> ratio clearly increased with decreasing speed, amounting to an increase of about 7% at speeds below 20 km/h compared to about 4% at speeds around 50 km/h. This was consistent with an earlier study on the speed dependence of the NO<sub>2</sub>/NO<sub>x</sub> fraction in vehicle exhaust by Lenner (1987). In 1994 and earlier there were probably only few cars equipped with catalytic converters (which became compulsory on all cars sold in Sweden starting with 1989 model). Our conclusion from the early data is that the NO<sub>2</sub>/NO<sub>x</sub> partition by the end of the 1980s and beginning of the 1990s was around 4-6%.

### 7.1.2 Measurements in a long road tunnel

To obtain a recent characterization of road traffic exhaust gas NO<sub>2</sub>/NO<sub>x</sub> partition for Gothenburg, measurements of NO, NO<sub>2</sub> and O<sub>3</sub> were taken in the middle of a 2-km-long road tunnel (the Lundby tunnel) between 2008-09-04 and 2008-09-15. Measurements of NO and NO<sub>2</sub> were taken with the ECO PHYSICS CLD 700 AL NO<sub>x</sub> analyser, the ozone concentrations were measured with an UV instrument, namely the Monitor Labs 8810. Measurements of NO, NO<sub>2</sub> and O<sub>3</sub> in the urban background were simultaneously performed at roof level in the city centre, some 3 km from the eastern end of the tunnel. Hourly mean concentrations were used in the calculations here.

The nitrogen dioxide concentrations originating from the primary emission ( $[\text{NO}_2]_{\text{primary}}$ ) as a function of the  $[\text{NO}_x]_{\text{primary}}$  (R6 – R9) are shown in Figure 27. The average NO<sub>2</sub>/NO<sub>x</sub> ratio of 13 % in the emission can be estimated from the slope of the linear regression line in the figure. If the average NO/NO<sub>x</sub> ratio is calculated for all hour-mean values exceeding 40 µg/m<sup>3</sup> NO<sub>2</sub> in Figure 27, an average of  $13 \pm 2$  % is obtained.

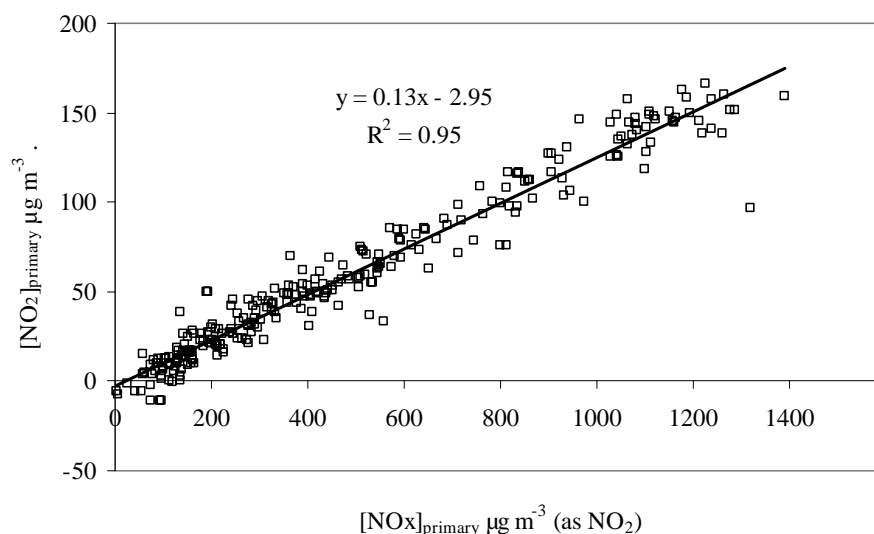


Figure 27. Calculated hourly NO<sub>2</sub> concentration in the tunnel originating from primary emission as a function of the calculated hourly NO concentration originating from primary emission.

### ***Nitrous acid concentrations***

On two occasions HNO<sub>2</sub> was measured in the Lundby tunnel using a filter pack. HNO<sub>2</sub> had earlier been measured using two carbonate-coated denuders in series (Ferm and Sjödin, 1985). The first one collects all HNO<sub>2</sub> plus a small fraction of NO<sub>2</sub> that is sorbed. The trapped amounts are identified as nitrite. The second denuder collects the small fraction of NO<sub>2</sub> that is sorbed. The denuders were made of glass and it was found that glass acted as a catalyst for reaction R1. It was pointed out by Febo (1986) that ozone could oxidize the nitrite formed in the denuder to nitrate. Instead of using glass denuders here, a filter pack made of polycarbonate was used to avoid catalysing R1. The first filter, which removes particulate matter was impregnated with sodium thiosulphate to remove ozone. The second and third filters were impregnated with potassium hydroxide and glycerine to trap HNO<sub>2</sub>. The HNO<sub>2</sub> concentration was calculated from the difference in the amount of nitrate in the second and the third filters.

As can be seen in Table 3, HNO<sub>2</sub> constituted a significant concentration compared to NO<sub>2</sub>. Thus, a fraction of the measured NO<sub>2</sub> could in fact be HNO<sub>2</sub>.

Table 3. HNO<sub>2</sub>, NO and NO<sub>2</sub> concentrations in the Lundby tunnel on two occasions.

Start	Stop	[HNO <sub>2</sub> ] ppb	[NO] ppb	[NO <sub>2</sub> ] ppb
2008-09-05 07:00	2008-09-05 11:00	13	246	77
2008-09-09 01:00	2008-09-09 05:00	11	114	32

## **7.2 Modelling**

To study the effects of all conversion and loss reactions of oxides of nitrogen as described in Chapter 1, a photochemical model of tunnel air mixing with the outside ambient air was constructed. Rates of the gas-phase reactions R1 – R4 are known from well-defined laboratory experiments (recommended values can be found in Atkinson et al., 1997, or Sander et al., 2006) and the effect of these reactions on the NO<sub>x</sub> chemistry can be simulated by a rather simple

photochemical model. Dry deposition rates of NO<sub>2</sub> are known; however, complex dynamic conditions in the tunnel introduce substantial uncertainties to quantification of this process. The rate of reaction R5, i.e. the heterogeneous formation of HONO from NO<sub>2</sub>, is also difficult to describe as the rate is not well determined and it varies with the composition and specific area of the surface of tunnel walls, its water content, and its coverage with other species etc. Kurtenbach et al. (2001) took measurements in the Kiesberg tunnel where they measured NO, NO<sub>2</sub>, HONO and CO<sub>2</sub> both under regular traffic conditions and in a closed tunnel pipe where they drove a vehicle under controlled conditions and added NO<sub>2</sub> along the tunnel wall. From observation of parallel NO<sub>2</sub> and HONO concentration decline, they derived a first-order NO<sub>2</sub> to HONO conversion rate  $k_{\text{hetR1}}^1 = (2.9 \pm 1.8) \times 10^{-3} \text{ min}^{-1}$ . This rate concurred with the findings of kinetic experiments performed on material scratched off the tunnel wall. Kurtenbach et al. (2001) also discussed heterogeneous conversion of NO<sub>2</sub> to HONO on fresh soot particles emitted in the tunnel. This process appeared to be important (ca. 30% of conversion on tunnel walls) if using the upper limit of the heterogeneous conversion rate published by Kalberer et al. (1999) and the particle surface area obtained from measurements in the tunnel. When using conversion rates from more recent publications of Amman et al. (2000) and Kleffmann et al. (1999), this process appeared to be unimportant. Kurtenbach et al. also used their measurements to derive direct HONO emissions. They found the HONO/NO<sub>x</sub> ratio in unprocessed exhaust to be 0.008 - a value consistent with earlier studies they reviewed in the same article.

### 7.2.1 Model description

In this study a model of a ventilated tunnel in order to study the role of the chemical and microphysical processes on NO<sub>2</sub>/NO<sub>x</sub> ratios in the tunnel was constructed. Two boxes of the model simulated air pollution outside the tunnel, one represented urban air, and the other a road just outside the tunnel. The third box simulated air inside the tunnel pipe (Figure 28). Mixing between the 'urban' and 'road' boxes simulated air pollution development in close vicinity of the road in order to obtain correct concentration of air entering the tunnel. Mixing between the 'road' and 'tunnel' boxes simulated self-ventilation of the tunnel.

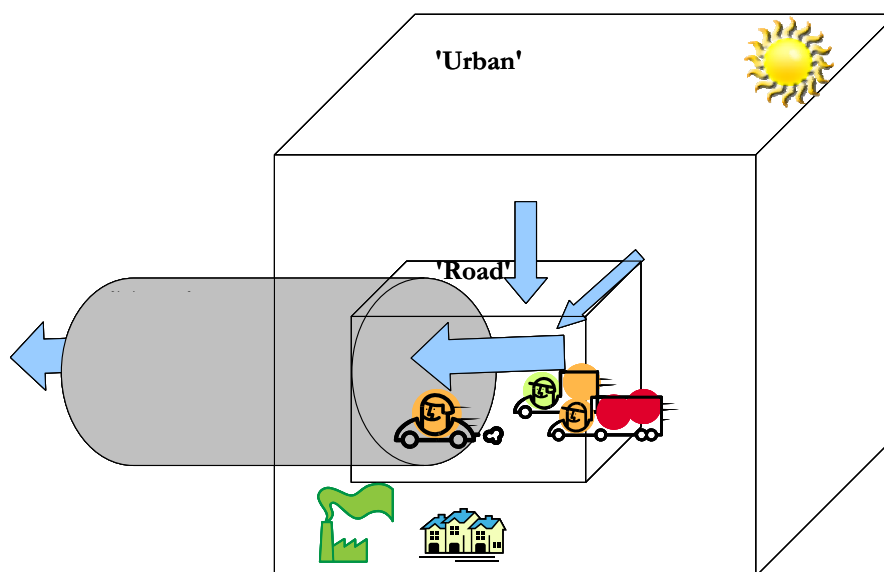


Figure 28. Schematic drawing of the tunnel box model.

In the outside boxes the chemistry was driven by solar radiation, and the photolytical rates in the model are a function of solar zenith angle. In the tunnel box the photolysis was switched off. The model included standard tropospheric chemistry of NO<sub>x</sub>, hydrogen species (HO<sub>x</sub>), Volatile Organic Compounds (VOC), CO and SO<sub>2</sub>. Heterogeneous reaction of NO<sub>2</sub> on a wet surface (R5) was included in the model using  $k_{\text{hetR1}}^1 = 3 \times 10^{-3} \text{ min}^{-1}$ . VOCs were treated as lumped species with Carbon Bond Mechanism IV (Gerry et al., 1989). Emissions of CO, NO, NO<sub>2</sub>, VOC, HONO were introduced to the model boxes using mean emissions of Gothenburg city in the urban box and same road emissions in the road and tunnel boxes. The dry deposition in the outside boxes was introduced by dry deposition rates corresponding to terrestrial surfaces. A mixing height of 1000 m and 50 m was chosen for the urban and road boxes respectively. In the tunnel the deposition was increased taking into account the surface/volume ratio of the tunnel. The air exchange rate of the tunnel was not measured at the time of the measurement campaign. The flow conditions had been, however, investigated thoroughly in another campaign and Figure 29 shows the wind speeds published in Rodler et al., 2005. Based on the measured wind speeds, the exchange rates of the tunnel were chosen as 10 min for high-traffic conditions and 30 min for low-traffic conditions (this corresponds to wind speeds ca. 3 and 1 m/s respectively).

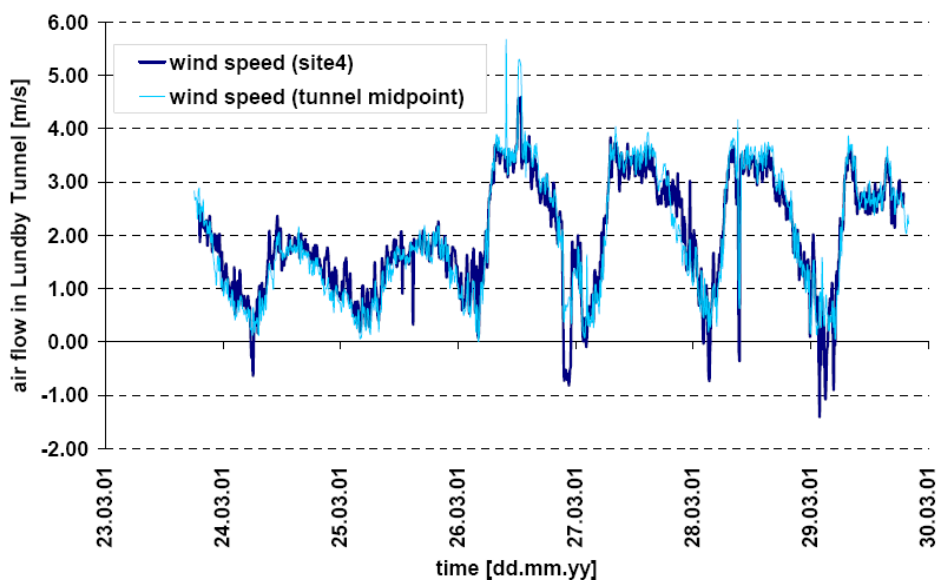


Figure 29. Air velocity measured with FLOWSIC at two sites for time intervals of 10 minutes.

## 7.2.2 Modelling results

A set of model simulations with varying strengths of emission source and ventilation rate was performed to investigate the role of chemistry and deposition on measured NO<sub>2</sub>/NO<sub>x</sub> ratios. The initial concentrations in the model corresponded to the conditions during the measurement campaign. Each simulation was performed for a 2-day period. On the second day, an extensive ozone formation due to accumulation of emissions was simulated in the 'urban' model box. This variability within each simulation enabled the study of the sensitivity of the processes to the ozone chemistry. Table 4 gives an overview of the simulations performed. Figure 30 shows the development of NO<sub>x</sub> and ozone concentrations in the 'urban' model box.

Table 4. Overview of the model simulations. ACR is the time-change rate of the tunnel. The Background category emissions are emissions to the 'Urban' model box, The Road category details emissions to the 'Road' and 'Tunnel' boxes. The NO<sub>2</sub>/NO<sub>x</sub> ratio in each simulation is the same for all three boxes.

Model simulation	ACR (min)	NO <sub>x</sub> emissions		NO <sub>2</sub> /NO <sub>x</sub>
		Background tonne/(year×km <sup>2</sup> )	Road tonne/(year*km)	
T1	10	11.4	4.15	0.13
T2	10	11.4	1.38	0.13
T3	30	11.4	4.15	0.13
T4	30	11.4	1.38	0.13

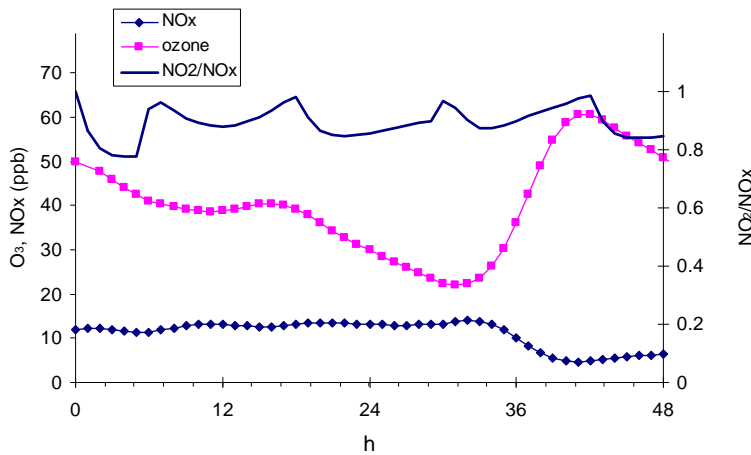


Figure 30. Ozone and NO<sub>2</sub> mixing ratios in the 'urban' model box and the corresponding NO<sub>2</sub>/NO<sub>x</sub> ratios. These background mixing ratios are the same for all model simulations. Time on the x-axis is time after model initialisation.

The results of the model show that the NO<sub>2</sub> removal processes indeed affect the NO<sub>2</sub>/NO<sub>x</sub> ratios. Figure 31 shows a plot of the NO<sub>2</sub>/NO<sub>x</sub> ratios in the 'Tunnel' box against the background ozone concentrations. We can see that at high ventilation rates (T1, T2) the NO<sub>2</sub>/NO<sub>x</sub> ratios are increased through titration of NO by the infiltrating ozone (R1). However, at lower ventilation rates the deposition processes decrease the initial ratio, sometimes below the emission ratio (0.13) by more than 30% (to ca. 0.08).

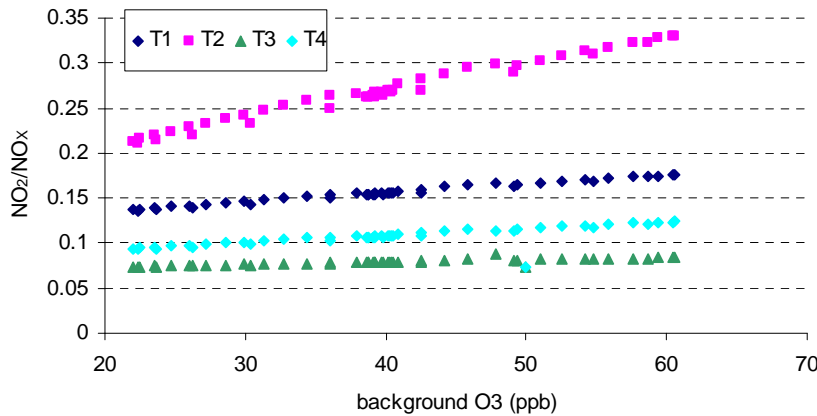


Figure 31. NO<sub>2</sub>/NO<sub>x</sub> ratios in the tunnel box plotted against ozone mixing ratios in the 'urban' model box for the 4 different model simulations.

Figure 32 shows what processes had the largest impact on changes in the NO<sub>2</sub>/NO<sub>x</sub> ratios in the ‘Tunnel’ box in the model simulations. The two most extreme cases, simulations T2 and T3 are shown. T2 was a fast-ventilation, low-emission case where R1 substantially increased the NO<sub>2</sub>/NO<sub>x</sub> ratios; however the NO<sub>2</sub> deposition was still significant (Figure 32a). T3 was a slow-ventilation, high-emission case where ozone titration did not substantially affect the NO<sub>2</sub>/NO<sub>x</sub> ratios but where both the NO<sub>2</sub> deposition and the HONO titration played a significant role. It can also be seen that in T3 HONO formation was important.

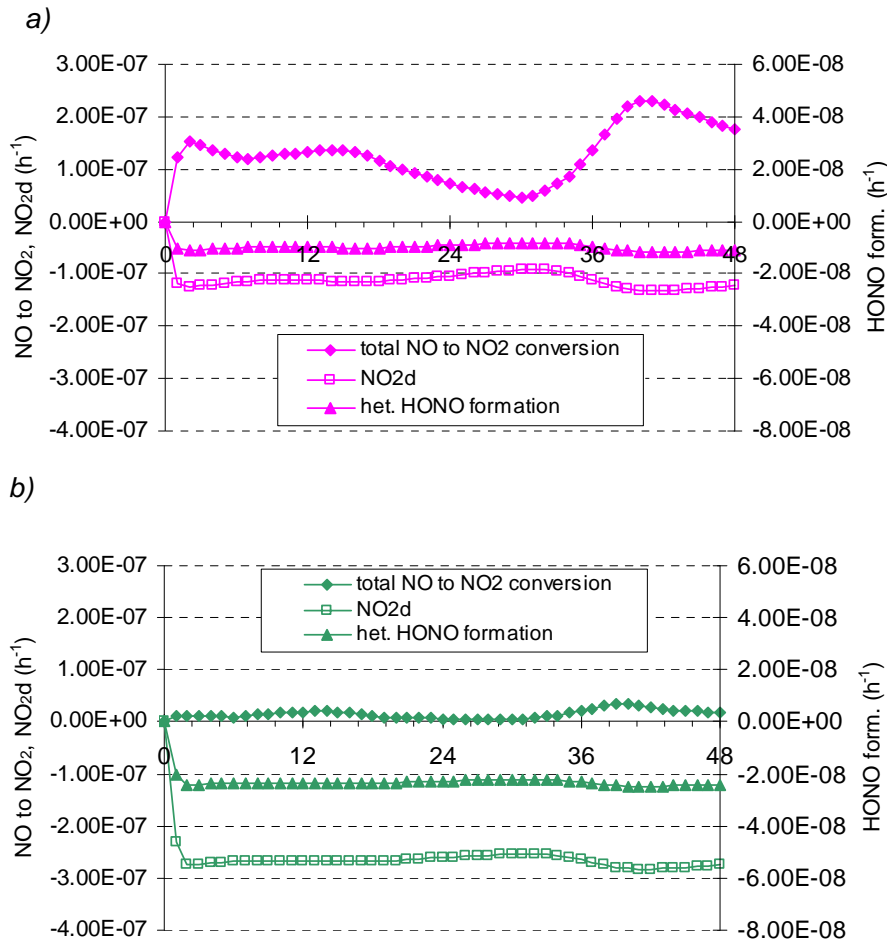


Figure 32. Chemical and microphysical processes affecting the NO<sub>2</sub>/NO<sub>x</sub> ratios in the tunnel. a) – simulation T2 (= fast ventilation, low emissions), and b) – simulation T3 (= slow ventilation, high emissions). The units were in mixing ratio/h, i.e. 1.00E-9 corresponded to 1 ppb/h vs. time (h). Observe that the HONO formation is on different axis with scale 1/5 of the primary y-axes.

Mixing ratios of HONO simulated by the model in the tunnel were in the order of 5-30 ppb, consistent with the mixing ratios presented in Table 3. These values were also consistent with the measurements of Kurtenbach et al. (2001) which were a result of using a similar description of the HONO processes in our model. Figure 33 shows the mixing ratios of HONO obtained from the four model simulations.

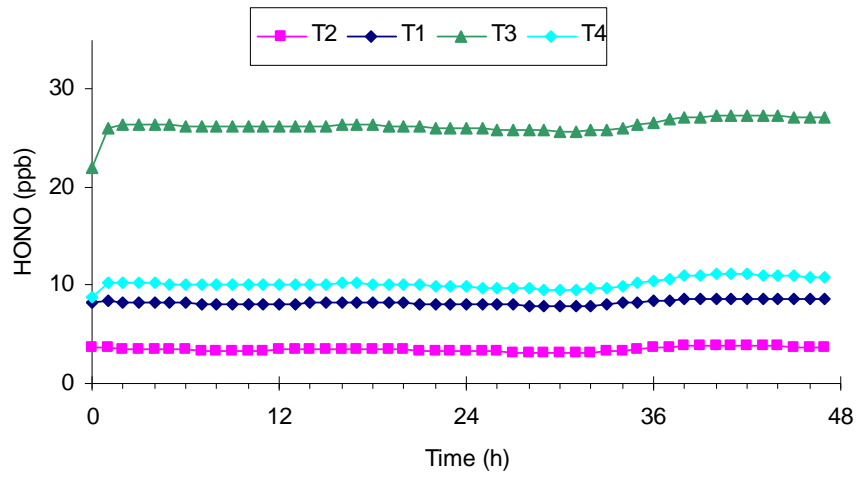
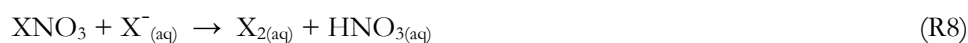
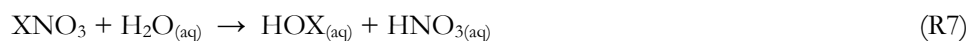


Figure 33. Mixing ratios of HONO simulated by model simulations T1 – T4.

## 8 Ship plume chemistry

Emissions from shipping are injected into the atmosphere in the form of coherent plumes. The chemical transformation of species in the plume is a non-linear process important both for formation of the secondary species, such as ozone and secondary NO<sub>2</sub>, and for removal of primary and secondary air pollutants from the atmosphere. Besides pollutant concentrations in the initial plume, there is also present the sea-salt aerosols, that readily affect chemical transformations in the plume, and which are characteristic for shipping emissions. Chemistry in complex meteorological air pollution models is in most cases kept simple in order to reduce their computational expenses. The simplifications are usually done through parameterisation of complex reaction pathways that are developed and tuned for land sources. As shipping is an significant source of NO<sub>x</sub> in coastal areas, it is of importance to investigate specificities of chemical conversions of emissions in more detail.

Davis et al. (2001) proposed that, in the plume, the reaction of NO with HO<sub>2</sub> leads to enhanced OH mixing ratios and thus to an enhanced rate of the main sink reaction for NO<sub>x</sub> (R3). Additional chemical loss of NO<sub>x</sub> can be through PAN formation (Chen et al.; 2005), through night-time formation of NO<sub>3</sub> and N<sub>2</sub>O<sub>5</sub>, followed by their heterogeneous oxidation on aerosol (R4) (Song et al., 2003), and through NO<sub>2</sub> oxidation by halogen oxides yielding halogen nitrates:



X in the chemical formulas represents the halogens Cl and Br. Halogen sources are autocatalytic halogen activation mechanisms on sea-salt aerosol (Vogt et al., 1996). Chen et al. (2005) inferred from measurements in a ship plume and from photo-stationary calculations with a box model, a chemical NO<sub>x</sub> lifetime of about 2 hours, almost four times shorter than calculated for background air, and showed that 80% of the loss was due to R3 and a remainder due to PAN formation. In highly concentrated parts of the plume, and in cases when the plume is emitted to a NO<sub>x</sub> pre-polluted background with already enhanced OH levels (which is often the case for ship emissions released close to the centre of Gothenburg), reaction R3, being also a sink for OH, can cause OH depletion in the plume, which can lead to increased NO<sub>x</sub> lifetime in the plume.

### 8.1 Plume-model description

The model for multiphase chemical reactions of ship plumes in the marine or urban boundary layers is based on the box Model Of Chemistry Considering Aerosols (MOCCA). Model results were published for the polluted marine boundary layer (MBL) (Sander et al., 1996) as well as for the remote MBL (Vogt et al., 1996, Pszeny et al, 2004). The chemical mechanism considers reactions both in the gas phase, in deliquesced sea salt and sulphate aerosols and on soot and dust particles. Photochemical reaction rates vary as a function of solar declination. In addition to the standard tropospheric HO<sub>x</sub>, CH<sub>4</sub>, and NO<sub>x</sub> chemistry, the reaction mechanism includes S, Cl, Br, and I compounds. Further, this version evaluates chemical processes involving different aerosol size fractions. The particle population is partitioned into eight mono-dispersed size bins with median diameters equal to the corresponding size interval of the modelled continuous distribution. The model can simulate conditions from the marine boundary layer to the lower stratosphere.



The original box version of the model has been extended to be able to perform plume simulations. It is possible to simulate multiple boxes with mixing. The plume mixing is described by the Gaussian approximation (Konopka, 1995, Schumann et al., 1995):

$$\sigma_h^2 = \frac{2}{3}s^2D_v\Delta t^3 + (2sD_s + s^2\sigma_{v0}^2)\Delta t^2 + 2(s\sigma_{s0} + D_h)\Delta t + \sigma_{h0}^2 \quad (\text{E1})$$

$$\sigma_s^2 = sD_v\Delta t^2 + (2D_s + s\sigma_{v0}^2)\Delta t + \sigma_{s0} \quad (\text{E2})$$

$$\sigma_v^2 = 2D_v\Delta t + \sigma_{v0}^2 \quad (\text{E3})$$

where  $\sigma_h$ ,  $\sigma_v$ , and  $\sigma_s$  are the horizontal, vertical and skewed standard deviations, respectively,  $\Delta t$  is the time from the beginning of the dispersion regime,  $D_h$ ,  $D_v$ , and  $D_s$  are the horizontal, vertical and skewed diffusion coefficients, and  $s$  is shear perpendicular to the plume main axes. The chemistry scheme of the model was extended by the CB-IV mechanism for hydrocarbon reactions (Gerry et al., 1989) and it can be chosen as an option in the model. The chemistry scheme used by TAPM model was implemented into the ship plume model in order to evaluate its performance.

## 8.2 Results

The model simulations performed in this study showed results that were in concordance with earlier studies: the NO<sub>x</sub> lifetime was reduced in plume due to increase of OH mixing ratio by a factor of 1.5 on average during the first 12 hours after the plume release (factor 1.3 when the plume was released in the evening) and an additional small decrease of lifetime due to the NO<sub>3</sub> and N<sub>2</sub>O<sub>5</sub>.

To quantify the amount of species in the plume that were produced or destroyed through different reaction channels in an expanding plume, the mixing ratios and reaction rates need to be multiplied by the volume of the unit length of the plume. In this study the amount of substance in the plume reacting through each reaction pathway was integrated over the volume of the plume parcel and accumulated in a budget variable defined for this purpose in the model. The budget variable was defined also for the reactions in the background air parcel and was integrated over the same volume of the plume parcel, allowing distinguishing between the mass of species reacting in the background air and in the plume.

Figure 34 shows the difference between the NO<sub>x</sub> sinks in the plume and in the background (simulation B1). Panel *a* of the figure shows the individual reactions integrated over 1 hour and the dominant influence of the OH+NO<sub>2</sub> sink (R3) in the plume released during daytime. It also shows the increasing importance of the heterogeneous sink reactions on sea salt and sulphate aerosol in later stages of the plume. Panel *b* of the figure shows the difference between the NO<sub>x</sub> sinks for plume released in the evening. During the first night, the sinks are in this case dominated by heterogeneous reactions (R6-R8) and by the N<sub>2</sub>O<sub>5</sub> formation, followed by the OH+NO<sub>2</sub> sink the following day. Panel *c* of the figure shows the accumulated specific budget of the total NO<sub>x</sub> sinks, showing that 0.16 M of NO<sub>x</sub> emitted to the plume parcel was oxidized during the first 24 hours in both cases and that some additional NO<sub>x</sub>, above the mass oxidized in background, was oxidized in the plume during the late stage of plume development due to changes in oxidation capacity.

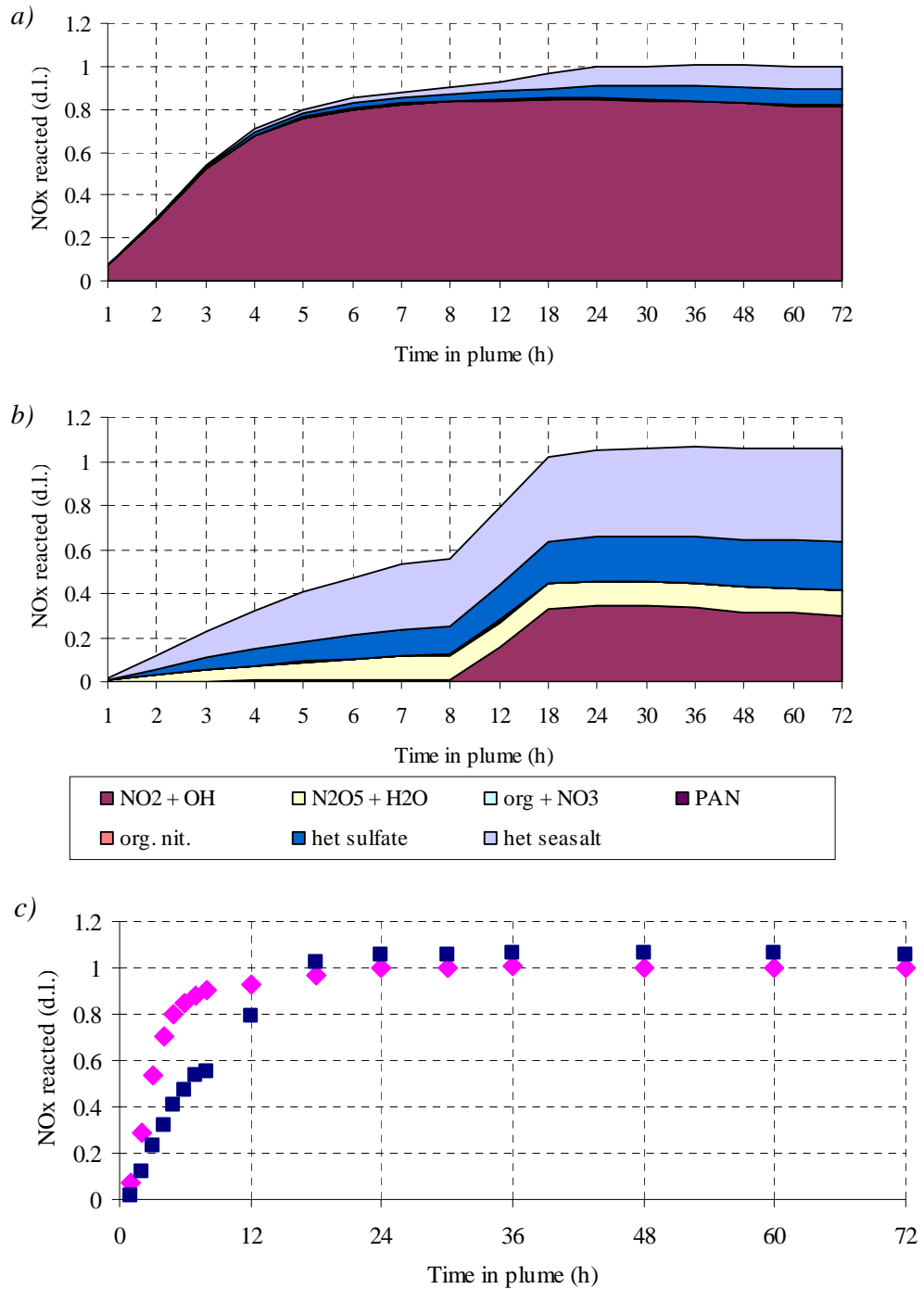


Figure 34. Sinks of oxides of nitrogen in a ship plume: The mass of NO<sub>x</sub> removed by the sink reactions in a unit length of the expanding plume was divided by the mass of NO<sub>x</sub> initially emitted into the unit length of the plume. The plots thus show the part of NO<sub>x</sub> removed from the plume. Plumes released at 12:00 and 20:00 are shown. Panel a) – Contribution of individual sink reactions to the sink of NO<sub>x</sub> in plume released at 12:00. The heterogeneous reactions include reactions of N<sub>2</sub>O<sub>5</sub>, BrNO<sub>3</sub> and ClNO<sub>3</sub>. Observe that the time axes are not linear. Panel b) –ditto but the plume was emitted at 20:00. Legend in Panel a) - applies also for this panel. Panel c) - Time evolution of the total relative NO<sub>x</sub> sink with linear time axes, cerise rhomb- plume at 12:00, dark blue square: plume at 20:00.

Performance of the TAPM chemistry on the ship plume was evaluated by comparison of two otherwise identical plume simulations, the first involving full MOCCA chemistry and the second the TAPM chemistry with 8 parameterized reactions for the  $\text{NO}_x$ -VOC-ozone chemistry. Both simulations calculated concentration development of two air parcels approaching Gothenburg from the sea, both gathering pollution from sources around the outer harbours and later the second one receiving emissions from the ship plume. Beyond that time, the air from the first air parcel is used for dilution of the second one. The simulations were performed for conditions simulated by the TAPM presented in Chapter 9. The ship plume was released at 12:00. Figure 35b shows that the difference between MOCCA and TAPM is small for the plume chemistry, with the MOCCA plume- $\text{NO}_2$  being higher by a few percent during the first hours and later, after the dusk, being lower than the TAPM plume. The background air parcels show quite close agreement during daylight hours but the  $\text{NO}_2$  sink is underestimated in TAPM during the dark, causing divergence of TAPM  $\text{NO}_2$  concentrations from the MOCCA scheme (Figure 35a). This is a result of missing  $\text{NO}_3$  chemistry that acts as a night sink for  $\text{NO}_2$  in the TAPM. The  $\text{NO}_3$  chemistry is also the reason for the relative decrease of the plume- $\text{NO}_2$  in MOCCA relatively to TAPM seen in Panel b) of the Figure 35.

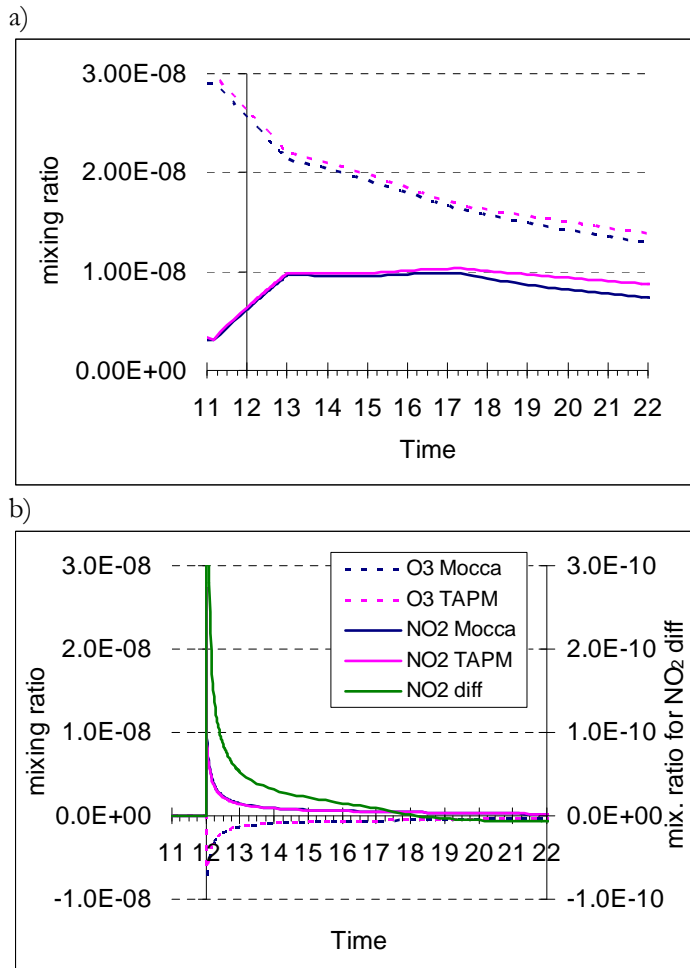


Figure 35. Development of mixing ratios of ozone and  $\text{NO}_2$  ( $1.0\text{E}-9 = 1\text{ppb}$ ) in the background air parcel passing Gothenburg (a) and the difference between the plume parcel and the background parcel in the same simulation (b) for the plume model with detailed chemistry (in blue) and with TAPM chemistry (in cerise). The difference between additional plume- $\text{NO}_2$  for the 2 chemical schemes is also shown (in green, note the different scale).

## 9 Dispersion modelling

### 9.1 The TAPM dispersion model

The local scale dispersion modelling in this project for Gothenburg was performed with two models, TAPM (see Appendix 1) and Enviman. Historically, Enviman is the model system that has been used by the Environmental Agency in Gothenburg. Nevertheless, TAPM has been widely used for various scales and purposes in Sweden. In this work mainly TAPM was used and Enviman was used for comparison.

The Air Pollution Model (TAPM model) has been used for the dispersion calculations of the Gothenburg area. The TAPM consists of two models, one meteorological and one dispersion model. TAPM was developed by the Australian CSIRO Atmospheric Research Division (Hurley et al, 2005). It is a 3D meteorological and chemical model for air pollution studies (see further Appendix 1).

### 9.2 The modelling

There is no emission database included within the TAPM model but it contains an external independent Access database as well as an external visualization tool. TAPM includes topography as well as land-use. On the basis of this, the model generates the meteorological parameters required for the dispersion modelling, such as temperature layering (inversions) and 3D-wind field, all based on daily synoptic (large scale) input data. As the calculations in TAPM are rather time consuming the grid resolution is usually kept coarse. Based on the synoptic input data, TAPM calculated the required meteorology on an hourly basis.

Enviman (Opsis 2000) is a complete modelling system that includes a detailed emissions database, a dispersion model and a visualization tool. Further, Enviman calculates the dispersion based on monitored meteorological input. The topography and land-use were not directly included in the calculations but some topographical effects may be captured by the meteorological measurements within the calculation area. Enviman uses a finer grid resolution for the results which may lead to a better description of, for example, dispersion along roads. For this study Enviman uses the "real weather" situations on an hourly basis.

In order to include long-distance transported air pollutants into the calculations, monitored hourly data of regional background concentrations for the parameters included in the study are used for the TAPM calculations. TAPM also includes chemistry such as NO/NO<sub>2</sub>, ozone, SO<sub>2</sub> and particle transformation. The result from Enviman was transformed to NO<sub>2</sub> from calculated NO<sub>x</sub> concentrations using the formula  $NO_2 = 11.27 * (NO_x^{0.44} - NO_x^{0.22}) - 3.64$  which is obtained based on monitoring data from Gothenburg (Gothenburg's Miljöförvaltning 2009). This formula also includes the long-distance transportation and the formula is based on the relationship between monitored NO<sub>x</sub> and NO<sub>2</sub> concentrations at Femman.

Both models predict hourly dispersion for the calculation area but TAPM also did it in 3D. In this work it is important to compare model results from TAPM with the results from Enviman since there was a long history of using Enviman in this area; thus, there is the possibility of checking that the transformed database for TAPM gives reasonable results regarding both the geographical

distribution and concentration levels. Further, since one purposes in this study is to analyse the role of shipping for the NO<sub>2</sub> concentrations in Gothenburg, it is crucial that the models include the chemical processes connected to the production of NO<sub>2</sub>. The simulations are performed for October 2008.

## 9.3 Results

### 9.3.1 Meteorological simulation with TAPM

In order to evaluate the dispersion modelling, comparisons were made between calculated and monitored meteorological and air pollution parameters. Figure 36 shows scatter plots comparing monitored and calculated meteorological parameters based on hourly data for February 2005. Similar data are also shown in a time series plot in Figure 37.

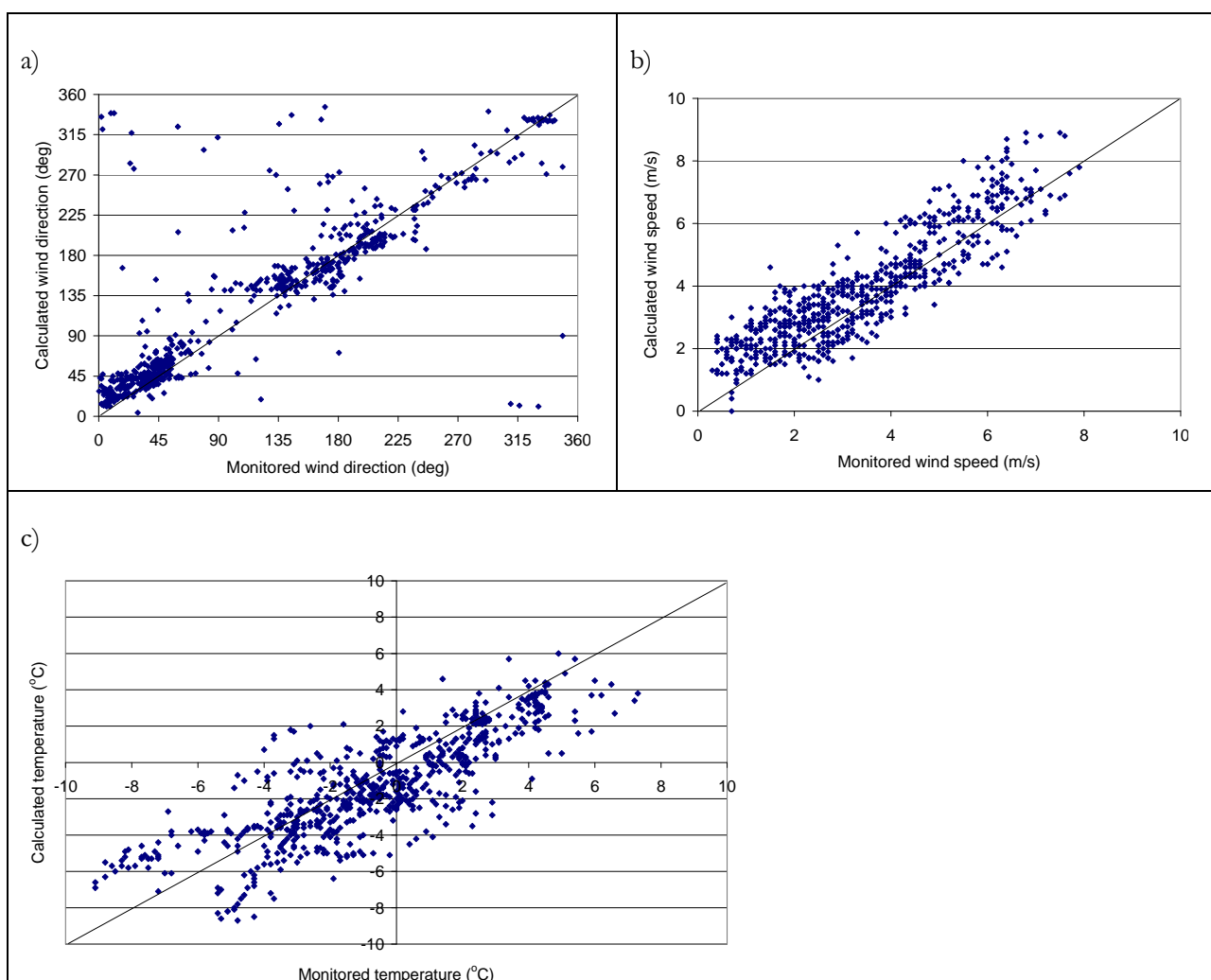


Figure 36. Comparison between calculated and monitored hourly data for February 2005 for the site Lejonet. Panel a) shows wind direction, b) wind speed, and c) temperature.

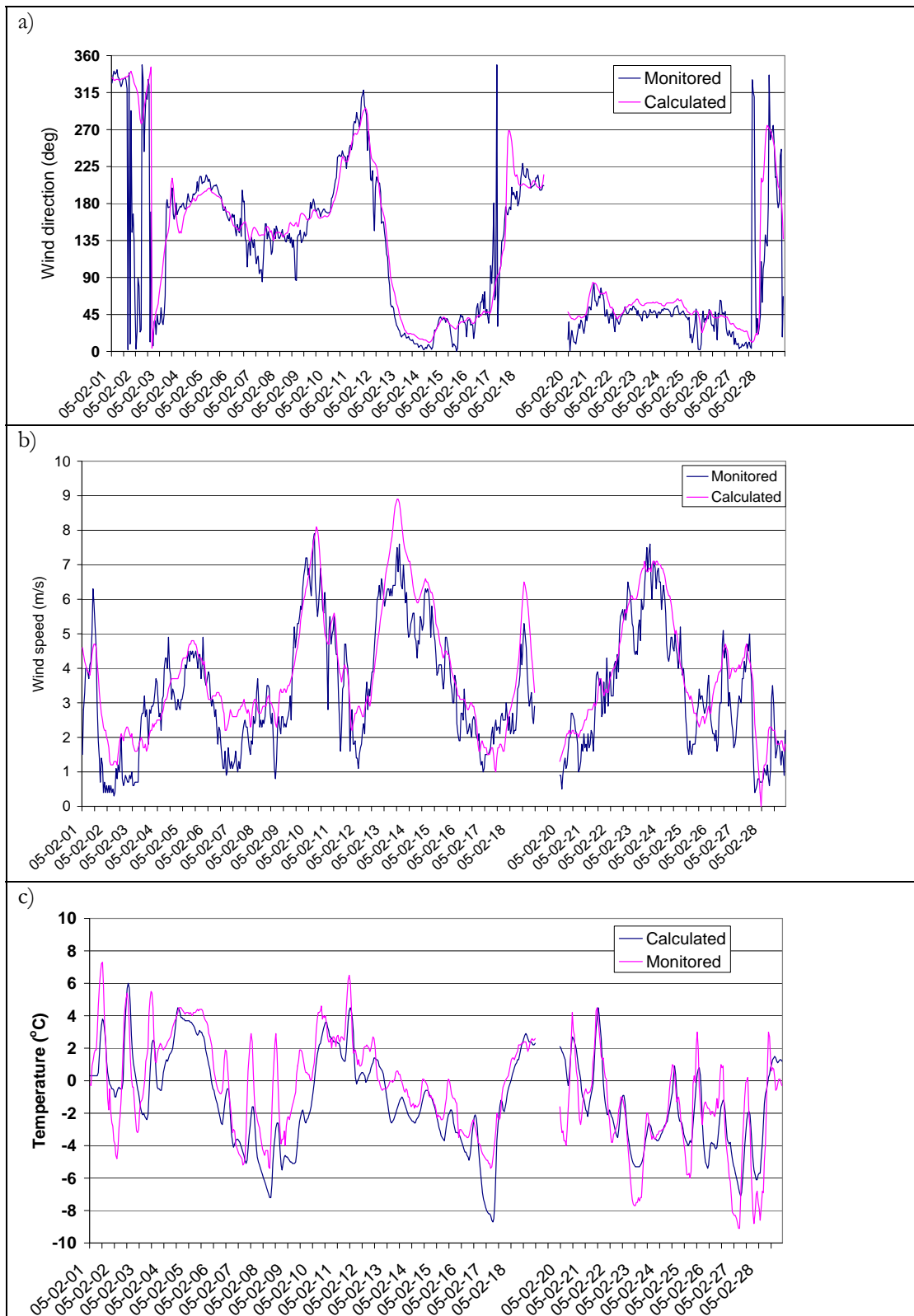


Figure 37. Comparison between calculated and monitored hourly data for February 2005 performed as time series data for the site Lejonet; Panel a) shows wind direction, b) wind speed, and c) temperature.

One commonly used method to show the dispersion conditions for air pollutants is the mixing height (z<sub>mix</sub> - height of the mixing layer) calculated with high time resolution. Within this parameter, both vertical and horizontal stability are included. However, the calculation of mixing height is difficult because vertical information about both wind speed and temperature are needed. This information is only available twice-a-day and only for a few sites in Sweden. The calculated mixing height had earlier been evaluated for rural conditions with available data at the airport outside Gothenburg (Haeger-Eugensson et al. 2002) with sufficient agreements. When the mixing height was low the dispersion was poor. According to these calculations there were both poor and effective dispersion conditions during the studied month. A simpler, but not as apparent, way to indicate the dispersion is the vertical temperature difference (for 2 - 10 m), which was monitored at the site Lejonet. Since the vertical temperatures could not be calculated for those heights with the TAPM model, the mixing height (Fig. 38) was used instead as a measure for the local dispersion at this site. A relationship was observed between the calculated mixing height and the monitored temperature decrease with height (Figure 39). Thus, this indicates that TAPM also could simulate local dispersion conditions within urban areas, which was even more difficult than for rural locations.

Normally, temperature decreases with height to various degrees depending on, among other things, humidity. For dry conditions the decrease is about 1 deg/100 m and for humid conditions it is less. In this case the normal decrease was between 0.25 and 0.5 degrees. Mixing heights below approximately 150-200 m were considered low in this area and occurred during inversion situations. During these occasions the temperature increased with height to various degrees depending on the strength of the inversion.

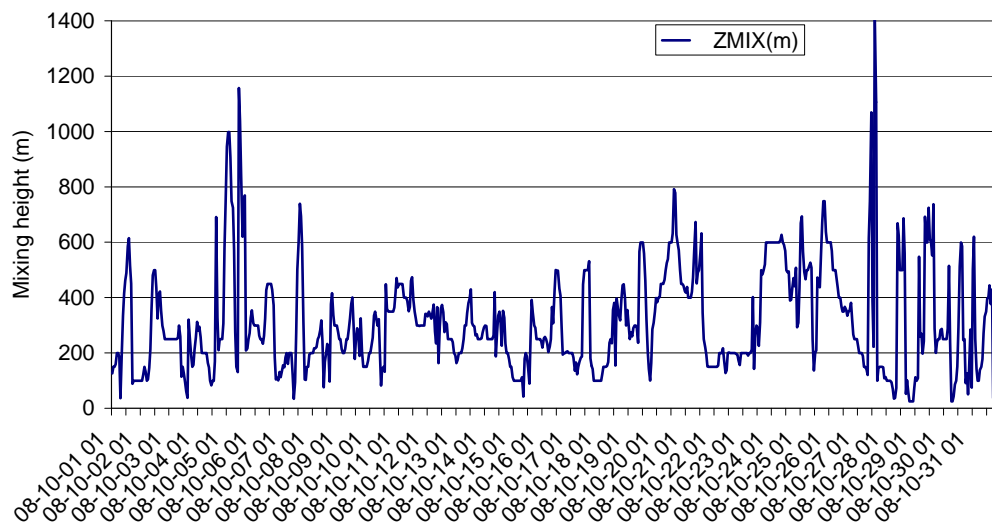


Figure 38. Calculated hourly mixing height data for February 2005 at the site Lejonet.

Apart from the instances with highly positive temperature differences in Figure 39 there was a linear decrease of the temperature difference with increasing mixing height (visible in the oval in the figure).

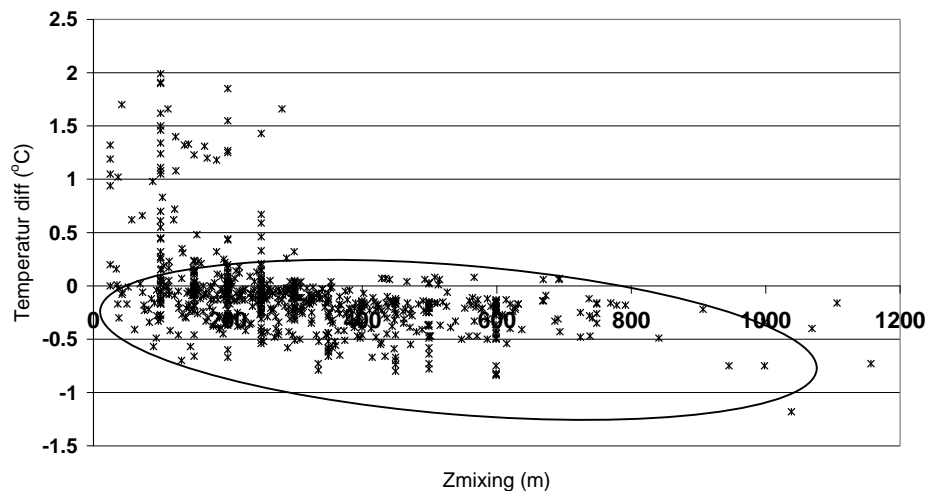


Figure 39. Comparison between calculated mixing height (height of the mixing layer) and monitored temperature decrease with height from 2- 46 m.

The results presented above show a very close agreement between calculated and monitored meteorological parameters. The calculated values captured different time scales due to both local and larger scale conditions. The TAPM model is therefore assumed to capture most of the meteorology which is crucial for giving realistic simulations of air pollution concentration in both local and mesoscales.

### 9.3.2 Dispersion calculations

As mentioned, besides using the TAPM model, the dispersion calculations were also carried out using Enviman. This modelling system is used by the local authorities and contains the emission database also used for TAPM.

#### 9.3.2.1 Calculations with TAPM

Using the previously described emission database (Chapter 4) as input to calculations with the TAPM dispersion model, the geographical distribution of ambient air concentrations for various parameters were obtained for the central part of Gothenburg. In Figure 40-Figure 43 the concentrations of NO<sub>2</sub>, NO<sub>x</sub>, SO<sub>2</sub> and O<sub>3</sub> are presented.



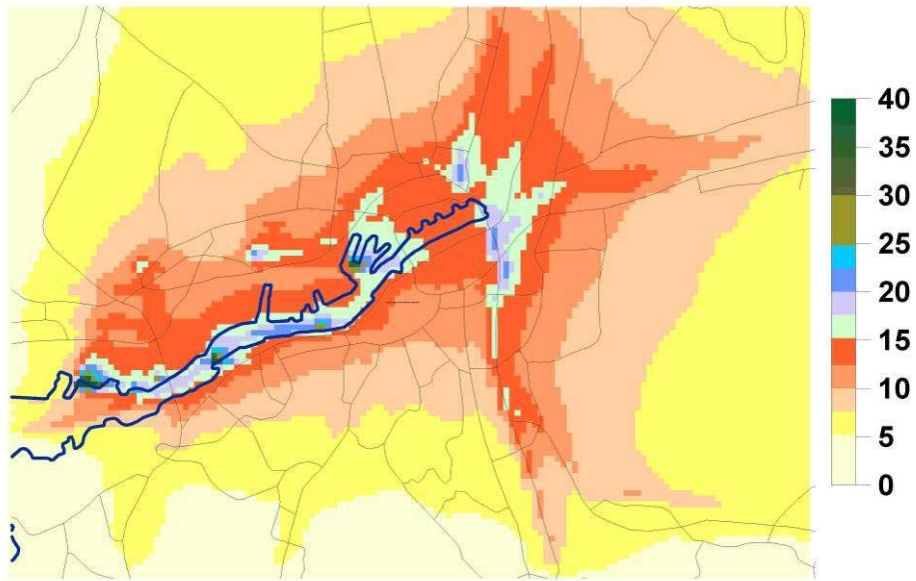


Figure 40. Total NO<sub>2</sub> concentration (□ g/m<sup>3</sup>) calculated with TAPM. The blue line indicates the main part of the harbour.

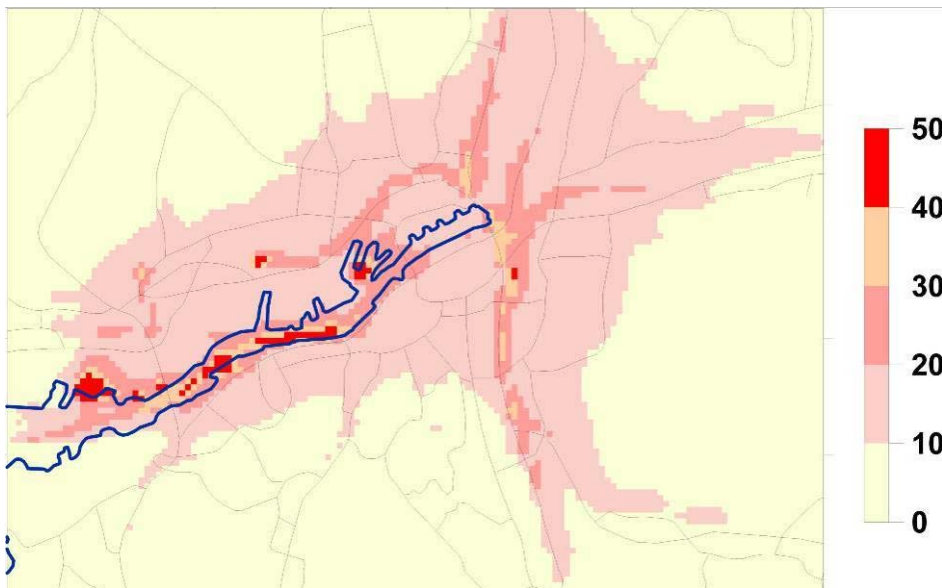


Figure 41. Total NO<sub>x</sub> concentration (µg/m<sup>3</sup>) calculated with TAPM. The blue line indicates the main part of the harbour.



Figure 42. Total SO<sub>2</sub> concentration (µg/m<sup>3</sup>) calculated with TAPM. The blue line indicates the main part of the harbour.

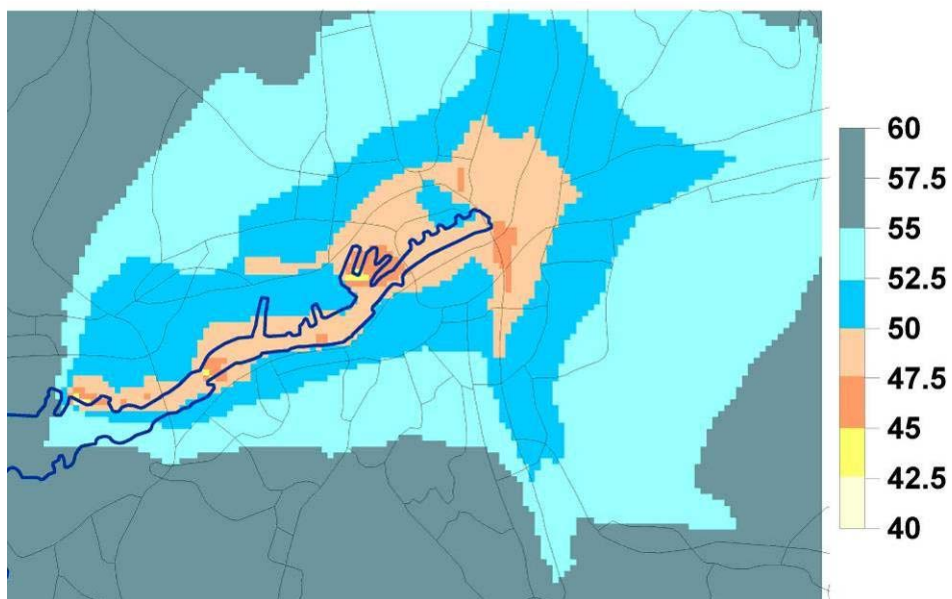


Figure 43. Total O<sub>3</sub> concentration (µg/m<sup>3</sup>) calculated with TAPM. The blue line indicates the main part of the harbour.

### 9.3.2.2 Calculations with Enviman

The calculations with Enviman, using the original database, for the Gothenburg area were performed for the same period as the calculations with TAPM. Maps showing concentrations of NO<sub>2</sub> and SO<sub>2</sub> are presented in Figure 44 and Figure 45, respectively.

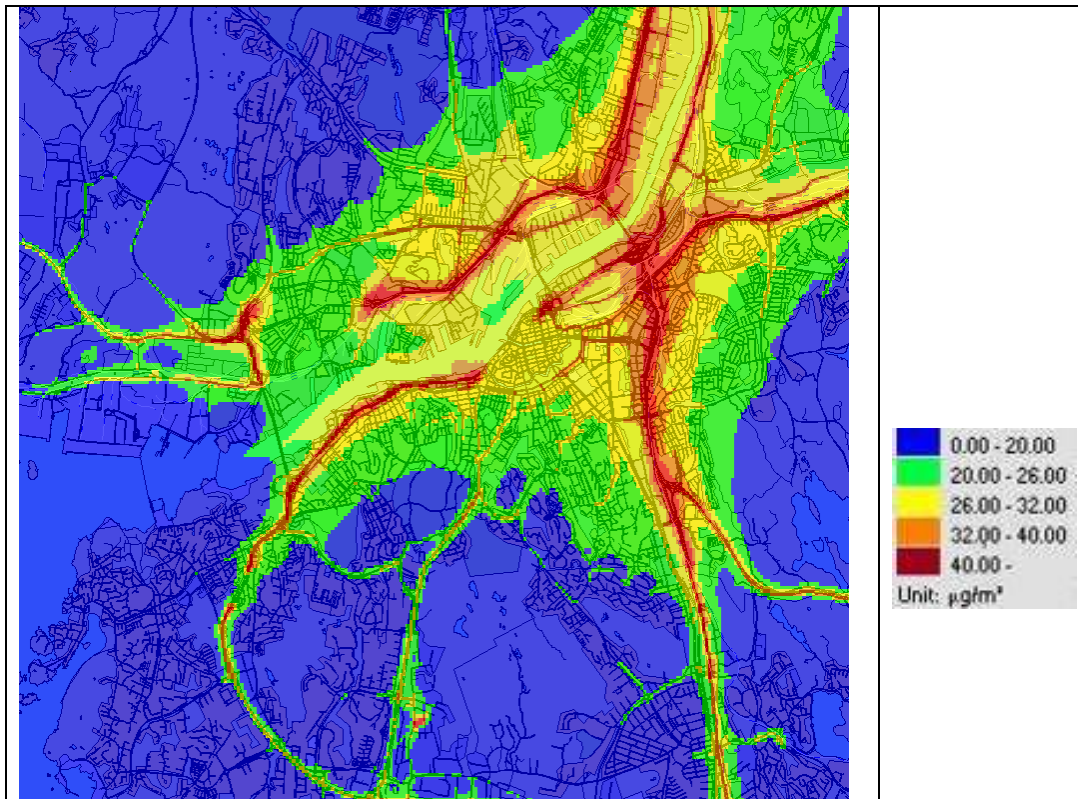


Figure 44. NO<sub>2</sub> concentrations (µg/m<sup>3</sup>) from traffic, ships and point sources calculated with Enviman.

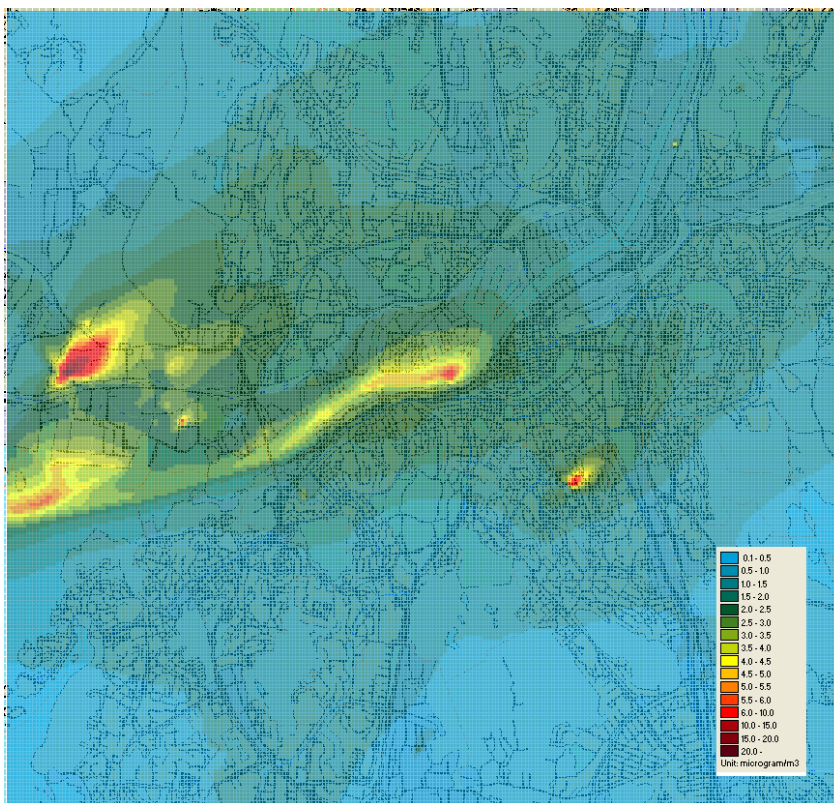


Figure 45. SO<sub>2</sub> concentrations (µg/m<sup>3</sup>) from traffic, ships and point sources calculated with Enviman.

### 9.3.3 Evaluation of air pollution calculations

In order to evaluate both the emissions data and model performance, some of the monitoring data presented in Table 5 were used. The location of the sites utilised is presented in Figure 46 and have been numbered according to Table 5.

Table 5. Name, numbering, coordinate and type of site used below.

Name of monitoring station	Number of monitoring station	Type of monitoring site	E-W coordinate	N-S coordinate
Amerikaskjulet	1	Passive sampling	1268983	6403869
Järntorget	2	Passive sampling	1270385	6403976
Kielterminalen	3	Passive sampling	1267985	6403245
Länsmansgården	4	Passive sampling	1266552	6406677
Masthuggskyrkan	5	Passive sampling	1269387	6403524
Suckarnas kaj	6	Passive sampling	1272319	6405829
Femman	7	Chemiluminescence	1271450	6404658
Lejonet	8	Chemiluminescence, meteorological	1272775	6405298

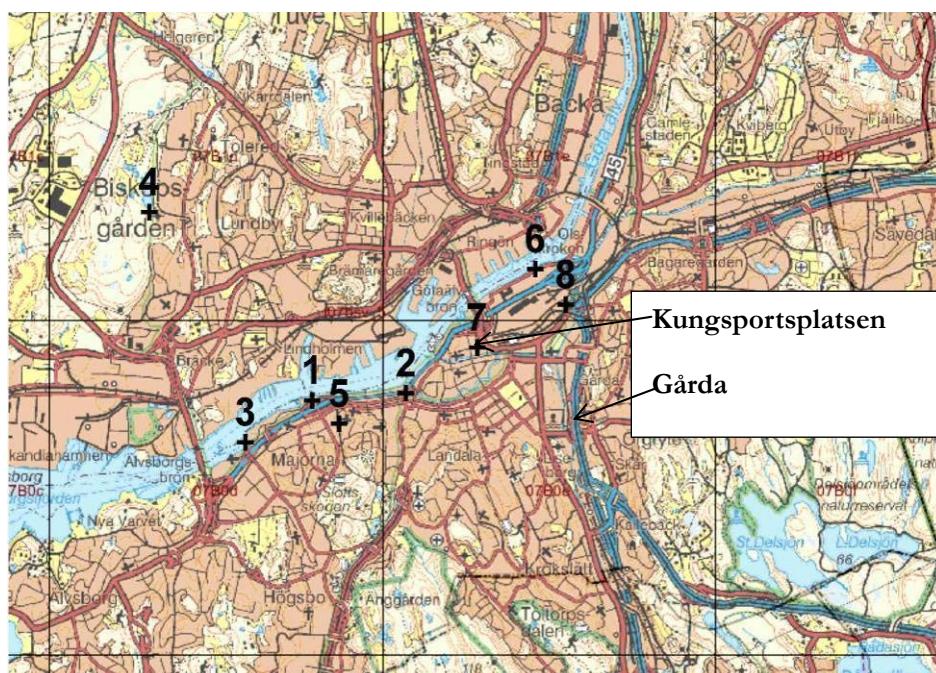


Figure 46. Map of the calculation area with the monitoring sites listed in Table 5.

An evaluation of the calculated (TAPM) air pollution concentrations was made by comparing calculated and monitored data of NO<sub>2</sub>, SO<sub>2</sub> and O<sub>3</sub> at sites 1 - 6 (Figure 47). To show if there was a general over- or under estimation, the ratios of calculated and monitored data were plotted for all sites (Figure 48).

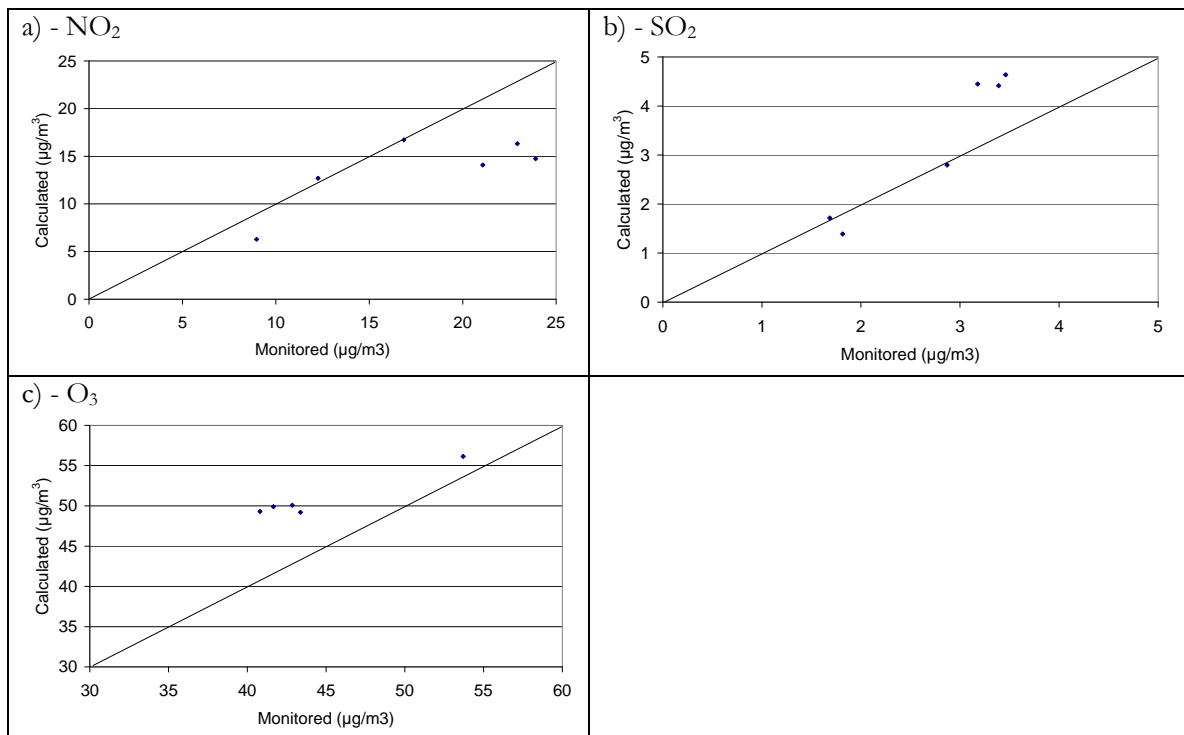


Figure 47. Comparison between calculated and monitored (see Chapter 5) a) NO<sub>2</sub>, b) SO<sub>2</sub> c) O<sub>3</sub>.

The results in Figure 47a show that the calculated NO<sub>2</sub> concentrations are about the same as the monitored concentrations at two of the sites and were underestimated by about 30% at four sites. In Figure 47b the comparison for SO<sub>2</sub> also shows a good agreement at two sites but these are different to the NO<sub>2</sub> sites where the differences were small. The calculated O<sub>3</sub> (Figure 47c) was, to varying degrees, overestimated at all sites, peaking at 20% over. The discrepancies between the different parameters and sites indicate that there was not a general under- or overestimation of either NO<sub>2</sub> or SO<sub>2</sub> emissions.

A comparison was also made between the calculated data and the continuously monitored air concentrations at the stationary site Femman (see Figure 47); these data were presented both as daily (Figure 48) and hourly means (Figure 50) of NO<sub>2</sub> concentrations. At this site the calculated data was in general underestimated by 25% compared to the monitored data. To compare the models, calculations were also made with Enviman and in Figure 49 a comparison is shown between the ratios of calculated/monitored concentrations from each of the models based on daily means. The result indicated that during most days both models showed similar trends even though TAPM more frequently underestimated the concentrations.

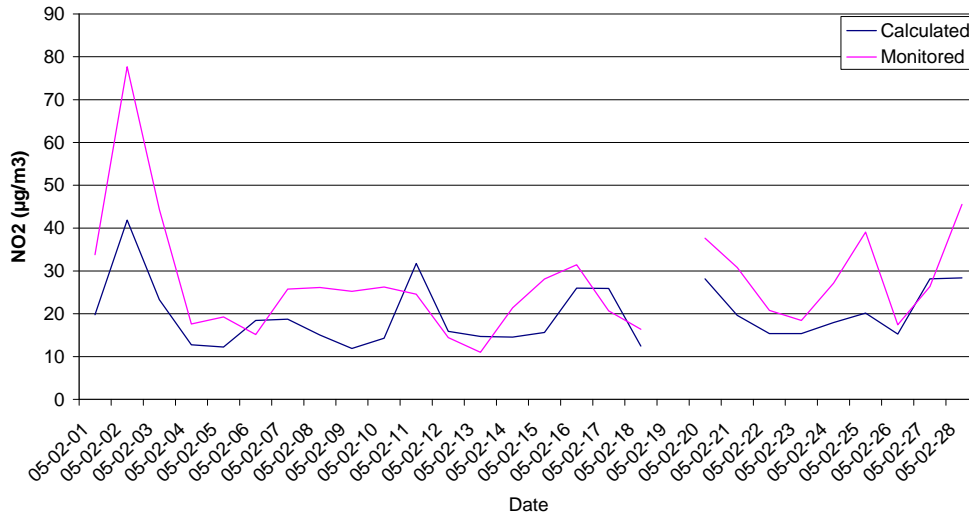


Figure 48. Daily mean NO<sub>2</sub> concentrations (µg/m<sup>3</sup>) at Femman calculated with TAPM.

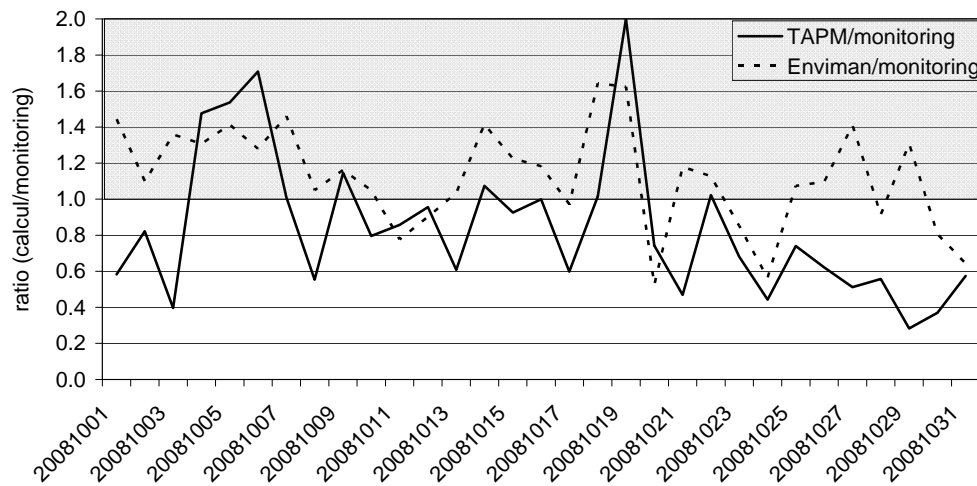


Figure 49. Comparison between the ratios of calculated and monitored concentrations of NO<sub>2</sub> from each model based on daily mean averages. In the shaded area of the figure, the calculated concentrations are overestimated compared to measurements.

In Figure 50 it is clear that the TAPM model capture also the hourly variations which are not only due to variations in emissions, but which also reflect the meteorological variations.

In Figure 52 and Figure 52 the ratios between calculated and monitored NO<sub>2</sub> concentrations are presented for both TAPM and Enviman calculations. Once again it can be noted that TAPM is underestimating the NO<sub>2</sub> concentration for many periods.

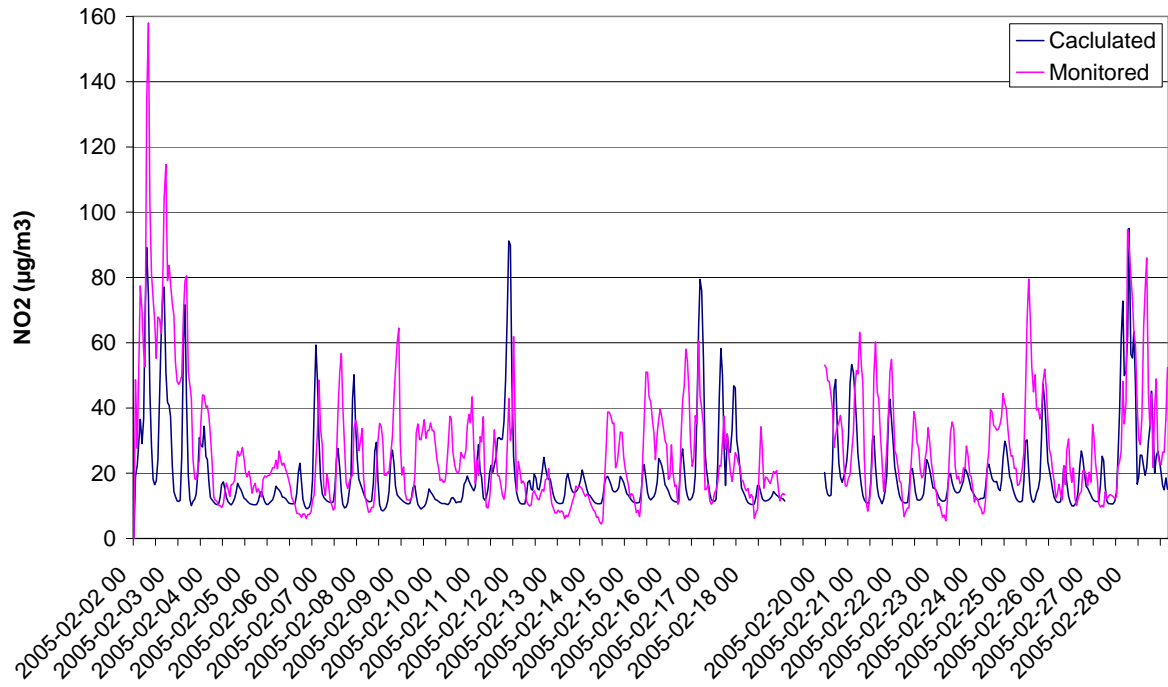


Figure 50. Comparison between measured and calculated (with TAPM) hourly means NO<sub>2</sub> concentrations (µg/m<sup>3</sup>) at Femman.

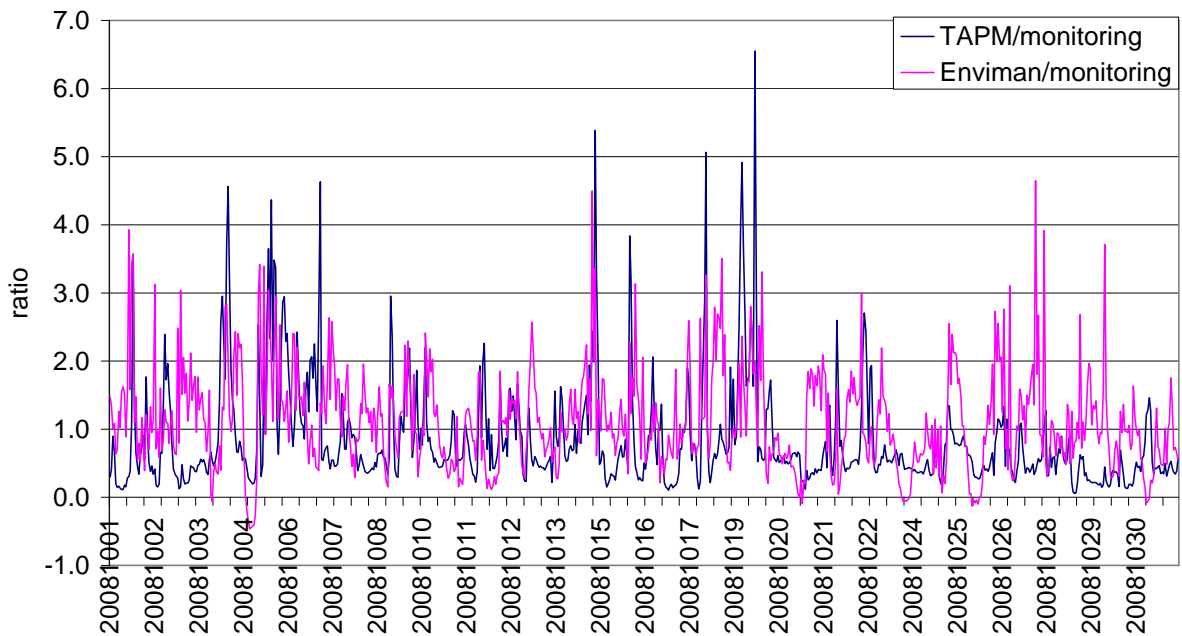


Figure 51. Comparison between the ratios of calculated and monitored concentrations of NO<sub>2</sub> from the two models based on hourly mean averages. Values > 1 indicate overestimated calculated concentrations compared to measurements.

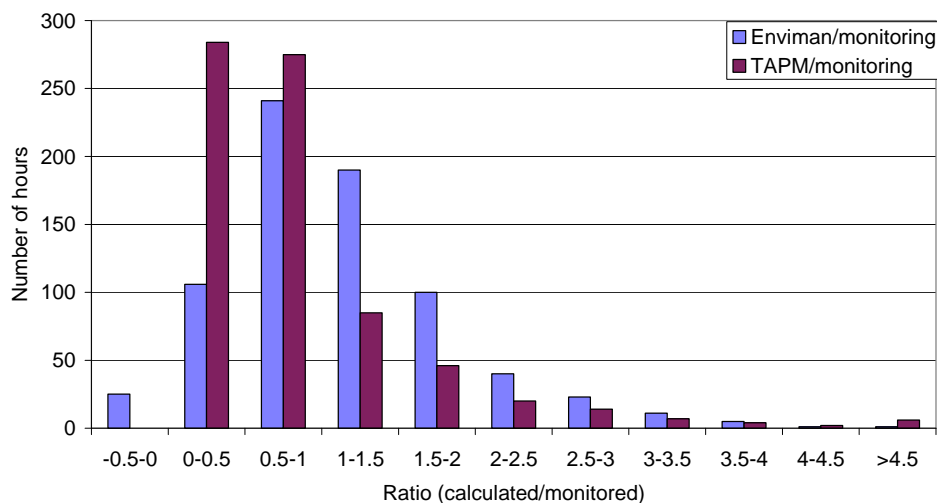


Figure 52. Comparison of the frequency of the ratio of calculated and monitored NO<sub>2</sub> concentrations from each model based on hourly mean averages from the two models.

In general it is more difficult to simulate finer timescales. However, the result presented in Figure 50 illustrates that the TAPM model captured fairly well the changes due to meteorology. According to Figure 53 most of the hours calculated with TAPM showed a ratio between calculated and monitored data that lays within the ranges 0-0.5 or 0.5-1. The data in the range 0-0.5 means a difference in the hourly NO<sub>2</sub> concentrations by 50% - 100%. The majority of the hours calculated with Enviman showed a ratio within the ranges 0.5-1 and 1-1.5. The negative values came from situations with calculated negative concentrations, possibly due to the NO<sub>2</sub>/NO<sub>x</sub> conversion routine.

In Figure 8 the monitored means of both the NO<sub>2</sub> and the SO<sub>2</sub> concentrations at Femman were shown to vary substantially depending on the wind direction. In Figure 53 the monitored NO<sub>2</sub> concentrations were split-up further into four different wind-speed classes. From this result it became clear that the highest concentrations occurred during low wind speed (1-2 m/s from all wind directions). The decrease of the NO<sub>2</sub> concentration was about the same for all wind directions for conditions with wind speed 1-2 as with speeds of 3-4 m/s. For the NO concentration there was a distinct difference between the very high concentrations when the wind came from the northerly directions (N, NE and NW) which imply that the source was close to Femman. For higher wind-speeds, which was typical for urban background air, the concentration difference of both NO<sub>2</sub> and NO was limited in the wind direction range of 135-315 degrees,

In Figure 54 the O<sub>3</sub> concentration is also presented in the different wind speed and wind direction classes for 2008. According to this result the development of the O<sub>3</sub> concentration pattern is nearly inverse to the NO pattern, at least for the two lowest wind speed classes. This indicates that it is a local effect, while for the higher wind speed classes it is a large-scale effect. Long-distance transportation of ozone might, for some wind directions, be the limiting parameter.



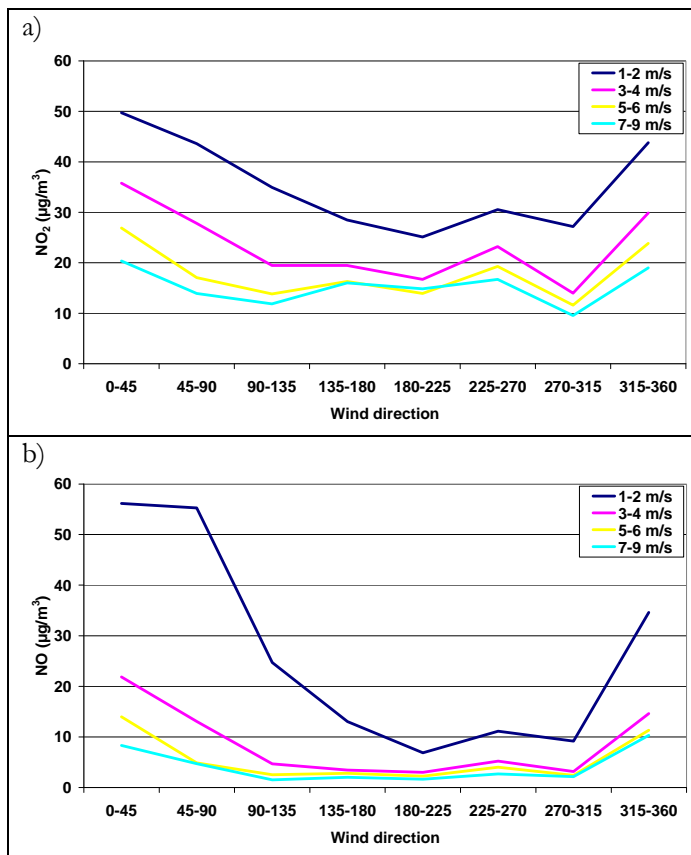


Figure 53. The monitored a) NO<sub>2</sub> and b) NO concentrations split-up into four different wind speed classes in the different wind directions.

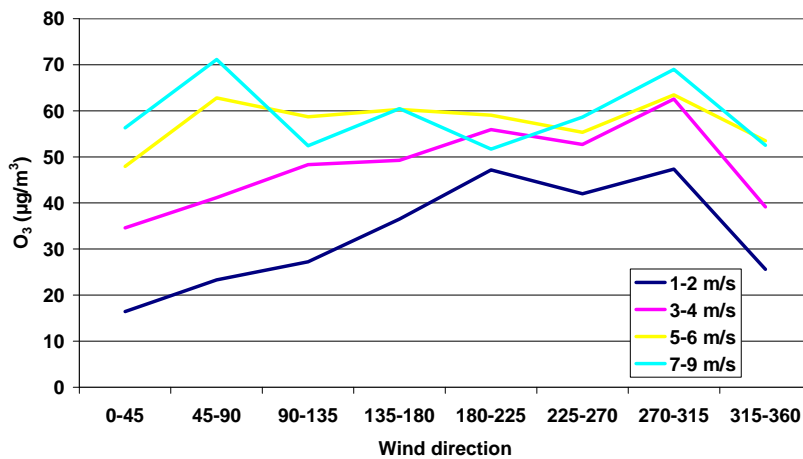


Figure 54. The O<sub>3</sub> concentrations split-up into four different wind speed classes in the different wind directions.

In Figure 55 the comparison between the mean calculated and monitored SO<sub>2</sub> concentrations at Femman from the different wind directions is shown. Not surprisingly the SO<sub>2</sub> pattern was very different from the NO<sub>2</sub> pattern since the sources for the two parameters are diverse. SO<sub>2</sub> peaks

occurred when the wind blew in a north easterly direction (22-90 degrees), from a southerly direction (200-225 degrees) and also from the west. Just north of Femman there is a large bus terminal but also the Göta Älv Bridge and river. South of Femman there is a heating plant and to the west there is the river with ships - both emitting SO<sub>2</sub>. Since the calculated SO<sub>2</sub> pattern coincided well with monitoring data, this indicated that the estimated emissions from ships and point sources were reliable.

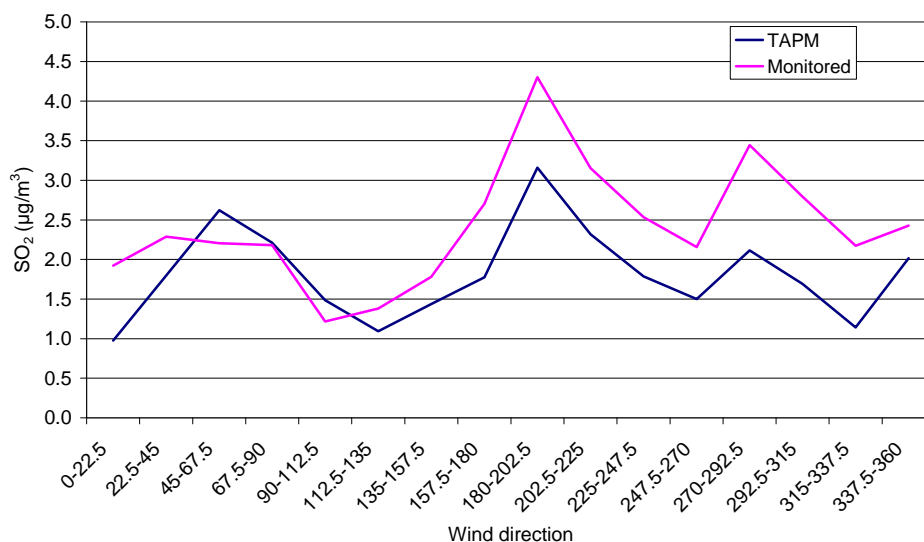


Figure 55. Mean SO<sub>2</sub> concentrations at the Femman site for each wind direction group (22.5 deg), for October 2008.

To sum up, both models were able to simulate the main features of the measured hourly NO<sub>2</sub> concentrations. The emissions used in TAPM were somewhat lower than the ones used in Enviman which could explain some of the discrepancy between the models. According to EU directives a calculated yearly mean concentration of both NO<sub>2</sub> and SO<sub>2</sub> should not differ by more than 30% compared to monitoring data while shorter time scales are allowed to vary by 50%. Both TAPM and Enviman meet these criteria (see Section 9.3.2).

### 9.3.4 Sensitivity study of the NO<sub>2</sub>/NO<sub>x</sub> emission ratio

In order to test the sensitivity of the effect of the NO<sub>2</sub> emission share in the NO<sub>x</sub> emissions the NO<sub>2</sub>/NO<sub>x</sub> emission ratio was increased from 5% to 20% in separate dispersion model calculations.

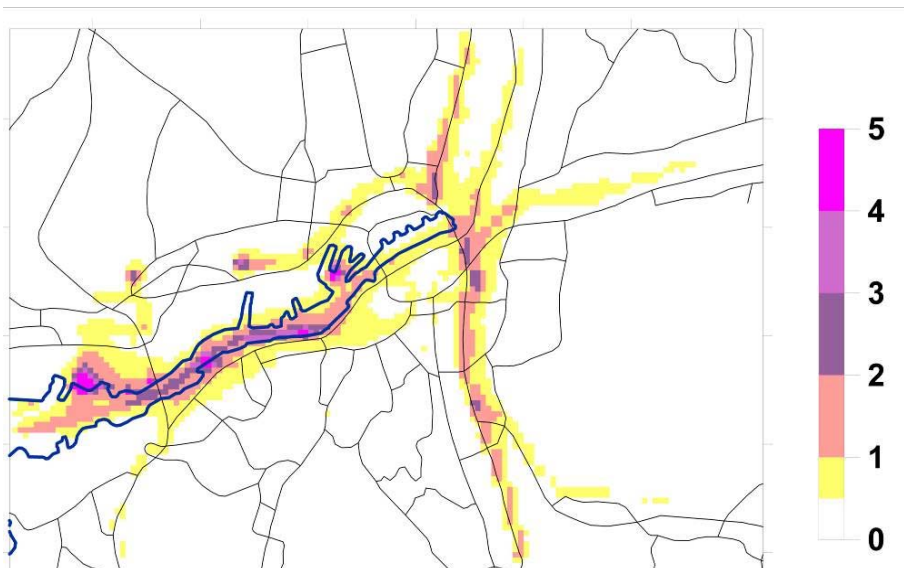


Figure 56. Difference in the NO<sub>2</sub> concentration (µg/m<sup>3</sup>) when the share of NO<sub>2</sub> in the NO<sub>x</sub> emissions is 20 % and 5 % respectively for the calculations of all emissions.

According to the calculations presented in Figure 56 an increase of the NO<sub>2</sub> share in the NO<sub>x</sub> emissions primarily affected the NO<sub>2</sub> concentrations close (500-600m) to roads or ships. The closer to the emission source, the more obvious was the impact. The effect of a 20% share of NO<sub>2</sub> also became larger at Femman at concentrations > 40 µg/m<sup>3</sup>(Figure 57).

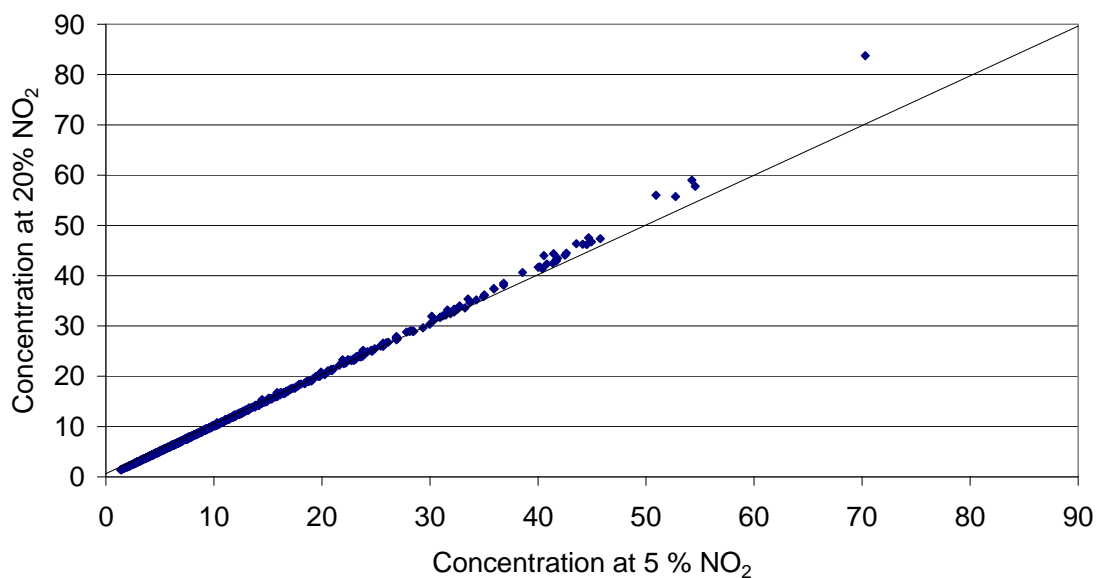


Figure 57. The effect of 5% and 20% NO<sub>2</sub> in the NO<sub>x</sub> emissions on the NO<sub>2</sub> concentration at the Femman site.

## 9.4 Separate calculations for different emission sources

Dispersion calculations were also made where one type of source at the time was excluded in order to study the geographical distribution of the emissions from each source. In Figure 58 the distribution pattern from road traffic, point and area sources are shown, while in Figure 59 the contribution from ships, point and area sources is shown. Calculations were also done of different concentration shares from the separate source types. In Figure 60 the NO<sub>2</sub> concentration shares and in Figure 61 the SO<sub>2</sub> concentration shares are shown for the sites defined in Figure 46. It seems as if a large fraction of both NO<sub>2</sub> and SO<sub>2</sub> came from ships at all sites except site 4; this is because all the monitoring sites were placed along the river and were thus close to the ship emissions. However, at site 4 the concentrations, both level and pattern, are quite different. This site is located on Hisingen relatively far away from both ship and road traffic emissions.

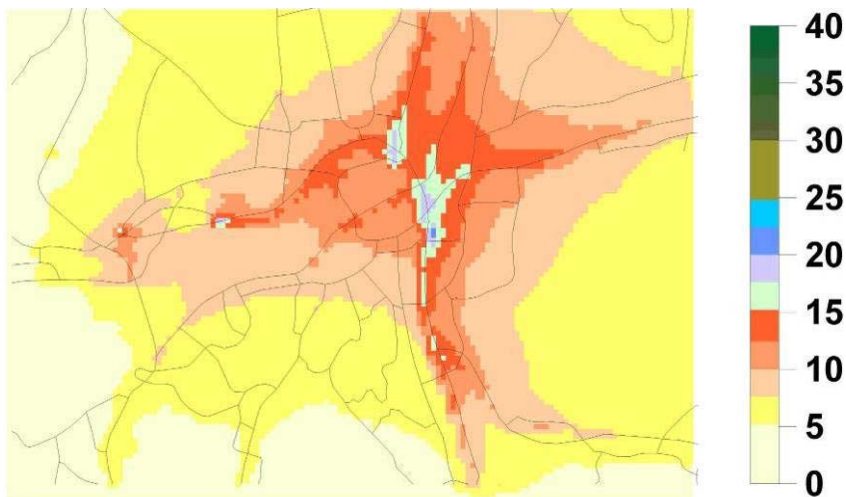


Figure 58. Calculated NO<sub>2</sub> concentration (µg/m<sup>3</sup>) from traffic, point- and area sources.

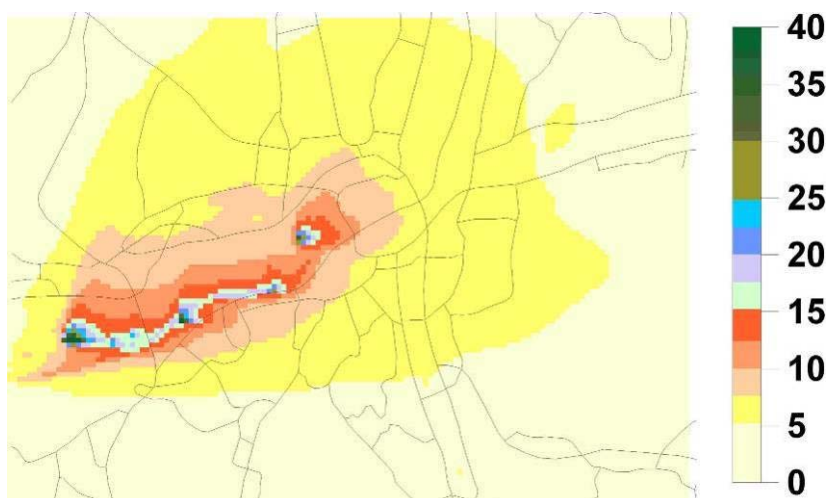


Figure 59. Calculated NO<sub>2</sub> concentration (µg/m<sup>3</sup>) from ships, point- and area sources.

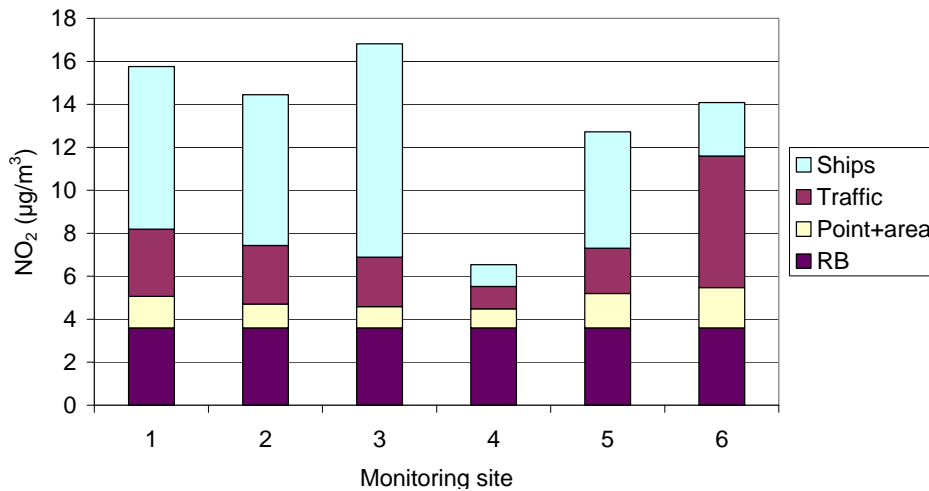


Figure 60. The shares of NO<sub>2</sub> from the different sources separately presented at the monitoring sites (Fig. 46).

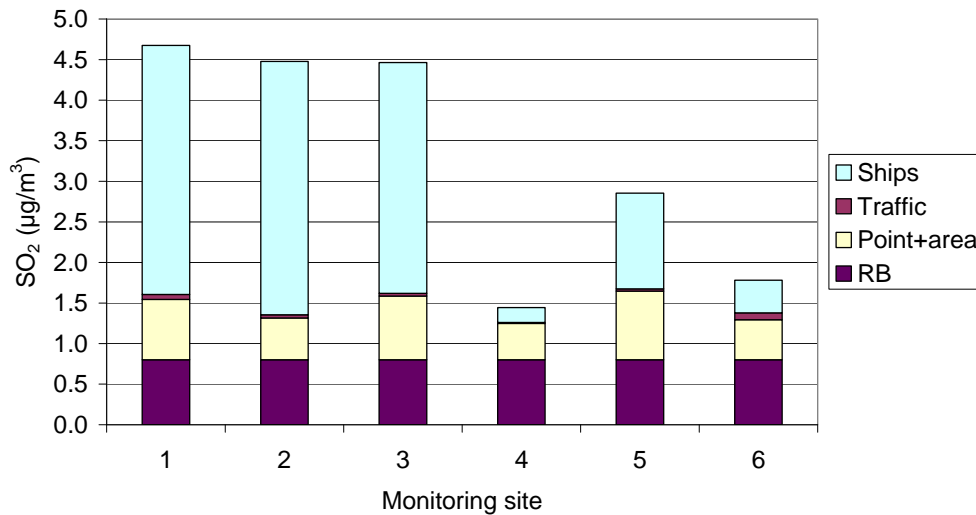


Figure 61. The shares of SO<sub>2</sub> from the different sources separately presented at the monitoring sites (Fig. 46).

In order to show the distribution variation over some other parts of the Gothenburg area, a comparison was also done for three other sites. Femman is also close to ship emissions, Kungsporsplatsen is located within the city centre where the traffic intensity is low (a largely pedestrianised area) and somewhat further away from the harbour area. Gårda is located very close to one of the most traffic-intensive roads in Gothenburg. The relationship between the different emission sources as shares of the NO<sub>2</sub> concentrations is shown in Figure 62 and as a percentage of the different shares in Figure 63. The calculations presented in a) are based on monthly means and in b) the data are for the 10 hours with the highest concentration.

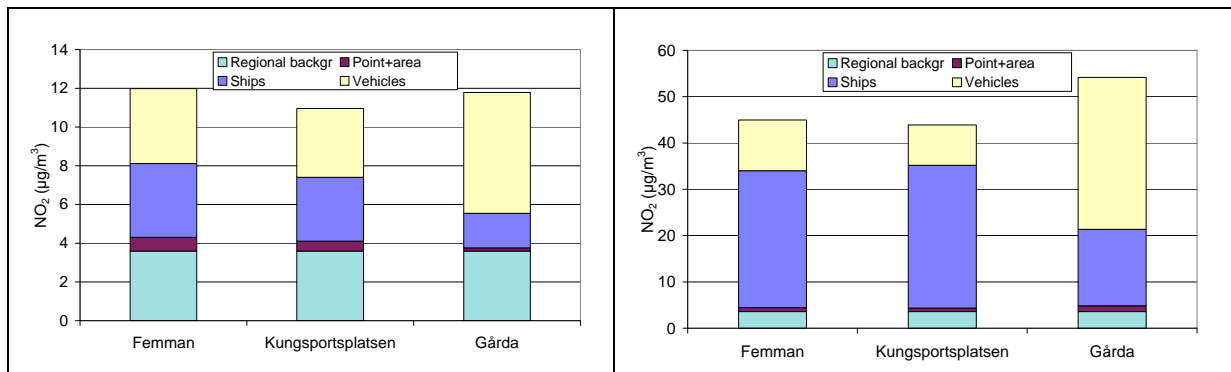


Figure 62. The shares of NO<sub>2</sub> concentrations from the different sources separately presented at the monitoring sites (Fig. 46); a) monthly means and b) means of the 20% hours with the highest concentration.

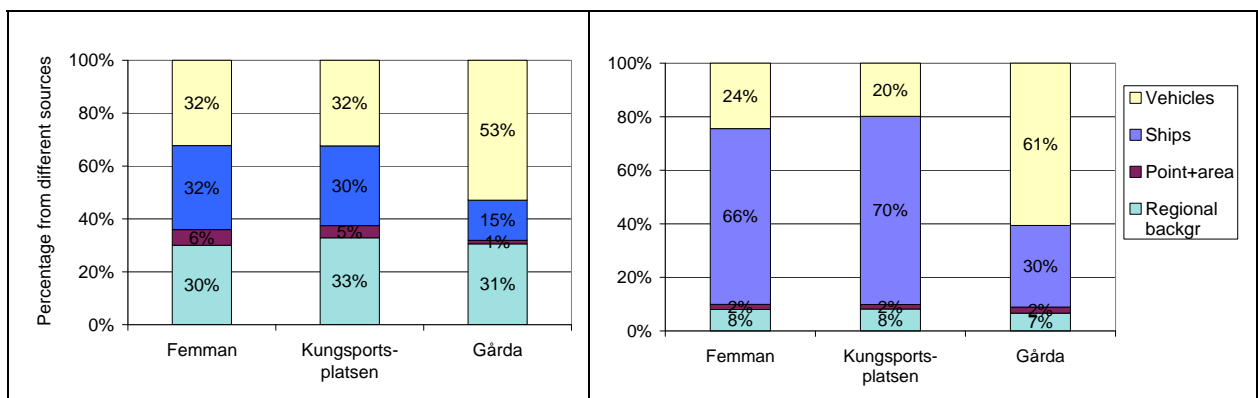


Figure 63. The percentage shares of NO<sub>2</sub> the concentration from the different sources separately presented at the monitoring sites (Fig. 46). a) Monthly means and b) means of the 20% hours with highest concentration.

According to the result presented in Figure 62a the share from road traffic was similar at both Femman and Kungsporsplatsen even though the concentration was lower at Kungsporsplatsen. The share from ships was similar to that of road traffic at both Kungsporsplatsen and Femman with the similar distance from the harbour at both sites. However, at Gårda the large influence from road traffic was obvious with 53% of the total concentration. The longer distance from the harbour area led to much lower influence from ship emissions with only 15 % of the concentration, compared to Femman where ship emissions contributed 32% to the concentration of NO<sub>2</sub>. In Figure 63b and Figure 62b, high concentration situations are presented. Here the distribution of shares was rather different compared to the long time mean calculations. The reason for this could be that the local, and possibly also the ground based emissions, governs the total concentrations more. The shares from ships were in this type of calculation very dominant at both Femman and Kungsporsplatsen while at Gårda the dominant share still came from the traffic.

## 10 Discussion

Two possible reasons for the high NO<sub>2</sub> levels in Gothenburg were investigated: 1) increased fraction of NO<sub>2</sub> in the NO<sub>x</sub> emissions from modern diesel engines, and 2) increasing total emission of NO<sub>x</sub> due to increasing contribution from shipping.

There has been a significant increase in primary emissions of NO<sub>2</sub> from traffic with time, mainly due to a larger use of diesel cars. This can also be observed in tunnel measurements where increasing NO<sub>2</sub> levels have been noted. However, the influence of this on the measured urban background NO<sub>2</sub> levels seems limited due to the rapid oxidation of NO with ozone.

It is observed that ship emissions have a large influence on the monitoring sites close to the harbour, however, it was also observed from the dispersion modelling that shipping emissions could have a significant influence also further from the harbour when it comes to the days with the highest observed levels.

The results also showed that local mixing conditions had a great influence on the dispersion of especially local and ground-based emissions (Figure 62 and Figure 63). This was mainly due to their main location within the Göta älv valleys where the dispersion becomes particularly poor during high pressure conditions. At sites within the valley, the share from different emission sources will thus differ depending on the dispersion, meaning that the share from, for example, shipping, calculated as long-time means, or parameters reflecting situations with poor dispersion, varies. Thus, the effect of ship emissions in the Gothenburg area is dominant along the harbour, but after about 1-2 km the ship contribution is still more than 30 % of the total concentration level.

There are also further factors that may affect the NO<sub>2</sub> concentrations in the Gothenburg city area, namely changes in local mixing conditions as a result of changing city shape and/or changing large-scale weather patterns as well as oxidation capacity of the atmosphere demonstrated by changing background ozone concentrations. Investigation of these factors demands further extensive modelling and data analysis, both on the small scale and on the continental scale which were not done in this study.

The calculated data were compared to measurements from diffusive sampling mainly along the river but also with the continuous monitoring at the Femman site. In general, the NO<sub>2</sub> concentrations were underestimated, the SO<sub>2</sub> mainly coincided well and the O<sub>3</sub> concentrations were somewhat overestimated in the calculations with the TAPM model. However, the variation due to the weather could be reproduced but the peaks are sometimes lower than the monitored concentration peaks. A brief analysis of the monitoring site Femman showed that the concentration levels for all the investigated parameters varied a great deal depending on the wind direction (see also Figure 8 and Figure 9). The obvious reason was the proximity to the harbour and also to areas with heavy traffic (N-NE). The ratio between NO<sub>x</sub>/NO<sub>2</sub> shows that this is also dependent on wind direction, indicating that the share of NO is also higher when the wind comes from heavy trafficked areas. This was also confirmed by the result presented in Figure 9 where the O<sub>3</sub> level was lowest when the wind blew from those directions.

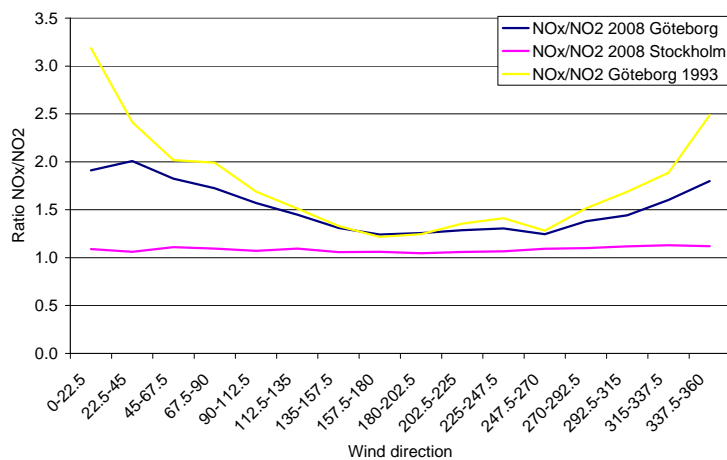


Figure 64. Variability of the ratio NO<sub>x</sub>/NO<sub>2</sub> at Femman 2008 and 1993 and Stockholm, Torkel Knutssongatan 2008.

A comparison with older monitoring data from Femman showed the NO<sub>x</sub>/NO<sub>2</sub> ratio has decreased from 1993 to 2008. To investigate whether this pattern was common at urban background sites, a site in Stockholm (for one year) was also investigated showing that there was hardly any variability at all.

The high concentration during northerly wind depended, on those occasions, on the fact that there were usually low wind-speed and inversion conditions. The reason why there was no variability during different wind directions in the Stockholm case, indicated a more evenly distributed emission pattern in Stockholm, at least in the close surroundings of the site Torkel Knutssongatan.

There are several reasons which explain the increased proportions of NO<sub>2</sub> in the primary emissions of NO<sub>x</sub>. It is the increase in the fraction of diesel vehicles by ca. 15% (as vehicle-km) during the last decade (see Figure 13 and (Figure 14). Diesel vehicles generally have a higher fraction of NO<sub>2</sub> in their NO<sub>x</sub> emissions than gasoline cars. On the top of this, the large increase of diesel vehicles over the last decade was also accompanied by a simultaneous increase of NO<sub>2</sub> part in NO<sub>x</sub> emissions from diesel trucks with Euro3 and Euro4 standards which became compulsory in 2000 and 2005, respectively (Figure 11). Measurements of NO<sub>2</sub> and NO<sub>x</sub> concentrations in tunnels, and at sites largely dominated by primary emissions, indicated an increase in the NO<sub>2</sub>/NO<sub>x</sub> partition from 4-6% in the 1980s, and at the beginning of the 1990s, to today's 13%. The tunnel-model study indicated that the actual NO<sub>2</sub>/NO<sub>x</sub> fraction could be even larger if effects of the NO<sub>2</sub> sinks in the tunnel are taken into account.

An increase in the NO<sub>2</sub> share of the primary NO<sub>2</sub> emissions was greatest close to sources because the NO in the primary emission reacted with ambient ozone forming NO<sub>2</sub> on a time-scale of minutes and the NO<sub>2</sub>/NO<sub>x</sub> ratio quickly increased, tending to approach a photo-stationary state between NO, NO<sub>2</sub> and ozone (see central part on Figure 10). The simultaneous measurements of NO<sub>2</sub>, NO (or NO<sub>x</sub>) and ozone indicated that the fraction of primary and secondary NO<sub>2</sub> in the city varied largely depending on mixing and photochemical conditions. The two measurement campaigns performed within the scope of this study showed an 81% share of the primary NO<sub>2</sub> emissions in the total increase of NO<sub>2</sub> concentration above the background in one case and a 26% share in the second. The high share of primary NO<sub>2</sub> was associated with low ozone concentrations and an excess of measured NO<sub>2</sub> above NO<sub>2</sub> calculated from background NO<sub>2</sub>, NO<sub>2</sub> formed by titration of emitted NO by ozone plus the direct emission of NO<sub>2</sub> (See Chapter 4). This discrepancy could indicate either that the background ozone concentration was too low (i.e.



background measurements do not correspond to Gothenburg background measurements in these conditions), that there was a larger share of secondary NO<sub>2</sub> in emissions, or that by the end of November there was an unusual ozone formation.

A sensitivity study with the city scale dispersion model was performed by raising the NO<sub>2</sub>/NO<sub>x</sub> emission ratio from 5 to 20%. The change in NO<sub>2</sub> concentrations showed that the effect of the higher share of NO<sub>2</sub> within the NO<sub>x</sub> emissions can affect the NO<sub>2</sub> concentration level close to the source up to a distance of about 500 - 600 m. Further, the effect also increased in tandem with increased concentration levels (Figure 57).

The chemical development in ship plumes was studied with a detailed photochemical plume model to ensure that the simple chemistry treatment of the TAPM model accurately described the processes affecting the NO/NO<sub>2</sub> distribution and NO<sub>x</sub> oxidation. Comparison of the detailed chemistry with the simplified version showed a significant similarity during day hours when chemistry is, to a large extent, driven by NO<sub>2</sub> photolysis. The night-time chemistry of NO<sub>x</sub>, driven by nitrate radical and oxidation of N<sub>2</sub>O<sub>5</sub> is not included in the TAPM chemical scheme which may lead to an underestimation of NO<sub>x</sub> oxidation during dark hours.

When it comes to measures to reduce the levels of NO<sub>2</sub> in the future it seems as if the ratio of NO<sub>2</sub> to NO in emissions is less important than the NO<sub>x</sub> emissions. However, it may still be a factor at street-level sites where the ozone levels can be lower. In the extreme case of tunnels it is certainly a factor. It would be of interest to study more in detail at what conditions (ozone-levels, traffic intensity, distance from roads, etc) the primary NO<sub>2</sub> emissions are important for the levels. Thus, for road traffic the important measure is to reduce the NO<sub>x</sub> emissions.

It will also have an impact if the NO<sub>x</sub> emissions from shipping can be reduced. Especially for days with high levels of NO<sub>2</sub>, i.e., situations where the most severe problems in relation to air quality standards occurs. It is likely that TIER III engines, with about 80% lower NO<sub>x</sub> emissions, will be introduced in the waters around Sweden from 2016. A rapid replacement of old engines with TIER III engines will reduce the emissions from shipping significantly. Further, a more widely use of on shore electricity for ships at berth may be important.

## 11 References

- Amman, M., Arens, F., Gutzwiller, L., Baltensperger, U., Gaggeler, H.W., 2000. The HONO formation capacity of primary and aged diesel soot particles. In: Vogt, R., Axelsdottir, G. (Eds.), Proceedings of the EC/EUROTRAC-2 Workshop, Aachen, FRG, ISBN: 3-00-005414-6, pp. 219–222.
- Atkinson, R., Baulch, D. L., Cox, R. A., Hampson Jr., R. F., Kerr, J. A., Rossi, M. J. and Troe, J., 1997. Evaluated kinetic, photochemical and heterogeneous data for atmospheric chemistry: Supplement V. Journal of Physical and Chemical Reference Data 26, 521-1011.
- Burgard, D.A., Dalton, T.R., Bishop, G.A., Starkey J.R., Stedman D.H. (2006) Nitrogen dioxide, sulfur dioxide, and ammonia detector for remote sensing of vehicle emissions. *Review of Scientific Instruments*, **77**:014101.1-014101.5.

- Chen, G., Huey, L.G., Trainer, M., Nicks, D., Corbett, J.J., Ryerson, T., Parrish, D., Neuman, J.A., Nowak, J., Tanner, D., Holloway, J., Brock, C., Crawford, J., Olson, J.R., Sullivan, A., Weber, R., Schauffler, S., Donnelly, S., Atlas, E., Roberts, J., Flocke, F., Hubler, G., Fehsenfeld, F. (2005). An investigation of the chemistry of ship emission plumes during ITCT 2002. *Journal of Geophysical Research*, **110**, D10S90, doi:10.1029/2004JD005236.
- Cofala, J., Amann, M., Heyes, C., Klimont, Z., Posch, M., Schöpp, W., Tarasson, L., Jonson, J., Whall, C., Stavrakaki, A., 2007. Final Report: Analysis of Policy Measures to Reduce Ship Emissions in the Context of the Revision of the National Emissions Ceilings Directive; International Institute for Applied Systems Analysis: Laxenburg, Austria, [www.iiasa.ac.at](http://www.iiasa.ac.at).
- Davis, D. D., Grodzinsky, G., Kasibhatla, P., Crawford, J., Chen, G., Liu, S., Bandy, A., Thornton, D., Guan, H., Sandholm, S. (2001). Impact of ship emissions on marine boundary layer NO<sub>x</sub> and SO<sub>2</sub> distributions over the Pacific Basin. *Geophysical Research Letters*, **28**, 235-238.
- Ekström, M., Sjödin, Andreasson, K. (2004) Evaluation of the COPERT III emission model with on-road optical remote sensing measurements. *Atmospheric Environment*, **38**, 6631–6641.
- Environmental Agency in Gothenburg
- Febo A., De Santis F. and Perrino C. (1986) Measurement of atmospheric nitrous and nitric acid by means of annular denuders. Proc. of the fourth European Symposium on Physico-Chemical Behaviour of Atmospheric Pollutants, 23-25 sept.1986 Stresa Italy (ed G. Angeletti and G. Restelli) pp. 121-125
- Ferm M. (2001) Validation of a diffusive sampler for ozone in workplace atmospheres according to EN838. Proc. from International Conference Measuring Air Pollutants by Diffusive Sampling, Montpellier, France 26-28 September 2001. p298-303
- Ferm M., Johansson C. and Persson K. (2008). Samband mellan kväveoxider och ozon i tätorter. Haltmätningar med diffusionsprovtagare. IVL rapport B1768
- Ferm M. and Rodhe H. (1997) Measurements of air concentrations of SO<sub>2</sub>, NO<sub>2</sub> and NH<sub>3</sub> at rural and remote sites in Asia. *Journal of Atmospheric Chemistry* **27**, 17-29
- Ferm M. and Svanberg P.-A. (1998) Cost-efficient techniques for urban- and background measurements of SO<sub>2</sub> and NO<sub>2</sub>. *Atmospheric Environment* **32**, 1377-1381
- Ferm M and Sjödin Å. (1983) Measurements of CO, NO<sub>2</sub> and NO inside and outside a car driving in the traffic. (In Swedish). IVL report B723
- Ferm M. and Sjödin Å. (1985) A sodium carbonate coated denuder for determination of nitrous acid in the atmosphere. *Atmospheric Environment* **19**, 979-983
- Ferm M. (2001) The theories behind diffusive sampling. Proc. from International Conference Measuring Air Pollutants by Diffusive Sampling, Montpellier, France 26-28 September 2001. p31-40
- Gerry, M. W., Whitten, G. Z., Killus, J. P., and Dodge, M. C. (1989) A photochemical mechanism for urban and regional scale computer modelling. *J. Geophys. Res.*, **94**, 12925-12956.
- Gothenburgs Miljöförvaltning (2009): Ren Stadsluft, [http://www.miljo.goteborg.se/luftnet/Ren\\_stadsluft](http://www.miljo.goteborg.se/luftnet/Ren_stadsluft)
- Haeger-Eugensson, M., (1999): Atmospheric stability and the interaction with local and meso-scale wind systems in an urban area. Earth Sciences Centre, Gothenburg university A39 1999.
- Haeger-Eugensson M., Borne K., Chen D., and Persson K (2002) Development of a New Meteorological Ventilation Index for Urban Air Quality Studies. IVL rapport L02/70.

- Hurley et al. (2005) The Air Pollution Model (TAPM) User manual. CSIRO Atmospheric Research International Paper No.31.
- Kalberer, M., Ammann, M., Arens, F., Gaggeler, H.W., Baltensperger, U., 1999. Heterogeneous formation of nitrous acid (HONO) on soot aerosol particles. *Journal of Geophysical Research* 104, 13825–13832.
- Kleffmann, J., Becker, K.H., Lackhoff, M., Wiesen, P., 1999. Heterogeneous conversion of NO<sub>2</sub> on carbonaceous surfaces. *Physical Chemistry Chemical Physics* 1, 5443–5450.
- Konopka, P., 1995: Analytical Gaussian solutions for anisotropic diffusion in a linear shear flow, *J. Non-Equilib. Thermodyn.*, **20**, 78-91.
- Kurtenbach, R., Becker, K.H., Gomes, J.A.G., Kleffmann, J., Lörzer, J.C., Spittler, M., Wiesen, P., Ackermann, R., Geyer, A., Platt, U., 2001, Investigations of emissions and heterogeneous formation of HONO in a road traffic tunnel. *Atmospheric Environment* 35, 3385–3394.
- Lenner, M. (1987) Nitrogen Dioxide in Exhaust Emissions from Motor Vehicles. *Atmospheric Environment* **21**, 37-43.
- Opsis (2000). User Guide. (www.enviman.com).
- Persson K, Sjöberg K. och Haeger-Eugensson M. (2007). Air quality in Sweden summer 2006 and winter 2006/07. Results from measurements within the Swedish Urban air quality network. (In Swedish). IVL report B1744
- Pszeny, A.A.P., Moldanová, J., Keene, W.C., Sander R., Maben J.R., Martinez-Harder, M. Crutzen, P.J., Perner, D. and Prinn, R.G. (2004) Aerosol pH and Inorganic Halogen Species in the Hawaiian Marine Boundary Layer, *Atmos. Chem. Phys.*, **4**, 147-168.
- Rodler, J., Sturm, P., Bacher, M., Sjödin, Å., Ekström, M., McCrae, I., Boulter, P., Kurtenbach, R., Wiesen, P., Lörzer, J., Petrea, M., Imhof, D., Prevot, A. S. H., Staehelin, J., Sangiorgio, C., Tona, B., Colberg, C. A., 2005. Validation -Final Report for ARTEMIS WP 1200. TUG report, Zurich.
- Sander, S. P., B. J. Finlayson-Pitts, R. R. Friedl, D. M. Golden, R. E. Huie, H. Keller-Rudek, C. E. Kolb, M. J. Kurylo, M. J. Molina, G. K. Moortgat, V. L. Orkin, A. R. Ravishankara and P. H. Wine "Chemical Kinetics and Photochemical Data for Use in Atmospheric Studies, Evaluation Number 15," JPL Publication 06-2, Jet Propulsion Laboratory, Pasadena, 2006.
- Sander, R., and Crutzen. P.J. (1996) Model study indicating halogen activation and ozone destruction in polluted air masses transported to the sea. *J. Geophys. Res.*, **101**, 9121-9138.
- Schumann, U., Konopka, P., Baumann, R., Busen, R., Gerz, T., Schlager, H., Schulte, P., Volkert, H. (1995) Estimate of diffusion parameters of aircraft exhaust plumes near the tropopause from nitric oxide and turbulence measurements. *J. Geophys. Res.*, **100**, 14147-14162
- Sjöberg K., Lövblad G., Ferm M., Ulrich E., Cecchini S. and Dalstein L. (2001) Ozone measurements at forest plots using diffusive samplers. Proc. from International Conference Measuring Air Pollutants by Diffusive Sampling, Montpellier, France 26-28 September 2001. p116-123.
- Sjöberg K, Haeger-Eugensson M., Forsberg B., Åström S, Hellsten S, Larsson K, Björk A., and Blomgren H. (2008). Quantification of population exposure to PM<sub>2.5</sub> and PM<sub>10</sub> in Sweden 2005. IVL report B 1792.
- Sjödin Å. and Ferm M. (1985) Measurements of nitrous acid in an urban area. *Atmospheric Environment* **19**, 985-992 The paper is discussed in *Atmospheric Environment* **20**, 408-411

- Sjödin, Å., Persson, K., Andreasson, K., Arlander, B., Galle, B. (1998) On-Road Emission Factors Derived from Measurements in a Traffic Tunnel. *Int. J. Vehicle Design* **20**, 147-158.
- Sjödin et al., 2000. Emissioner i trafikttunnlar - jämförelse mellan mätningar och modellberäkningar, IVL Svenska Miljöinstitutet AB.
- Sjödin, Å., Jerksjö M., Sandström C., Erlandsson L., Almén J., Ericsson E., Larsson H., Hammarström U., Mohammed-Reza Y., Johansson H. (2009) Implementering av ARTEMIS Road Model i Sverige.
- Song, C. H., Chen, G., Hanna, S. R., Crawford, J., Davis, D. D. (2003) Dispersion and chemical evolution of ship plumes in the marine boundary layer: Investigation of O<sub>3</sub> /NO<sub>y</sub> /HO<sub>x</sub> chemistry version. *Journal of Geophysical Research*, **108**, 4143, doi:10.1029/2002JD002216.
- Thomar M. (2008) A study of NO<sub>2</sub> emissions from vehicles in traffic situations, Master of Science Thesis, Chalmers.
- Vogt, R., Crutzen, P. J., and Sander, R (1996). A mechanism for halogen release from sea-salt aerosol in the remote marine boundary layer, *Nature*, **382**, 327-330.

## Appendix 1. Description of the TAPM model

TAPM, The Air Pollution Model, was developed by the Australian CSIRO Atmospheric Research Division. Air pollution models typically use either observed meteorological data from a surface-based meteorological station or a diagnostic wind field model based on available observations. TAPM is different from these approaches in that it solves the fundamental fluid dynamics and scalar transport equations to predict meteorology and pollutant concentration for a range of pollutants important for air pollution applications - *this eliminates the need of site-specific meteorological observations*. Instead, the model predicts the flows important to local-scale air pollution transport, such as sea breezes and terrain-induced flows, against a background of larger-scale meteorology provided by synoptic analyses. It predicts meteorological and pollution parameters directly on local, city or inter-regional scales.

### ***Meteorology model***

The meteorological component of TAPM is an incompressible, non-hydrostatic, primitive equation model with a terrain-following vertical coordinate for three-dimensional simulations. The model solves the momentum equations for horizontal wind components, the incompressible continuity equation for vertical velocity, and scalar equations for potential virtual temperature and specific humidity of water vapour, cloud water and rainwater. Explicit cloud micro-physical processes are included. Turbulent kinetic energy and eddy dissipation rates are calculated for determining the turbulence terms and the vertical fluxes. Further, surface energy budget is considered to compute the surface temperature. A vegetative canopy and soil scheme is used at the surface. Radiative fluxes at the surface and at upper levels are also calculated. Also, TAPM was confirmed to have strong ability in simulating thermally-driven meso- and local scale wind systems, such as sea-to-land breeze and urban heat-island effects. Investigations have shown that the model performs well in simulating air temperature and wind, which are the two most important fields to drive air pollution modelling.

### ***Air pollution model***

The air pollution component of TAPM, which uses predicted meteorology and turbulence from the meteorological component, includes three modules. The Eulerian Grid Module (EGM) solves prognostic equations for concentration and for cross-correlation of concentration and virtual potential temperature. The Lagrangian Particle Module (LPM) can be used to represent near-source dispersion more accurately, while the Plume Rise Module is used to account for plume momentum and buoyancy effects for point sources. The model also has gas-phase photochemical reactions based on the generic reaction set, and gas- and aqueous-phase chemical reactions for sulphur dioxide and particles. In addition, wet and dry deposition effects are also included. See more information about the TAPM at [www.dar.csiro.au/tapm/index.html](http://www.dar.csiro.au/tapm/index.html).

### ***Verification of the model***

IVL has performed a validation of the modelling system for European conditions with very satisfying results. TAPM has also been verified for many regions in Australia and overseas. CSIRO has verified the model in Kwinana, Perth and the Pilbara (WA), Cape Grim (TAS), Melbourne (VIC), Newcastle and Sydney (NSW), Mt Isa (QLD), Port Pirie (SA), Kuala Lumpur (Malaysia), as well as for Kincaid and Indianapolis (USA) international tracer datasets. (See further the list of publications and Technical Paper on verification and list of relevant papers from CSIRO can also be found at the above-mentioned website).

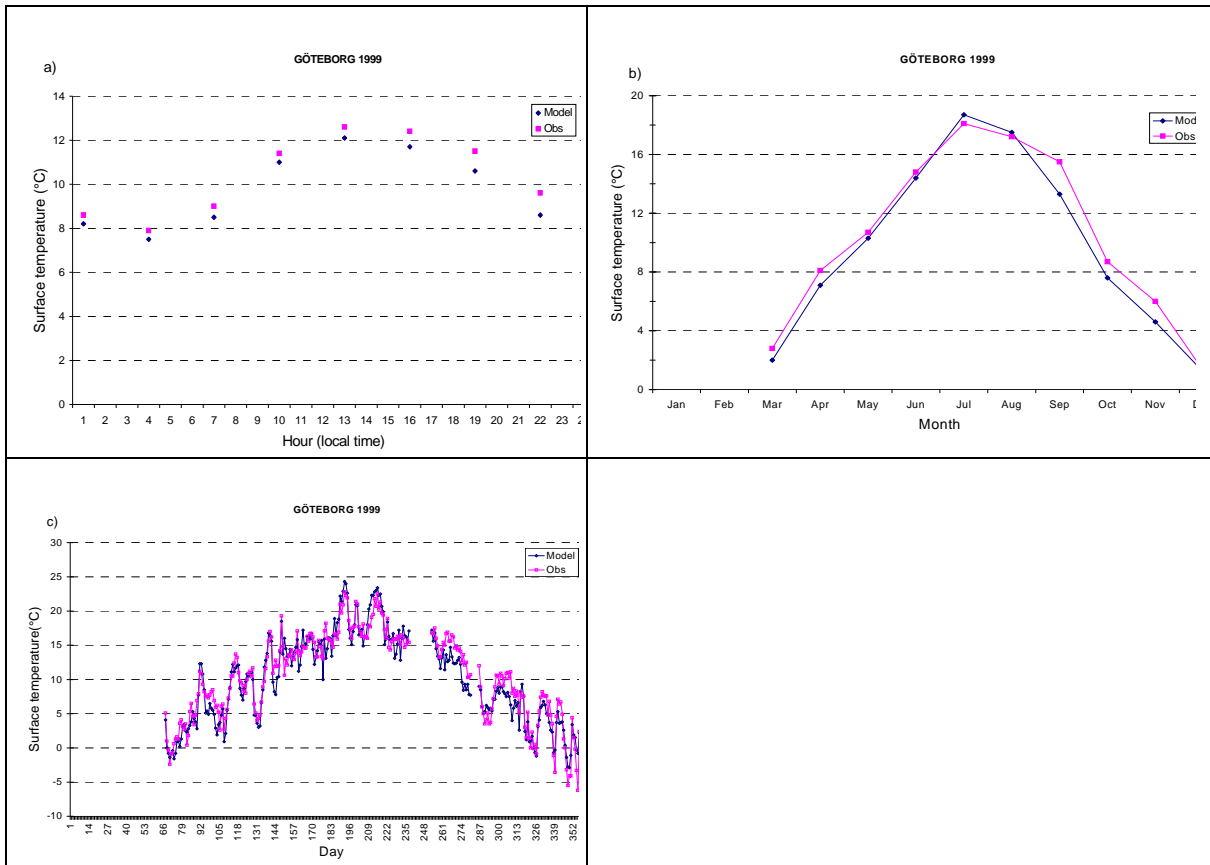


Figure A1. Monitored and simulated air temperature in Gothenburg 1999 (a) hourly; (b) seasonal; (c) daily variation.

In Figure A2 a comparison of monitored and simulated wind speed at Säve.

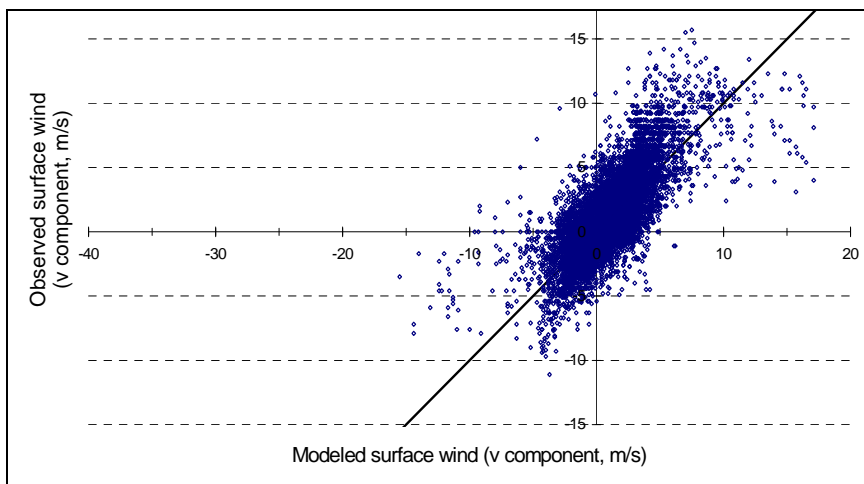


Figure A2. Comparison between monitored and simulated wind speed at Säve 1999.

Comparison between monitored and simulated ozone and NO<sub>2</sub> concentrations from Australia (see Figure A3).

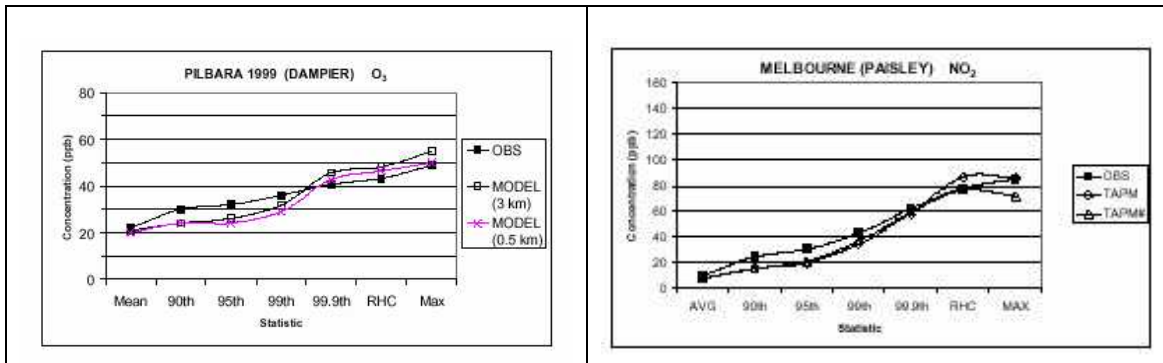


Figure A3. Comparison between monitored and simulated ozone and NO<sub>2</sub> concentrations in Australia, grid resolution 3 km x 3 km.